Analytical Solutions of 3D Heat Conduction in Flux Channels with Nonuniform Properties and Complex Structures

by

© **Belal Al-Khamaiseh**

A thesis submitted to the School of Graduate Studies
in partial fulfillment of the requirements for the
degree of Doctor of Philosophy.

Department of Mathematics and Statistics

Memorial University

April 2018

St. John's, Newfoundland and Labrador, Canada

Abstract

In the microelectronics industry, thermal issues due to self-heating are major problems that affect the performance, efficiency, and reliability of devices. The recent trend of producing advanced devices with smaller sizes, high power densities, and extreme performance makes thermal management an increasingly important factor in the development of microelectronic systems. In most applications, the microelectronic systems are modeled as rectangular flux channels, where heat is generated in one or more small heat-source areas and flows by conduction through the system to spread the heat into a larger convective heat-sink area, where the generated heat is then transferred by convection into an ambient fluid.

In this work, analytical solutions for the temperature distribution and thermal resistance in three-dimensional (3D) flux channels with nonuniform properties and complex structures are obtained. First, general analytical solutions in 3D isotropic flux channels with nonuniform heat transfer coefficients along the sink plane are presented using the method of separation of variables combined with the method of least squares. Different parametric studies have been conducted to study the effect of different variable heat transfer coefficient functions with the same average conductance on the temperature field. Second, general analytical solutions of 3D isotropic flux channels with temperature-dependent thermal conductivities and a uniform heat transfer coefficient along the sink plane are presented by means of the Kirchhoff transform method. The solutions are used to study the effect of the temperature-dependent thermal conductivity on the temperature rise and thermal resistance for different conductivity functions. Third, general analytical solutions in 3D flux channels of multilayered structures consisting of a finite number of orthotropic layers with constant and temperature-dependent thermal conductivities are obtained. All the analytical solutions have been verified by conducting numerical simulations based on the finite element method (FEM) using the Analysis of Systems (ANSYS) software package.

To my parents

Acknowledgements

First and foremost, I owe my deepest gratitude to my supervisor Dr. Serpil Kocabiyik and my co-supervisor Dr. Yuri Muzychka for providing me the opportunity to pursue this work. I would also like to thank them for their distinguished supervision, continuous support, motivation, enthusiasm, and immense knowledge. This work would not have been possible without them.

I am grateful for the financial support provided by the Natural Sciences and Engineering Research Council of Canada (NSERC) in the form of research grants of my supervisors, and by the School of Graduate Studies (SGS) in the form of a graduate fellowship. I am also grateful for the partial financial support provided by the Department of Mathematics and Statistics in the form of a teaching assistantship during my doctoral studies.

I acknowledge the support of the Department of Mathematics and Statistics and the Faculty of Engineering and Applied Science for providing the computational facilities which were important for this work.

Last but not the least, I must express my very profound gratitude to my parents, brothers, sisters, and friends for providing me with unfailing support and continuous encouragement throughout my years of study and through the process of researching and writing this thesis.

Statement of contribution

This thesis contributes to the area of heat transfer. It introduces analytical solutions for the temperature distribution and thermal resistance in 3D flux channels with nonuniform properties and complex structures. This contribution includes developing analytical solutions for the temperature field in flux channels with nonuniform heat transfer coefficients, multilayered structures with orthotropic conductivity tensor and interfacial conductance, nonlinear conduction in single and multilayered structures. A variety of different mathematical models, techniques, and transformations are used to illustrate the construction of the developed analytical solutions. Moreover, numerical simulations based on the FEM are conducted in order to verify these analytical solutions and to demonstrate their robustness.

This work is considered of significant importance for thermal analysts and engineers in the microelectronics industry as it provides computational algorithms and tools for obtaining the precise thermal behavior and the optimal configuration of the microelectronic devices rather than conducting the challenging experimental work. In fact, the developed analytical solutions can be used in other transport phenomena, such as mass transfer according to some analogies that can be made between the transport phenomena laws.

The findings presented in Chapters 2-6 are considered original scholarship and distinct contributions to knowledge.

Table of contents

List of tables

List of figures

List of symbols

A_c	=	Area, m^2.
$\mathbf{A}$	=	Linear system matrix.
$\mathbf{A}^j$	=	jth linear system matrix.
$A_{mn},\ B_{mn}$	=	Fourier coefficients.
$A^*_{mn},\ B^*_{mn}$	=	Multiple-heat-source Fourier coefficients.
$A,\ B,\ C$	=	Arbitrary constants.
Bi	=	Biot number.
$a,\ b,\ c,\ d$	=	Linear dimensions, m.
$\bar{b},\ \bar{d}_i$	=	Transformed linear dimensions, m.
$\mathbf{b}$	=	Linear system right-hand-side vector.
$\mathbf{b}^j$	=	jth linear system right-hand-side vector.
$C_{mn},\ D_{mn}$	=	Fourier coefficients.
$\hat{C}_{mn}$	=	Modified Fourier coefficients.
$\mathbf{C}$	=	Fourier coefficients vector.
$\mathbf{C}^j$	=	jth Fourier coefficients vector.
c_j	=	Least squares modeling function parameters.
c_p	=	Specific heat, J/kg·K.
F	=	Transcendental function.
f	=	Prescribed temperature boundary condition function.
h_0	=	Reference conductance, W/m^2·K.
h_c	=	Interfacial conductance, W/m^2·K.
h_e	=	Conductance along the edges, W/m^2·K.
h_s	=	Sink-plane conductance, W/m^2·K.
$h(x)$	=	1D heat transfer coefficient function, W/m^2·K.
$h(x,y)$	=	2D heat transfer coefficient function, W/m^2·K.
I	=	Sum of squared residuals.

I_{MN}	=	Least squares integral.
g	=	Prescribed heat flux boundary condition function.
$\dot{g}$	=	Internal heat generation, W/m^3.
$K\{\}$	=	Kirchhoff transform.
$k(T)$	=	Temperature-dependent thermal conductivity, W/m·K.
$\hat{k}(T)$	=	Functional relationship of temperature.
k	=	Thermal conductivity, W/m·K.
k_0	=	Reference thermal conductivity, W/m·K.
k_i	=	Effective layer conductivities, W/m·K.
$\bar{\bar{k}}$	=	Thermal-conductivity tensor.
$m,\ n$	=	Indices for summations.
M	=	Number of terms in summations.
N	=	Number of terms in summations.
	=	Number of layers.
N_c	=	Number of heat sources.
$N(\cdot)$	=	Norm.
p	=	Power in the sink-conductance function.
$p(x)$	=	Real-valued function.
q	=	Heat flux, W/m^2.
Q	=	Heat flow rate, W.
R	=	Thermal resistance, K/W.
R_{mn}	=	Spreading resistance components, K/W.
r	=	Residual.
$\hat{r}$	=	Position vector, $\equiv (x, y, z)$.
$S(x, y)$	=	Source-plane boundary condition function.
T	=	Temperature, K or °C.
T_∞	=	Ambient temperature, K or °C.
$\hat{T}$	=	Centroidal temperature, K or °C.
t	=	Thickness, m.
$\bar{t}_i$	=	Effective layer thickness, m.
U	=	Original Kirchhoff transform variable.
$u(x)$	=	Eigenfunction of the Sturm-Liouville problem.
	=	Continuous function.
$\tilde{u}$	=	Least squares approximate function.

$v(x),\ w(x)$	=	Real-valued functions.
$X,\ Y,\ Z$	=	Separating functions.
$X_c,\ Y_c$	=	Location of the heat-source center, m.
$\overline{Y}_c$	=	Transformed Y_c, m.
$x,\ y,\ z$	=	Cartesian coordinates, m.
$\vec{x}$	=	Multidimensional position vector.
y_i	=	Orthotropic transform variable, m.

Operators

∇	=	Gradient.
$\nabla\cdot$	=	Divergence.
∇^2	=	Laplacian.
$\dfrac{\partial}{\partial n}$	=	Outward normal derivative.

Greek Symbols

β_{mn}	=	Eigenvalues of the double Fourier expansion, $\equiv \sqrt{\lambda_m^2 + \delta_n^2}$ m^{-1}.
γ	=	Dummy eigenvalue variable, m^{-1}.
δ_n	=	Eigenvalues of the Fourier expansion in y-direction, m^{-1}.
ϵ	=	Heat-source-size aspect ratio.
ζ_i	=	Orthotropic transform variables, m.
θ	=	Temperature excess, $\equiv T - T_\infty$ K or °C.
	=	Apparent temperature, K.
λ	=	Eigenvalue of the Sturm-Liouville problem.
λ_m	=	Eigenvalues of the Fourier expansion in x-direction, m^{-1}.
μ_i	=	Mixed conductivities ratio, $\equiv \dfrac{k_{1,x}k_{i,y}}{k_{1,y}k_{i,x}}$.
ρ	=	Density, kg/m^3.
σ	=	Square root of the first-layer conductivities ratio, $\equiv \sqrt{k_{1,y}/k_{1,x}}$.
τ	=	Thickness aspect ratio.
	=	Variable in the Kirchhoff transform.
ϕ	=	Spreading function.
φ	=	Trial function.
ψ	=	Least squares Fourier coefficients function.
	=	Inverse Kirchhoff transform function, $\equiv K^{-1}\{\}$.
Ω	=	Bounded domain.

ω	=	Temperature coefficient of thermal conductivity, 1/K.

Subscripts

c	=	Source.
e	=	Edge.
$i,\ j$	=	Indices for Eigenvalues and Fourier coefficients.
	=	Denote layer i and heat source j, respectively.
s	=	Sink.
sp	=	Spreading.
t	=	Total.

Superscripts

t	=	Transpose.
$*$	=	Dimensionless.
$\overline{(\cdot)}$	=	Mean value, transformed dimension.

List of abbreviations

ANSYS	Analysis of Systems
BP	Black Phosphorus
1D	One Dimensional
2D	Two Dimensional
3D	Three Dimensional
FEM	Finite Element Method
Fig.	Figure
ICs	Integrated Circuits
LEDs	Light Emitting Diodes
ODE	Ordinary Differential Equation
PDE	Partial Differential Equation
TSR	Thermal Spreading Resistance

Chapter 1

Introduction and Overview

1.1 Motivation

In the electronics industry, the development of electronic equipment has come a long way from large and low power performing devices to advanced devices with smaller sizes and high power densities. In the past few decades, the development of electronic devices has received significant attention in producing smaller, more flexible, and higher power density devices. This includes the development of new materials, tools, processes, and design methodologies [1, 2].

As electronic devices are rapidly shrinking in size while their power density continues to increase, thermal management becomes an increasingly important factor in the development of electronic devices to improve their functionality, performance, and reliability. In most electronic devices, such as transistors, light emitting diodes (LEDs), integrated circuits (ICs), and microprocessors, heat is generated by the flow of an electrical current in the device, where the amount of the generated heat is proportional to the power output of the device.

In many electronic devices, the geometry of the device is considered as a 3D

(a) (b)

Figure 1.1: (a) Schematic layout of a 3D flux channel. (b) A sample of a microelectronic device [4].

flux channel, where heat is generated in the system in one or more small regions. The regions are usually referred to as heat sources, and the generated heat flows by conduction through the system to spread into a convective heat sink, where it is transferred from the system into an ambient fluid, using any of the cooling techniques, as shown in Fig. 1.1. As a result of this process, the temperature excess in the electronic system may rise until it stabilizes at a point where the generated heat in the system is equal to the removed heat from the system [3].

The importance of thermal management in electronic systems has served to push engineers, physicists, and mathematicians to obtain precise thermal behaviors of the developed electronic systems using experimental work, numerical simulations, and by developing analytical solutions for the temperature field. However, among the three techniques, analytical solutions are most advantageous since they are obtained and illustrated in closed forms that can be applied directly to several applications. In addition, analytical solutions are more flexible and practical for optimization studies.

1.2 Objectives

In the modern microelectronics industry, the development of microelectronic systems involves using new anisotropic materials, multilayered structures, different heat-sink structures, and different cooling techniques in manufacturing the electronic systems. In particular, the different heat-sink structures and the different cooling techniques might present a nonuniform heat transfer coefficient along the sink plane. Further, some anisotropic materials with different thermal conductivities in the three spatial directions (orthotropic) have received significant attention in the development of microelectronic systems of single or multilayered structures. In most of these materials, the thermal conductivities are temperature dependent. Hence, the development of analytical solutions for the temperature field of such complex structures becomes more challenging. In most cases, the development of analytical solutions for the temperature distribution in the microelectronic systems requires the employment of some advanced mathematical transformations and techniques. The main objectives of the present work are as follows:

- Develop analytical solutions for the temperature distribution and total thermal resistance of an isotropic 3D flux channel with a nonuniform heat transfer coefficient along the sink plane and study the effect of different heat transfer coefficient distributions on thermal analysis, see Fig. 1.2a.

- Present analytical solutions for the temperature distribution and total thermal resistance of an isotropic 3D flux channel with a temperature-dependent thermal conductivity and study the effect of different temperature-dependent thermal conductivity functions on thermal analysis.

- Develop analytical solutions for the temperature distribution and total thermal resistance of a multilayered 3D flux channel, consisting of N-layers of orthotropic

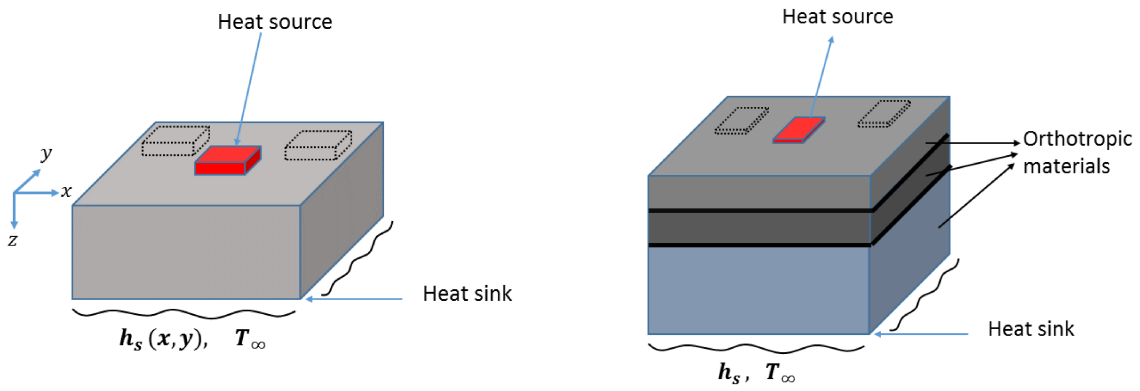

(a) (b)

Figure 1.2: Schematic layout of different 3D flux channels. (a) Single layer with nonuniform convection. (b) Multilayered with uniform convection.

materials with different thermal conductivities in the three spatial directions in each layer and interfacial thermal resistance between the adjacent layers, see Fig. 1.2b.

- Obtain analytical solutions for the temperature distribution and total thermal resistance of a multilayered 3D flux channel consisting of N-layers of temperature-dependent orthotropic thermal conductivities in each layer.

- Verify all the developed analytical solutions by conducting numerical simulations based on the FEM using the ANSYS commercial software package.

1.3 Heat Conduction and Spreading Resistance

1.3.1 Governing Equations

The general heat conduction equation for a stationary solid is given by [5, 6]:

$$\rho c_p \frac{\partial T}{\partial t} = \nabla \cdot (\bar{\bar{k}}\, \nabla T) + \dot{g}, \tag{1.1}$$

where ρ is the material density, c_p is the specific heat constant, $\dot{g}$ is the internal heat generation rate per unit volume, and $\bar{\bar{k}}$ is the thermal conductivity tensor of the material. In the steady-state case with no internal generation, the general heat conduction equation reduces to:

$$\nabla \cdot (\bar{\bar{k}} \, \nabla T) = 0. \tag{1.2}$$

The thermal conductivity of the medium is presented in tensor form and is kept included within the divergence operator $(\nabla\cdot)$ to account for anisotropic materials and temperature-dependent thermal conductivity relationships. The general form of the thermal conductivity tensor $\bar{\bar{k}}$ is considered as a second-order tensor that involves nine components given by [5, page 615]:

$$\bar{\bar{k}} = \begin{bmatrix} k_{11} & k_{12} & k_{13} \\ k_{21} & k_{22} & k_{23} \\ k_{31} & k_{32} & k_{33} \end{bmatrix}, \tag{1.3}$$

where $\{k_{ij}\}_{i,j=1}^{3}$ are the conductivity coefficients with i, j corresponding to the three Cartesian coordinates x, y, and z, i.e., $x \equiv 1, y \equiv 2, z \equiv 3$. Moreover, the conductivity coefficients k_{ij} might be constants or presented as temperature-dependent functional relationships, i.e., $k_{ij} = k_{ij}(T)$, depending on the material's properties. Furthermore, when the off-diagonal elements of the conductivity tensor matrix vanish, i.e., $k_{ij} = 0$ for $i \neq j$, the system is called orthotropic and the conductivity tensor matrix becomes:

$$\bar{\bar{k}} = \begin{bmatrix} k_{11} & 0 & 0 \\ 0 & k_{22} & 0 \\ 0 & 0 & k_{33} \end{bmatrix} = \begin{bmatrix} k_x & 0 & 0 \\ 0 & k_y & 0 \\ 0 & 0 & k_z \end{bmatrix}, \tag{1.4}$$

and the steady-state conduction equation becomes:

$$\frac{\partial}{\partial x}\left(k_x \frac{\partial T}{\partial x}\right) + \frac{\partial}{\partial y}\left(k_y \frac{\partial T}{\partial y}\right) + \frac{\partial}{\partial z}\left(k_z \frac{\partial T}{\partial z}\right) = 0. \tag{1.5}$$

Moreover, in the case of equal diagonal components in the orthotropic system, i.e., $k_x = k_y = k_z = k$, the system is called isotropic and the steady-state heat conduction equation reduces to:

$$\nabla \cdot (k\ \nabla T) = 0, \tag{1.6}$$

which is reduced in the case of constant thermal conductivity to the Laplace equation given by:

$$\nabla^2 T = 0. \tag{1.7}$$

1.3.2 Boundary Conditions

The main linear boundary conditions that may appear on the system's boundaries can be classified into three types:

1. **Boundary conditions of the first type (prescribed temperature or Dirichlet conditions)**.

   This boundary condition is considered when the temperature distribution is specified along the boundary surface as:

   $$T|_{boundary} = T_0, \quad \text{or} \quad T|_{boundary} = f(\hat{r}), \tag{1.8}$$

   where the boundary temperature can be a constant or changing with position according to the function $f(\hat{r})$, where $\hat{r}$ is the position vector ($\hat{r} = (x, y, z)$).

2. **Boundary conditions of the second type (prescribed heat flux or Neumann conditions)**.

   This boundary condition is considered when the heat flux is specified along the boundary surface as:

$$k_n \frac{\partial T}{\partial n}\bigg|_{boundary} = q, \quad \text{or} \quad k_n \frac{\partial T}{\partial n}\bigg|_{boundary} = g(\hat{r}), \tag{1.9}$$

   where $\partial/\partial n$ denotes the derivative along the outward normal at the boundary surface and k_n is the normal thermal conductivity component. The heat flux at the boundary surface can be a constant or changing with position according to the function $g(\hat{r})$. As a special case, when no heat flow enters or leaves the system though the boundary surface, the surface is called adiabatic or perfectly insulated, i.e.,

$$\frac{\partial T}{\partial n}\bigg|_{boundary} = 0. \tag{1.10}$$

3. **Boundary conditions of the third type (convection or Robin conditions)**.

   This boundary condition is considered when the heat is transferred from a conductive medium into a surrounding ambient fluid, defined by:

$$-k_n \frac{\partial T}{\partial n}\bigg|_{boundary} = h_s(T|_{boundary} - T_\infty), \tag{1.11}$$

   where T_∞ is a reference temperature of the surrounding ambient fluid and h_s is the heat transfer coefficient which is usually taken as a constant. However, it can be a function of position $h_s(\hat{r})$ with nonuniform values along the boundary surface.

1.3.3 Thermal Spreading Resistance

Thermal resistance is a measurement of a temperature gradient that represents how an object resists a heat flow. In modeling microelectronic devices and cooling systems, the measurement of the thermal resistance plays a significant role in the thermal management of the systems as it gives an index of the effectiveness of the cooling systems, where it is always desirable to minimize the thermal resistance of the system. Thermal spreading resistance (TSR) occurs as heat flows by conduction from a small source to a larger sink with different cross-sectional areas, as shown in Fig. 1.3. Thermal spreading resistance is an increasingly important topic in thermal management of microelectronic systems because, in some cases, it has a large contribution of more than 50% to the total thermal resistance.

For a single heat source spreading heat to a larger extended sink area, the total thermal resistance of the system can be defined as [7, 8]:

$$R_t = \frac{\overline{T}_c - T_\infty}{Q}, \tag{1.12}$$

where $\overline{T}_c$ is the mean temperature over the heat-source area, and Q is the total heat input of the system.

1.4 Methodology

Throughout the thesis, the following mathematical methods, techniques, and transformations are used to obtain the solutions for the temperature distribution and thermal resistance of the different models under study.

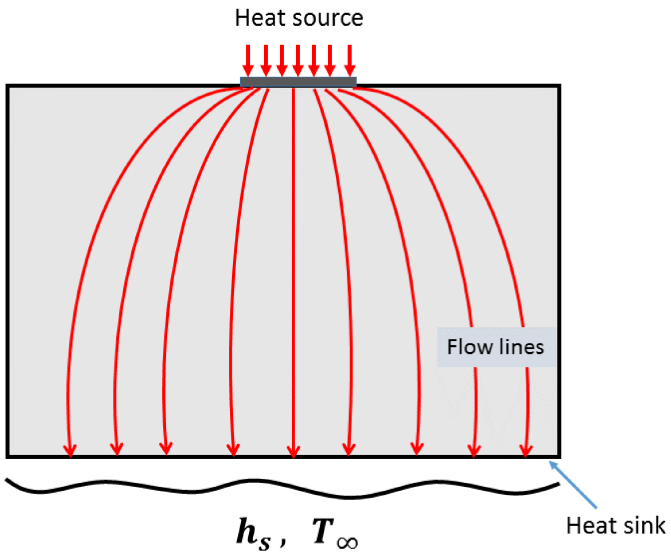

Figure 1.3: Example of spreading heat flow (channel's vertical cross section).

1.4.1 Separation of Variables

Separation of variables is a widely used method in solving linear partial differential equations (PDEs) including the heat equation, the wave equation, and the Helmholtz equation. The main idea of the method of separation of variables is to seek solutions to a PDE represented in the form of products of functions, each of which depends on one variable [9], in which the PDE is separated into ordinary differential equations (ODEs) that can be solved individually. Thereafter, the solutions of the ODEs are used to find the solution of the original PDE [10]. However, the direct application of the method has some requirements on the PDE and the boundary conditions of the system under study. Such requirements include [5]:

- Linear PDE and linear boundary conditions;
- Homogeneous PDE;
- For steady-state problems, all the boundary conditions are homogeneous with

the exception of a single nonhomogeneous boundary condition;

- For transient problems, all the boundary conditions are homogeneous and the initial condition is nonhomogeneous.

If the above requirements are not satisfied, other approaches have to be applied first before using separation of variables, such as the principle of superposition, shifting, splitting the problem, using mathematical transformations, or other mathematical techniques.

The application of the separation of variables method to a linear PDE defined in an orthogonal coordinate system (like, Cartesian, cylindrical, and spherical coordinate systems) can be applied by expressing the dependent variable of the PDE in a separable form of the orthogonal coordinates. For example, when considering the linear steady-state heat conduction equation in the Cartesian coordinate system, represented by the Laplace equation given in Eq. (1.7), the method of separation of variables can be employed to obtain a general series solution of the problem. This solution can be obtained by assuming that the solution will take the following product form:

$$T(x, y, z) = X(x) \cdot Y(y) \cdot Z(z), \tag{1.13}$$

and when substituting this form into the Laplace equation, we can obtain a system of ODEs, each of its equations depends on one variable and separation constants [11]. Moreover, the use of the method of separation of variables reduces the PDE into a system of ODEs that involves the well known Sturm-Liouville problem. The general Sturm-Liouville equation for $u(x)$ defined on the interval $[a, b]$ can be expressed by the following linear homogeneous ODE [10, 12, 13]:

$$\frac{d}{dx}\left[p(x)\frac{du}{dx}\right] + [v(x) + \lambda w(x)]u(x) = 0, \tag{1.14}$$

subject to boundary conditions of the following types:

1. $A_1u(a) + A_2u'(a) = 0, \qquad A_1^2 + A_2^2 > 0,$

2. $B_1u(b) + B_2u'(b) = 0, \qquad B_1^2 + B_2^2 > 0,$

3. $u(a) = u(b)$ and $p(a)u'(a) = p(b)u'(b)$;

4. $u(a)$ and $u'(a)$ are finite with $p(a) = 0$,

5. $u(b)$ and $u'(b)$ are finite with $p(b) = 0$,

where $p(x)$, $v(x)$, $w(x)$, and $p'(x)$ are real-valued continuous functions over $[a, b]$ and $p(x) > 0$ and $w(x) > 0$ over (a, b). The Sturm-Liouville problem is called regular when the boundary conditions associated with Eq. (1.14) are of the first two types and $p(x) > 0$ and $w(x) > 0$ over the bounded interval $[a, b]$, which we are mainly concerned with in this work. The values of λ for which the regular Sturm-Liouville problem has a nontrivial solution are called the eigenvalues, and the corresponding solutions $u(x, \lambda)$ are called the eigenfunctions. A regular Sturm-Liouville problem has an infinite set of real eigenvalues that are arranged in ascending order $\lambda_1 < \lambda_2 < \lambda_3 < \dots$, i.e., $\lambda_i < \lambda_{i+1}$ $(i = 1, 2, 3, \dots)$ and $\lambda_i \to \infty$ as $i \to \infty$ [12, 14]. Moreover, the set of corresponding eigenfunctions $u_i(x, \lambda_i)$ is an orthogonal set with respect to the weighting function $w(x)$, i.e.,

$$\int_a^b u_n(x, \lambda_n)u_m(x, \lambda_m)w(x)dx = \begin{cases} 0, & n \neq m, \\ N(\lambda_n), & n = m, \end{cases} \tag{1.15}$$

where $N(\lambda_n)$ is the norm of the eigenfunction $u_n(x, \lambda_n)$.

When considering the steady-state heat conduction equation given in Eq. (1.7)

(Laplace equation), defined on a 3D finite rectangular domain in the Cartesian coordinate system subject to linear boundary conditions of the types presented in Section 1.3.2 with all homogeneous boundary conditions except one nonhomogeneous boundary condition, the application of the separation of variables method will reduce the PDE into a system of ODEs. This system involves the regular Sturm-Liouville problem in the homogeneous directions of the form:

$$\frac{d^2u}{dx^2} + \lambda u = 0, \qquad a \leq x \leq b, \tag{1.16}$$

with respect to the following boundary conditions:

$$A_1 u(a) + A_2 u'(a) = 0, \qquad A_1^2 + A_2^2 > 0, \tag{1.17}$$

$$B_1 u(b) + B_2 u'(b) = 0, \qquad B_1^2 + B_2^2 > 0. \tag{1.18}$$

This problem has nontrivial solutions for positive values of λ (and $\lambda = 0$ when $A_1 = B_1 = 0$) and the general solutions can be expressed as:

$$u_i(x) = C_i \cos(\sqrt{\lambda_i}x) + D_i \sin(\sqrt{\lambda_i}x), \qquad \text{for positive } \lambda_i, \tag{1.19}$$

$$u_i(x) = C_0 + D_0 x, \qquad \text{for } \lambda_0 = 0 \text{ (when } A_1 = B_1 = 0), \tag{1.20}$$

where the eigenvalues $\{\lambda_i\}_{i=0}^{\infty}$ are obtained based on the specific boundary conditions of the problem, which can be obtained explicitly or can be represented by a transcendental equation $F(\lambda_i) = 0$ [5].

Once the solutions of the ODEs are obtained, the principle of superposition can be used to represent the general solution of the original PDE, where the nonhomogeneous direction boundary conditions are used to find the unknown coefficients in the general solution. It is worth mentioning that the definition of the boundary conditions

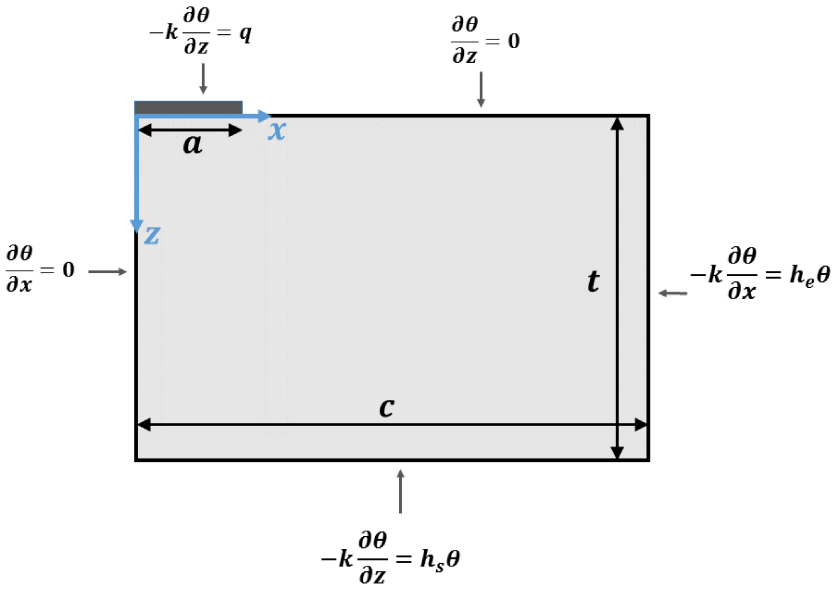

Figure 1.4: Configuration of the 2D flux channel problem.

has a significant effect on the general solution representation. Usually, when these boundary conditions are linear with constant coefficients, the Fourier coefficients in the general series solution can be obtained explicitly by employing the orthogonality of the homogeneous direction eigenfunctions. Moreover, the general solution can be presented as an exact infinite series analytical solution. However, when variable coefficients are present (as we will see in Chapters 2 and 3) in the definition of the boundary conditions, the classical Sturm-Liouville theory might not be applied directly, where approximate analytical solutions, that represent a good approximation to the true solution, are needed in some cases. In order to illustrate this clearly and to distinguish between the exact and approximate solutions that have been adopted in this thesis, we will present the solution procedure for a two-dimensional (2D) flux channel with different boundary conditions.

Consider a 2D rectangular flux channel with a constant heat flux over a part of one end and a convective cooling along the opposite end, as shown in Fig. 1.4. The heat conduction for the temperature excess $\theta = T - T_\infty$ in the flux channel is governed

by Laplace's equation:

$$\nabla^2\theta = \frac{\partial^2\theta}{\partial x^2} + \frac{\partial^2\theta}{\partial z^2} = 0, \tag{1.21}$$

with respect to the following boundary conditions. Along the line $z = 0$, the boundary condition is given by:

$$-k\left.\frac{\partial\theta}{\partial z}\right|_{z=0} = \begin{cases} q, & 0 < x < a \\ 0, & a < x < c. \end{cases} \tag{1.22}$$

Along the two side edges, the boundary conditions are given by:

$$\left.\frac{\partial\theta}{\partial x}\right|_{x=0} = 0, \tag{1.23}$$

$$-k\left.\frac{\partial\theta}{\partial x}\right|_{x=c} = h_e\theta(c, z), \tag{1.24}$$

where h_e is the lateral heat transfer coefficient, which is considered constant. Moreover, the convective-cooling boundary condition along the line $x = c$ can be turned to an adiabatic condition when $h_e \to 0$. Along the line $z = t$, a convective-cooling boundary condition is considered, given by:

$$-k\left.\frac{\partial\theta}{\partial z}\right|_{z=t} = h_s\theta(x, t). \tag{1.25}$$

The sink heat transfer coefficient h_s is of most importance as it plays the major role in removing the heat out of the system. This coefficient might be defined as a constant or as a function of position ($h_s \equiv h_s(x)$), where the two different definitions have significant effects on the representation of the general solution. For the time being, we will consider a constant value of the sink heat transfer coefficient and proceed to the general solution of the problem. The method of separation of variables can be used to obtain the general solution of the problem, where we attempt to determine solutions

in the product form $\theta(x,z) = X(x) \cdot Z(z)$ [6, 11, 15, 16]. Applying the method of separation of variables and using the side boundary conditions (homogenous-direction boundary conditions) yield the following general solution:

$$\theta(x,z) = \sum_{m=1}^{\infty} \cos(\lambda_m x) \left[C_m \cosh(\lambda_m z) + D_m \sinh(\lambda_m z) \right], \tag{1.26}$$

where λ_m are the eigenvalues in the x-direction, which can be obtained by solving the following transcendental equations:

$$\lambda_m \sin(\lambda_m c) = \frac{h_e}{k} \cos(\lambda_m c), \qquad m = 1, 2, \ldots, \tag{1.27}$$

C_m and D_m are the Fourier coefficients. The following result is obtained for the Fourier coefficients when the sink boundary condition is applied (Eq. (1.25)):

$$D_m = -\phi_m C_m, \tag{1.28}$$

where ϕ_m is the spreading function defined by:

$$\phi_m = \frac{\lambda_m \tanh(\lambda_m t) + [h_s/k]}{\lambda_m + [h_s/k] \tanh(\lambda_m t)}. \tag{1.29}$$

Thus, the general solution can be rewritten as:

$$\theta(x,z) = \sum_{m=1}^{\infty} C_m \cos(\lambda_m x) \left[\cosh(\lambda_m z) - \phi_m \sinh(\lambda_m z) \right]. \tag{1.30}$$

Finally, the nonhomogenous boundary condition, given in Eq. (1.22), is used to find

the Fourier coefficients C_m by taking Fourier series expansions of the boundary condition and using the orthogonality of the eigenfunctions to get:

$$C_m = \frac{q}{k\lambda_m \phi_m} \frac{\int_0^a \cos(\lambda_m x)\, dx}{\int_0^c \cos^2(\lambda_m x)\, dx} = \frac{2q \sin(\lambda_m a)}{ck\lambda_m^2 \phi_m}, \tag{1.31}$$

which completes the representation of the general solution as an exact infinite series analytical solution. On the other hand, when the sink heat transfer coefficient is defined as a function of position ($h_s(x)$), the general solution of problem can not be represented as an exact infinite series analytical solution anymore since the classical representation of the infinite Fourier series solution is violated. This can be seen clearly when we employ the sink boundary condition to find a relationship between the Fourier coefficients C_m and D_m, where the relationship represented by the spreading function becomes a function of x as:

$$\phi_m = \phi_m(x) = \frac{\lambda_m \tanh(\lambda_m t) + [h_s(x)/k]}{\lambda_m + [h_s(x)/k] \tanh(\lambda_m t)}, \tag{1.32}$$

and this violates the assumptions of the separation of variables methodology as the Fourier coefficients are no longer constants. However, an approximate solution of the problem can be constructed based on the separation of variables methodology. This approximate solution might be constructed as:

$$\theta(x,z) = \sum_{m=1}^{M} C_m \cos(\lambda_m x) \left[\cosh(\lambda_m z) - \phi_m(x) \sinh(\lambda_m z)\right], \tag{1.33}$$

This solution is constructed by following a similar technique to some variational calculus methods that usually used for obtaining approximate solutions, like the Ritz method and the Kantorovich method [15, 17], in which a general form of an approximate solution is constructed with unknown coefficients or functions that are usually

determined using variational calculus. However, in our solution, we apply the method of least squares to find the unknown Fourier coefficients C_m with an extension to 3D problems, as we will see in Chapters 2 and 3.

1.4.2 Least Squares Method

The method of least squares is a widely used method in approximating functions, and it is considered a standard technique in regression analysis, data fitting, and approximating a function by a combination of other functions. Least squares problems can be classified into linear least squares and nonlinear least squares, depending on the general form of the modeling (approximating) function. We will focus on linear least squares, where the modeling function can be expressed as a linear combination of some linearly independent set of functions. For example, a one-dimensional (1D) modeling function can be expressed in the form:

$$\tilde{u}(x, c_1, c_2, \ldots, c_M) = \sum_{j=1}^{M} c_j \varphi_j(x), \tag{1.34}$$

where $\{c_j\}_{j=1}^{M}$ are the modeling-function parameters to be determined. For discrete data represented by a set of points (x_i, y_i), $i = 1, 2, \ldots, N$, the least squares method can be applied to find the best approximate continuous modeling function $\tilde{u}(x, c_1, c_2, \ldots, c_M)$. The idea behind the method of least squares is to determine the values of the parameters $\{c_j\}_{j=1}^{M}$ such that the modeling function minimizes the sum of the squares of the residuals represented by [18]:

$$I = \sum_{i=1}^{N} r_i^2, \tag{1.35}$$

where r_i is the residual defined by the difference between the ith discrete value y_i and the corresponding value predicted by the modeling function, i.e.,

$$\begin{aligned} r_i &= y_i - \tilde{u}(x_i, c_1, c_2, \ldots, c_M), \\ r_i &= y_i - \sum_{j=1}^{M} c_j \varphi_j(x_i). \end{aligned} \tag{1.36}$$

The modeling-function parameters $\{c_j\}_{j=1}^{M}$ are obtained to minimize the sum of the squared residuals I represented in Eq. (1.35) by setting the gradient of I with respect to the parameters to zero:

$$\frac{\partial I}{\partial c_m} = 2 \sum_{i=1}^{N} r_i \frac{\partial r_i}{\partial c_m} = 0, \qquad m = 1, 2, \ldots, M, \tag{1.37}$$

which leads to the following system:

$$\sum_{j=1}^{M} c_j \left(\sum_{i=1}^{N} \varphi_j(x_i) \varphi_m(x_i) \right) = \sum_{i=1}^{N} y_i \varphi_m(x_i), \qquad m = 1, 2, \ldots, M. \tag{1.38}$$

Equation (1.38) represents a system of m-equations and m-unknown parameters that has to be solved for the parameters $\{c_j\}_{j=1}^{M}$. These equations are called the normal equations for the least squares problem [18, 19].

The same procedure can be used for approximating a continuous function $u(x)$ defined on a bounded interval $[a, b]$ by a linear combination of other functions as defined in (1.34). This can be done by viewing the function $u(x)$ as a vector of infinitely many points. Hence, the sum of the squared residuals can be defined in an integral form as [19]:

$$I = \int_a^b \left[u(x) - \sum_{j=1}^{M} c_j \varphi_j(x) \right]^2 dx, \tag{1.39}$$

and the parameters of the modeling function $\{c_j\}_{j=1}^{M}$ are found to minimize I using [20]:

$$\frac{\partial I}{\partial c_m} = 0, \qquad m = 1, 2, \ldots, M, \tag{1.40}$$

which leads to the following linear system of normal equations, represented by:

$$\sum_{j=1}^{M} c_j \int_a^b \varphi_j(x)\varphi_m(x)dx = \int_a^b u(x)\varphi_m(x)dx, \qquad m = 1, 2, \ldots, M. \tag{1.41}$$

Furthermore, the least squares method can be used, in general, for a multidimensional function $u(\vec{x})$ defined on a bounded domain Ω by considering:

$$I = \int_\Omega \left[u(\vec{x}) - \tilde{u}(\vec{x}, c_1, c_2, \ldots, c_M)\right]^2 d\Omega, \tag{1.42}$$

and following the same procedure for the 1D least squares method.

1.4.3 Stretched Coordinate Transformations

Stretched coordinate transformations are mathematical transformations that can be used to transform a system of governing equations defined on a physical domain into an equivalently convenient system defined on a new logical domain. Under this kind of transformation, the physical domain can be extended or squeezed in one or more directions to obtain the new logical domain, in which the transformed governing equations are presented in a simpler form [21]. We will confine our attention to the use of stretched coordinate transformations for the heat conduction equation of an orthotropic medium. Consider the 3D steady-state heat conduction equation for an orthotropic medium with constant thermal conductivities given by:

$$k_x \frac{\partial^2 T}{\partial x^2} + k_y \frac{\partial^2 T}{\partial y^2} + k_z \frac{\partial^2 T}{\partial z^2} = 0, \tag{1.43}$$

defined on the following rectangular domain:

$$0 < x < c, \qquad 0 < y < d, \qquad 0 < z < t. \tag{1.44}$$

The stretched coordinate transformations can be applied to this system by considering the following new independent variables ζ_1, ζ_2, and ζ_3 defined by [5]:

$$\zeta_1 = x\sqrt{k_0/k_x}, \qquad \zeta_2 = y\sqrt{k_0/k_y}, \qquad \zeta_3 = z\sqrt{k_0/k_z}, \tag{1.45}$$

where k_0 is a reference conductivity. Under these transformations, the heat conduction equation for the orthotropic medium given in Eq. (1.43) is transformed to the following heat conduction equation with isotropic properties:

$$k_0 \left(\frac{\partial^2 T}{\partial \zeta_1^2} + \frac{\partial^2 T}{\partial \zeta_2^2} + \frac{\partial^2 T}{\partial \zeta_3^2} \right) = 0, \tag{1.46}$$

defined on the following transformed logical domain:

$$0 < \zeta_1 < c\sqrt{k_0/k_x}, \qquad 0 < \zeta_2 < d\sqrt{k_0/k_y}, \qquad 0 < \zeta_3 < t\sqrt{k_0/k_z}. \tag{1.47}$$

1.4.4 Kirchhoff Transform

When thermal properties of a material vary with temperature, the general heat conduction equation becomes nonlinear, and the general heat conduction equation for an isotropic medium becomes of the form [16]:

$$\rho(T) c_p(T) \frac{\partial T}{\partial t} = \nabla \cdot (k(T)\ \nabla T) + \dot{g}, \tag{1.48}$$

where $\rho(T)$, $c_p(T)$, and $k(T)$ are temperature dependent. In particular, the thermal conductivity of any material depends on the chemical composition, physical structure, and state of the material. Moreover, it also depends on the temperature variation interval under consideration [6]. In most cases, the thermal conductivity varies with temperature according to some functional relationship, e.g.,

$$k(T) = k_0[1 + \omega T], \tag{1.49}$$

where k_0 is a reference conductivity, and ω is the temperature coefficient of thermal conductivity. When the temperature variation interval under consideration is not too wide or the functional dependency of the thermal conductivity on temperature is not too strong, the variation of thermal conductivity with temperature may be neglected and it can be approximated by a constant [6, 16]. However, when the temperature variation interval is wide or the functional dependency between the thermal conductivity and temperature is quite strong, the assumption of a constant thermal conductivity becomes unacceptable.

The Kirchhoff transform is considered a convenient method for solving nonlinear transient and steady-state heat conduction problems with temperature-dependent properties. However, the method is more attractive for solving steady-state problems, as the method can be used to obtain exact solutions without considering any assumptions or approximations [16]. The idea behind the Kirchhoff transform is to present a new variable as an integral function of the temperature-dependent thermal conductivity, where the nonlinear system can be transformed under the Kirchhoff transform into a linear system in terms of the new variable. Moreover, the linearized system can be solved using existing analytical methods for solving linear problems, after which the solution of the linear system can be transformed back to the solution of the nonlinear

system through the inverse Kirchhoff transform. The original Kirchhoff transform is presented by defining a new dependent variable in the form [15, 16, 22, 23]:

$$U = K\{T\} = \frac{1}{k_0}\int_0^T k(\tau)d\tau, \tag{1.50}$$

where $U \equiv U(T)$, and k_0 is a constant reference conductivity. We will only present the application of the Kirchhoff transform to the nonlinear steady-state problems with no heat generation term, defined by:

$$\nabla \cdot (k(T)\ \nabla T) = 0. \tag{1.51}$$

From Eq. (1.50), we have the following relation [24, 25]:

$$\frac{dU}{dT} = \frac{k(T)}{k_0}. \tag{1.52}$$

Hence, using the result in Eq. (1.52), we get the following relations:

$$\nabla U = \frac{dU}{dT}\nabla T = \frac{k(T)}{k_0}\nabla T, \tag{1.53}$$

$$\nabla^2 U = \frac{1}{k_0}\left[\nabla \cdot (k(T)\ \nabla T)\right]. \tag{1.54}$$

In other words, the nonlinear heat equation given in Eq. (1.51) can be transformed under the Kirchhoff transform defined in Eq. (1.50) to the Laplace linear equation in terms of the new variable U:

$$\nabla^2 U = 0, \tag{1.55}$$

which can be solved using the existing analytical methods for solving linear problems,

provided that the boundary conditions can be transformed into linear boundary conditions. The boundary conditions associated with the problem can be transformed under the Kirchhoff transform according to their types. Now, we will examine the transformation for the different linear types of boundary conditions presented in Section 1.3.2. To illustrate the application of the transformation to the boundary conditions with a practical example, we will assume that the thermal conductivity depends on temperature in the form presented in Eq. (1.49). The boundary conditions can be transformed under the Kirchhoff transform as follows [16]:

1. **Prescribed temperature**.

   For a prescribed temperature boundary condition addressed by:

$$T|_{boundary} = f(\hat{r}), \tag{1.56}$$

   the boundary condition can be transformed directly under the Kirchhoff transform by substituting the function $f(\hat{r})$ into the Kirchhoff integral given in Eq. (1.50), i.e.,

$$U|_{boundary} = \frac{1}{k_0}\int_0^{f(\hat{r})} k(\tau)d\tau = \int_0^{f(\hat{r})} (1+\omega\tau)d\tau = f(\hat{r}) + \frac{\omega}{2}f^2(\hat{r}), \tag{1.57}$$

   which is again a prescribed temperature boundary condition for the new variable U. Moreover, when the temperature along the boundary is considered to be constant, i.e., $f(\hat{r}) = T_0$, the transformed boundary condition is also a constant temperature along the boundary given by:

$$U|_{boundary} = T_0 + \frac{\omega}{2}T_0^2. \tag{1.58}$$

2. **Prescribed heat flux**.

   For a prescribed heat flux boundary condition addressed by:

$$k(T)\frac{\partial T}{\partial n}\bigg|_{boundary} = g(\hat{r}), \tag{1.59}$$

   which is a nonlinear boundary condition, the transformation of this kind of boundary conditions is straightforward, by using the following result:

$$k(T)\frac{\partial T}{\partial n} = k(T)\frac{\partial T}{\partial U}\cdot\frac{\partial U}{\partial n} = k_0\frac{\partial U}{\partial n}. \tag{1.60}$$

   Thus, the transformed boundary condition is addressed by:

$$k_0\frac{\partial U}{\partial n}\bigg|_{boundary} = g(\hat{r}), \tag{1.61}$$

   which is a linear boundary condition for U.

3. **Convection boundary conditions**.

   Although the prescribed temperature and prescribed heat flux boundary conditions can be transformed easily into linear boundary conditions through the Kirchhoff transform for the new variable U, this is not the case, in general, when considering a convection boundary condition of the form:

$$-k(T)\frac{\partial T}{\partial n}\bigg|_{boundary} = h_s(T|_{boundary} - T_\infty), \tag{1.62}$$

   and when the Kirchhoff transform is considered, the boundary condition can be transformed to:

$$-k_0\frac{\partial U}{\partial n}\bigg|_{boundary} = h_s(K^{-1}\{U|_{boundary}\} - T_\infty), \tag{1.63}$$

which is a nonlinear boundary condition, since $K^{-1}\{U\}$ is, in general, a nonlinear function of U. In fact, when convection boundary conditions are present in the problem, the transformed boundary conditions are, in general, nonlinear boundary conditions [16, 22].

1.4.5 Finite Element Method and ANSYS Software

Although the scope of this work is to obtain analytical solutions for the temperature distribution and thermal resistance in various flux channel problems, verifications of the developed analytical solutions have been conducted in comparison with solving the problems numerically based on the FEM using the ANSYS commercial software package. The FEM is a powerful and widely used numerical method for solving initial- and boundary-value problems arising in different real-life problems. The main idea of the FEM is to divide the physical domain of the problem into a finite number of subdomains (elements) for which the solution is approximated over these subdomains based on some basis functions using the variational or weighted residual methods [26–28]. The ability to discretize complex and irregular domains and the flexibility of refining the grid in regions of interest with the FEM make the method an attractive analysis tool for many problems.

Solving practical problems using the FEM requires either the development of an FEM computer program or the use of available FEM software products, packages, and libraries. ANSYS is a finite element analysis software used to simulate a wide variety of engineering disciplines including fluid dynamics and thermal analysis. The software has been developed extensively over the past few decades to include several physical phenomena and to improve the power of solving complex systems. Nowadays, ANSYS with its user friendly interface (Workbench) is considered one of the most trusted and widely used numerical simulation software packages [28, 29].

In thermal analysis simulations, the construction of the solution using the ANSYS software can be summarized by the following three steps [28]:

1. **Preprocessing**.

   The first step corresponds to the model generation process, in which the geometry of the problem is determined and the material properties are defined. Moreover, the finite element mesh is generated in this step, where many options can be specified within the meshing generation process such as element type, mesh refinement regions, real constants required by the element type, etc.

2. **Solution Processing**.

   In this step, the boundary conditions of the problem are specified along the geometry boundaries and the solution can be obtained.

3. **Postprocessing**.

   In this step, the results are reviewed and can be exported into result files in tabular format which can be used for data analysis purposes.

1.5 Thesis Organization

This thesis is presented in a manuscript (research paper) format. It contains seven chapters including five chapters that are published (3), accepted (1), and submitted (1) to international peer-reviewed journals. In Chapter 1, an introduction and overview is presented. This chapter summarizes the motivations, objectives, and literature review of the problems addressed in this thesis. It also presents the mathematical methods, techniques, and transformations used throughout the thesis to address the

problems under study. Chapter 2 is published in the IEEE Transactions on Components, Packaging and Manufacturing Technology [30]. In this chapter, the temperature distribution and thermal resistance of a 3D flux channel with a nonuniform heat transfer coefficient along the sink plane are modeled and analyzed analytically. The solutions are obtained by using the method of separation of variables combined with the method of least squares. A single concentric heat source is considered in the source plane, while the conductance along the sink plane is modeled by a symmetric 1D conductance function. Chapter 3 is submitted to the ASME-Journal of Heat Transfer. In this chapter, analytical solutions for the temperature distribution and thermal resistance of a 3D flux channel with eccentric heat source and a variable heat transfer coefficient that varies in the two horizontal dimensions are developed by using the method of separation of variables combined with the method of least squares. Chapter 4 is accepted for publication in the AIAA-Journal of Thermophysics and Heat Transfer. In this chapter, analytical solutions for the temperature distribution and thermal resistance of a 3D flux channel with temperature-dependent thermal conductivity are discussed and used to study the effect of the temperature-dependent thermal conductivity on the temperature rise and spreading resistance for different conductivity functions. Chapter 5 is published in the ASME-Journal of Heat Transfer [31]. In this chapter, general analytical solutions for the temperature distribution and thermal resistance of a multilayered orthotropic system are obtained. The system is considered as a compound 3D flux channel consisting of N-layers with different thermal conductivities in the three spatial directions of each layer. A single eccentric heat source is considered in the source plane, while a uniform heat transfer coefficient is considered along the sink plane. The solutions account for the effect of interfacial conductance between the layers and for considering multiple eccentric heat sources in the source plane. Chapter 6 is published in the AIAA-Journal of Thermophysics and

Heat Transfer [32]. In this chapter, analytical solutions for the temperature rise and thermal resistance of a multilayered 3D flux channel with orthotropic temperature-dependent thermal conductivities are addressed by means of the Kirchhoff transform. Chapter 7 summarizes the problems considered in this thesis and presents suggestions for further investigation.

1.6 Literature Review

Thermal analysis and thermal resistance in microelectronic devices have been studied extensively in the past few decades. The significant importance of thermal management in microelectronics has served to put considerable demands on researchers to conduct different analytical, numerical, and experimental studies in the field of thermal analysis. For the analytical studies, which are the scope of this thesis, the geometry of the microelectronic devices is usually considered as a rectangular flux channel or a cylindrical flux tube. A general review of the literature on thermal analysis and thermal spreading resistance shows that several analytical solutions have been developed for obtaining the precise thermal behavior and thermal resistance of different flux channels and flux tubes with different structures.

Kennedy started the research on thermal spreading resistance of cylindrical shaped semiconductor devices [33]. He obtained analytical solutions for the temperature distribution and thermal resistance in a finite flux tube with a constant heat flux over a part of one end and an isothermal-sink boundary condition along the other end. Thereafter, a number of relevant analytical studies have been presented on thermal analysis and thermal spreading/constriction resistance in different systems with finite and semi-infinite domains [7, 8, 34–59].

A general literature review on thermal analysis and thermal spreading resistance

of microelectronics in the past fifty years is discussed in detail in a recent review paper [60]. The authors presented a review of the most important research studies on thermal spreading/constriction resistance in the past five decades starting from the work of Kennedy in 1960 up to the most recent studies. However, in the following subsections, we will describe and focus on some studies that are related directly to the scope of this thesis.

1.6.1 Single-Layer Flux Channels

Different analytical solutions for the temperature field and thermal resistance have been investigated for single-layer flux channels with different aspects. Such aspects include: considering isotropic materials [7, 36–38, 51, 58], anisotropic materials [49, 51, 54, 57], materials with temperature-dependent thermal conductivity [57, 58], concentric heat source [36–38, 49], eccentric heat source [7, 51, 54, 57, 58], single heat source [36–38, 57], multiple heat sources [7, 49, 51, 54, 57, 58], isothermal-sink boundary conditions [37, 57], convective-sink boundary conditons [7, 36, 38, 49–51, 58], and others.

Kadambi and Abuaf started the research on obtaining analytical solutions for the temperature field in 3D finite rectangular flux channels with convective sink for the first time [36]. They obtained analytical solutions for the transient and steady-state temperature field in 2D and 3D rectangular isotropic flux channels with a concentric isoflux heat source, convective sink, and insulated sides. A similar model has been analytically studied by Krane [37], but changes the heat-sink boundary condition to an isothermal boundary condition.

Muzychka et al. [7, 8, 49–53] have done extensive research on different thermal spreading resistance problems, including different geometries, boundaries, and properties. Muzychka et al. [7] developed a general solution for the spreading resistance of

a rectangular eccentric heat source with convective-sink boundary conditions. Their solution accounts for multiple discrete heat sources distributed over the source plane and for compound flux channel structures consisting of two isotropic layers in perfect contact. They extended their solution to account for transversely isotropic and compound systems in [49]. Moreover, Muzychka et al. [51] presented the influence coefficient method as an efficient and convenient method for calculating the temperature field in the source plane for multiple isoflux heat sources in isotropic, transversely isotropic, and compound flux channels.

Ditri [57] studied a single-layer flux channel with orthotropic temperature-dependent thermal conductivities and a fixed-temperature boundary condition along the sink plane. Bagnall et al. [58] studied the temperature rise in problems with temperature-dependent thermal conductivities and convection boundary conditions along the sink plane using the Kirchhoff transform. Gholami and Bahrami [54] obtained analytical solutions for the spreading resistance of a single orthotropic flux channel with different constant thermal conductivities in the three spatial directions (i.e., $k_x \neq k_y \neq k_z$), and discrete inward and outward heat fluxes along both sides of the channel.

Although many analytical studies have been done on different aspects of thermal spreading resistance and thermal management, attention has been focused on problems with a uniform heat transfer coefficient, uniform temperature, and uniform heat flux boundary conditions along the sink plane. Recently, Razavi et al. [61] studied the thermal resistance of a 2D flux channel with nonuniform heat transfer coefficients along the sink plane. However, usually the heat sources are of different dimensions in both horizontal directions compared to the dimensions of the horizontal cross section of the flux channel. Hence, the nature of heat flow is 3D through the flux channel. Moreover, analytical solutions for the temperature field and thermal spreading resistance in flux channels with temperature-dependent thermal conductivities and

convective boundary conditions are limited [58] because of the restricted applicability of the Kirchhoff transform to boundary conditions of the first and second kinds.

1.6.2 Multilayered Flux Channels

In the microelectronics industry, multilayered structures are found extensively, where the microelectronic device/system is manufactured as a compound system of different materials. A variety of analytical studies have been conducted for the temperature field and thermal resistance in multilayered flux channels.

Kokkas [35] studied thermal analysis in multilayered rectangular structures with isotropic materials and isothermal-sink boundary conditions. Bonani and Ghione [56] used the Kirchhoff transform to study a composite medium consisting of two perfectly attached layers with temperature-dependent and piecewise inhomogeneous thermal conductivity. Yovanovich et al. [38] obtained a general analytical solution for the spreading resistance of an isoflux rectangular concentric heat source on a two-layer flux channel with isotropic properties and a convective-sink boundary condition. In Muzychka et al. [7, 49], the authors extended their solution to account for eccentric heat sources and transversely isotropic compound systems.

Recently, Muzychka et al. [8] analytically modeled the thermal spreading resistance of compound transversely isotropic two-layer systems with equal thermal conductivities in the in-plane directions that are different than the through-plane thermal conductivity (i.e., $k_x = k_y \neq k_z$). Bagnall et al. [59] developed an analytical solution for the thermal spreading resistance in multilayered flux channels with isotropic and transversely isotropic properties. Their solution accounts for the effect of the interfacial conductance between the adjacent layers.

Recently, a variety of new materials have emerged in the microelectronics industry with properties superior to Silicon, enabling new devices with extreme performance. Such materials include β-Gallium-oxide (β-Ga_2O_3) [62] and Black Phosphorus (BP) [63], which are acknowledged to have orthotropic thermal conductivity tensors with different thermal conductivities in the three spatial directions. A review of the literature reveals that analytical solutions for the temperature field and thermal resistance of multilayered othrotropic systems with different thermal conductivities in the three spatial directions, i.e., $k_x \neq k_y \neq k_z$ in each layer, have not yet been analyzed.

References

[1] C. J. M. Lasance, "Advances in high-performance cooling for electronics," https://www.electronics-cooling.com/2005/11/advances-in-high-performance-cooling-for-electronics/, 2005.

[2] A. L. Moore and L. Shi, "Emerging challenges and materials for thermal management of electronics," *Mater. Today*, vol. 17, no. 4, pp. 163–174, May 2014.

[3] D. S. Steinberg, *Cooling Techniques for Electronic Equipment.* Hoboken, NJ, USA: Wiley, 1980.

[4] http://www.freiberginstruments.com/branches/microelectronic-industry.html.

[5] D. W. Hahn and M. N. Özisik, *Heat Conduction.* Hoboken, NJ, USA: Wiley, 2012.

[6] S. Kakac and Y. Yener, *Heat Conduction, 3rd ed.* Malabar, FL, USA: Taylor & Francis, 1993.

[7] Y. S. Muzychka, J. R. Culham, and M. M. Yovanovich, "Thermal spreading resistance of eccentric heat sources on rectangular flux channels," *J. Electron. Packag.*, vol. 125, no. 2, pp. 178–185, Jun. 2003.

[8] Y. S. Muzychka, K. R. Bagnall, and E. N. Wang, "Thermal spreading resistance and heat source temperature in compound orthotropic systems with interfacial

resistance," *IEEE Trans. Compon., Packag., Manuf. Technol.*, vol. 3, no. 11, pp. 1826–1841, Nov. 2013.

[9] R. L. Street, *Analysis and Solution of Partial Differential Equations.* Monterey, CA, USA: Brooks/Cole, 1973.

[10] J. W. Dettman, *Mathematical Methods in Physics and Engineering.* New York, NY, USA: McGraw-Hill, 1969.

[11] R. Haberman, *Applied Partial Differential Equations with Fourier Series and Boundary Value Problems.* Upper Saddle River, NJ, USA: Pearson, 2004.

[12] L. Debnath, *Nonlinear Partial Differential Equations for Scientists and Engineers.* New York, NY, USA: Birkhäuser Boston, 2005.

[13] J. D. Logan, *An Introduction to Nonlinear Partial Differential Equations.* Hoboken, NJ, USA: Wiley, 2008.

[14] J. W. Brown and R. V. Churchill, *Fourier Series and Boundary Value Problems.* New York, NY, USA: McGraw-Hill, 2008.

[15] V. Arpaci, *Conduction Heat Transfer.* New York, NY, USA: Addison-Wesley, 1966.

[16] M. N. Özisik, *Boundary Value Problems of Heat Conduction.* Scranton, PA, USA: International Textbook, 1968.

[17] L. V. Kantorovich and V. I. Krylov, *Approximate Methods of Higher Analysis.* Groningen, Netherlands: Noordhoff, 1958.

[18] R. L. Burden and J. D. Faires, *Numerical Analysis, 9th ed.* Boston, MA, USA: Brooks/Cole, 2011.

[19] W. Gautschi, *Numerical Analysis*. New York, NY, USA: Springer, 2012.

[20] R. B. Kelman, "Least squares Fourier series solutions to boundary value problems," *Soc. Ind. Appl. Math.*, vol. 21, no. 3, pp. 329–338, Jul. 1979.

[21] W. Wu, *Computational River Dynamics*. Boca Raton, FL, USA: CRC Press, 2007.

[22] H. S. Carslaw and J. C. Jaeger, *Conduction of Heat in Solids*. UK: Oxford Univ. Press, 1959.

[23] J. H. Knight and J. R. Philip, "Exact solutions in nonlinear diffusion," *J. Eng. Math.*, vol. 8, no. 3, pp. 219–227, Jul. 1974.

[24] L. M. Jiji, *Heat Conduction*. Berlin, Germany: Springer, 2009.

[25] P. Vadasz, "Analytical solution to nonlinear thermal diffusion: Kirchhoff versus Cole-Hopf transformations," *J. Heat Transf.*, vol. 132, no. 12, pp. 121 302–1–121 302–6, Dec. 2010.

[26] J. N. Reddy, *An Introduction to the Finite Element Method*. New York, NY, USA: McGraw-Hill, 1993.

[27] O. C. Zienkiewicz, R. L. Taylor, and J. Z. Zhu, *The Finite Element Method: Its Basis and Fundamentals*. Oxford, UK: Elsevier Butterworth-Heinemann, 2005.

[28] E. Madenci and I. Guven, *The Finite Element Method and Applications in Engineering Using ANSYS*. New York, NY, USA: Springer, 2006.

[29] H. H. Lee, *Finite Element Simulations with ANSYS Workbench 16*. KS, USA: SDC Publications, 2015.

[30] B. Al-Khamaiseh, M. Razavi, Y. S. Muzychka, and S. Kocabiyik, "Thermal resistance of a 3D flux channel with nonuniform heat convection in the sink plane," *IEEE Trans. Compon., Packag., Manuf. Technol.*, 2017, advance online publication. doi:10.1109/TCPMT.2017.2776601.

[31] B. Al-Khamaiseh, Y. S. Muzychka, and S. Kocabiyik, "Spreading resistance in multilayered orthotropic flux channels with different conductivities in the three spatial directions," *ASME-Journal of Heat Transfer*, vol. 140, no. 7, pp. 1–10, 2018, doi:http://doi.org/10.1115/1.4038712.

[32] ——, "Spreading resistance in multilayered orthotropic flux channel with temperature-dependent thermal conductivities," *AIAA-Journal of Thermophysics and Heat Transfer*, vol. 32, no. 2, pp. 392–400, 2018, doi:http://doi.org/10.2514/1.T5337.

[33] D. P. Kennedy, "Spreading resistance in cylindrical semiconductor devices," *J. Appl. Phys.*, vol. 31, no. 8, pp. 1490–1497, 1960.

[34] T. N. Veziroglu and S. Chandra, "Thermal conductance of two dimensional constrictions," in *Prog. Astron. Aeron.*, vol. 21, 1969, pp. 617–620.

[35] A. G. Kokkas, "Thermal analysis of multiple-layer structures," *IEEE Trans. Electron Devices*, vol. Ed-21, no. 11, pp. 674–681, Nov. 1974.

[36] V. Kadambi and N. Abuaf, "An analysis of thermal response for power chip packages," *IEEE Trans. Electron Devices*, vol. 32, no. 6, pp. 1024–1033, Jun. 1985.

[37] M. J. M. Krane, "Constriction resistance in rectangular bodies," *J. Electron. Packag.*, vol. 113, no. 4, pp. 392–396, Dec. 1991.

[38] M. M. Yovanovich, Y. S. Muzychka, and J. R. Culham, "Spreading resistance in isoflux rectangles and strips on compound flux channels," *J. Thermophys. Heat Transf.*, vol. 13, no. 4, pp. 495–500, 1999.

[39] G. Ellison, "Extensions of a closed form method for substrate thermal analyzers to include thermal resistances from source-to-substrate and source-to-ambient," in *7th IEEE Semi-Therm Symp.*, Feb. 1991, pp. 140–148.

[40] ——, "Thermal analysis of microelectric packages and printed circuit boards using an analytic solution to the heat conduction equation," *Adv. Eng. Softw.*, vol. 22, no. 2, pp. 99–111, 1994.

[41] ——, "Thermal analysis of circuit boards and microelectronic components using an analytical solution to the heat conduction equation," in *20th IEEE Semi-Therm Symp.*, Mar. 1996, pp. 144–150.

[42] M. M. Yovanovich, "General expression for constriction resistances due to arbitrary flux distribution at non-symmetric, coaxial contacts," in *AIAA 13th Aerosp. Sci. Meeting*, Pasadena, CA, USA, 1975, pp. 381–396.

[43] ——, "Thermal constriction resistance of contacts on a half-space: Integral formulation," in *AIAA Prog. in Astron. Aeronautics, Radiat. Transf. Thermal Control*, vol. 49, New York, NY, USA, 1976, pp. 397–418.

[44] T. F. Lemczyk and M. M. Yovanovich, "Thermal constriction resistance with convective boundary conditions, part 1: Half-space contacts," *Int. J. Heat Mass Transf.*, vol. 31, no. 9, pp. 1861–1872, 1988.

[45] ——, "Thermal constriction resistance with convective boundary conditions, part 2: Layered half-space contacts," *Int. J. Heat Mass Transf.*, vol. 31, no. 9, pp. 1873–1883, 1988.

[46] M. M. Yovanovich, "Constriction resistance of planar isoflux heat sources within semi-infinite conductors: Image method," in *4th ASME/JSME Thermal Eng. Joint Conf.*, Maui, HI, USA, Mar. 1995, pp. 19–24.

[47] ——, "Thermal resistances of circular source on finite circular cylinder with side and end cooling," *J. Electron. Packag.*, vol. 125, no. 2, pp. 169–177, Jun. 2003.

[48] ——, "Four decades of research on thermal contact, gap and joint resistance in microelectronics," *IEEE Trans. Compon. Packag. Technol.*, vol. 28, no. 2, pp. 182–206, Jun. 2005.

[49] Y. S. Muzychka, M. M. Yovanovich, and J. R. Culham, "Thermal spreading resistance in compound and orthotropic systems," *J. Thermophys. Heat Transf.*, vol. 18, no. 1, pp. 45–51, Jan.-Mar. 2004.

[50] ——, "Influence of geometry and edge cooling on thermal spreading resistance," *J. Thermophys. Heat Transf.*, vol. 20, no. 2, pp. 247–255, 2006.

[51] Y. S. Muzychka, "Influence coefficient method for calculating discrete heat source temperature on finite convectively cooled substrates," *IEEE Trans. Compon. Packag. Technol.*, vol. 29, no. 3, pp. 636–643, Sep. 2006.

[52] ——, "Spreading resistance in compound orthotropic flux tubes and channels with interfacial resistance," *J. Thermophys. Heat Transf.*, vol. 28, no. 2, pp. 313–319, Mar. 2014.

[53] ——, "Thermal spreading resistance in a multilayered orthotropic circular disk with interfacial resistance and variable heat flux," in *ASME 2015 Int. Tech. Conf. and Exhibition on Packag. and Integ. of Electron. and Photon. Microsys.* San Francisco, California: Paper No. IPACK2015-48243, Jul. 6-9 2015.

[54] A. Gholami and M. Bahrami, "Thermal spreading resistance inside anisotropic plates with arbitrarily located hotspots," *J. Thermophys. Heat Transf.*, vol. 28, no. 4, pp. 679–686, Oct.-Dec. 2014.

[55] A. M. Darwish, A. J. Bayba, and H. A. Hung, "Thermal resistance calculation of AlGaN-GaN devices," *IEEE Trans. Microwave Theory Tech.*, vol. 52, no. 11, pp. 2611–2620, Nov. 2004.

[56] F. Bonani and G. Ghione, "On the application of the Kirchhoff transformation to the steady-state thermal analysis of semiconductor devices with temperature-dependent and piecewise inhomogenous thermal conductivity," *Solid-State Electron.*, vol. 38, no. 7, pp. 1409–1412, 1995.

[57] J. Ditri, "Heat conduction in microwave devices with orthotropic and temperature-dependent thermal conductivity," *IEEE Trans. Microwave Theory Tech.*, vol. 55, no. 3, pp. 555–560, Mar. 2007.

[58] K. R. Bagnall, Y. S. Muzychka, and E. N. Wang, "Application of the Kirchhoff transform to thermal spreading problems with convection boundary conditions," *IEEE Trans. Compon., Packag., Manuf. Technol.*, vol. 4, no. 3, pp. 408–420, Mar. 2014.

[59] ——, "Analytical solution for temperature rise in complex, multilayer structures with discrete heat sources," *IEEE Trans. Compon., Packag., Manuf. Technol.*, vol. 4, no. 5, pp. 817–830, May 2014.

[60] M. Razavi, Y. S. Muzychka, and S. Kocabiyik, "Review of advances in thermal spreading resistance problems," *J. Thermophys. Heat Transf.*, vol. 30, no. 4, pp. 863–879, 2016.

[61] ——, "Thermal resistance in a rectangular flux channel with nonuniform heat convection in the sink plane," *J. Heat Transf.*, vol. 137, no. 11, pp. 111 401–1–111 401–9, Nov. 2015.

[62] M. Higashiwaki, K. Sasaki, A. Kuramata, T. Masui, and S. Yamakoshi, "Development of gallium oxide power devices," *Phys. Status Solidi A*, vol. 211, no. 1, pp. 21–26, 2014.

[63] J. Zhu, J. Y. Chen, H. Park, X. Gu, H. Zhang, S. Karthikeyan, N. Wendel, S. A. Campbell, M. Dawber, X. Du, M. Li, J. P. Wang, R. Yang, and X. Wang, "Revealing the origins of 3D anisotropic thermal conductivities of black phosphorus," *Adv. Electron. Mater.*, vol. 2, no. 5, pp. 1 600 040–1–1 600 040–9, 2016.

Statement of co-authorship

This statement describes the authors' research contributions in the following journal manuscript.

Title: **Thermal Resistance of a 3D Flux Channel with Nonuniform Heat Convection in the Sink Plane**
Located in Chapter 2.

The following people contributed to the conception of this paper:
Author 1: Belal Al-Khamaiseh
Author 2: Dr. Masood Razavi
Author 3: Dr. Yuri S. Muzychka
Author 4: Dr. Serpil Kocabiyik

Belal Al-Khamaiseh was the primary author of this research. He played a major role in developing the analytical solutions, conducting the computational part, analyzing the results, and comparing the analytical results with numerical results for verification purposes. Dr. Masood Razavi contributed to the literature search and the mathematical model of the problem. Dr. Yuri S. Muzychka played a significant role in presenting the idea of the research and together he and Dr. Serpil Kocabiyik contributed to the conception and design of this research. They also guided it's analytical and computational components.

Chapter 2

Thermal Resistance of a 3D Flux Channel with Nonuniform Heat Convection in the Sink Plane

2.1 Introduction

Thermal spreading resistance is an increasingly important topic in thermal management and thermal analysis of mechanical and electronic devices because, in some devices, more than 50% of the total thermal resistance is confined in spreading resistance. Thermal spreading resistance occurs when heat enters the system through a small region and flows by conduction. A proper analysis of the temperature rise and thermal resistance is essential for designing a durable device. For this purpose, different analytical, experimental and numerical methods are used to determine the

Published in the IEEE Transactions on Components, Packaging and Manufacturing Technology [1].

precise thermal behavior of the device. For the analytical methods, the geometry of the device is usually simplified to a rectangular flux channel or a cylindrical flux tube in order to accommodate the Cartesian or cylindrical coordinate systems.

Kennedy [2] began the research on the thermal spreading resistance of cylindrical shaped semiconductor devices. Ellison [3–5] analytically studied the thermal spreading resistance in electronic devices. Yovanovich [6–9] studied different spreading resistance problems for more than forty years. Lemczyk and Yovanovich [10, 11] studied the thermal spreading/constriction resistance in systems with convective boundary conditions. Muzychka et al. [12–14] and Muzychka [15] have done comprehensive research on different aspects of thermal spreading resistance problems including different geometries, boundaries, and properties. Muzychka et al. [12] modeled and obtained a solution for the spreading resistance of rectangular flux channels with eccentric heat sources, adiabatic edges and a uniform heat transfer coefficient along the sink plane. Furthermore, they studied the effects of geometry and edge cooling on thermal spreading resistance [13]. Muzychka [16] developed a computationally efficient method for calculating the temperature of flux channels with discrete heat sources and uniform conductance along the sink plane. Recently, Muzychka et al. [14] analytically modeled the thermal spreading resistance for a two-layer transversely isotropic system with interfacial resistance between the layers. Muzychka [15] also developed a similar model for cylindrical flux tubes. Bagnall et al. [17] studied the effect of temperature-dependent thermal conductivity on the temperature rise in systems with a uniform heat transfer coefficient along the sink plane where the Kirchhoff transform has been used to linearize the heat conduction equation. Moreover, they developed an analytical solution for spreading resistance in multilayered flux channels by finding a recursive formula for solving problems with an arbitrary number of layers [18].

Although many comprehensive studies have been done on different aspects of thermal spreading resistance and thermal management, attention has been focused on problems with a uniform heat transfer coefficient along the sink plane. However, in most devices, the sink configuration is not uniform, which can help in reducing the material and distributing convection cooling based on the temperature distribution along the sink plane where intense cooling is more necessary in high-temperature regions than low-temperature regions, as shown in Fig. 2.1. Recently, Razavi et al. [19] studied the thermal resistance of a two-dimensional (2D) flux channel with nonuniform heat transfer coefficient along the sink plane. However, in most devices, the heat sources are of different dimensions in both the horizontal directions compared to the dimensions of the horizontal cross-sectional of the device, and the heat-source area is much smaller than the cross-sectional area. Hence, the nature of heat flow is three-dimensional (3D) through the flux channel. The aim of this study is to analytically investigate the effect of a nonuniform heat transfer coefficient along the sink plane of a 3D flux channel on thermal resistance. In order to develop analytical solutions for such problems, the method of separation of variables, along with the method of least squares, is used. Then the analytical solution is used to evaluate and study the dimensionless total thermal resistance of different heat-source-size and channel-thickness aspect ratios for different Biot numbers and different conductance distribution profiles along the sink plane.

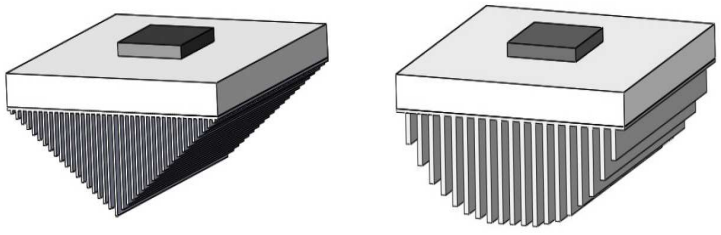

Figure 2.1: Flux channels with a nonuniform heat transfer coefficient.

2.2 Mathematical Theory

In this section, the problem under consideration is modeled and illustrated mathematically where the governing equation of the temperature distribution as well as the boundary conditions are stated, after which the analytical solution of the problem is presented. The total thermal resistance is then presented based on the analytical solution, and the nondimensional total thermal resistance as a function of some aspect ratio factors is then introduced.

2.2.1 Problem Statement

The system under consideration is a 3D rectangular flux channel with a concentric heat source, convective cooling along the lateral edges and a variable heat transfer coefficient along the sink plane, as shown in Fig. 2.2. The system is modeled in Cartesian coordinates such that the origin is at the center of the heat source.

The heat conduction in the flux channel is governed by Laplace's equation:

$$\frac{\partial^2 T}{\partial x^2} + \frac{\partial^2 T}{\partial y^2} + \frac{\partial^2 T}{\partial z^2} = 0, \tag{2.1}$$

or, by defining the temperature excess $\theta = T - T_\infty$:

$$\frac{\partial^2 \theta}{\partial x^2} + \frac{\partial^2 \theta}{\partial y^2} + \frac{\partial^2 \theta}{\partial z^2} = 0, \tag{2.2}$$

with respect to the following boundary conditions based on the configuration shown in Fig. 2.2 and by using the symmetry of the system in the x- and y-directions. Along the source plane, a discrete heat flux is specified over the heat-source region, whereas the area outside the heat-source region is considered as adiabatic. Hence, the source-plane

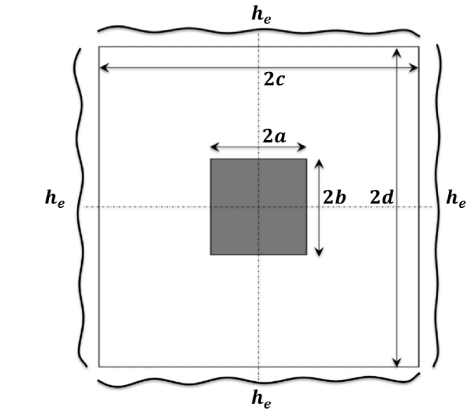

(a)

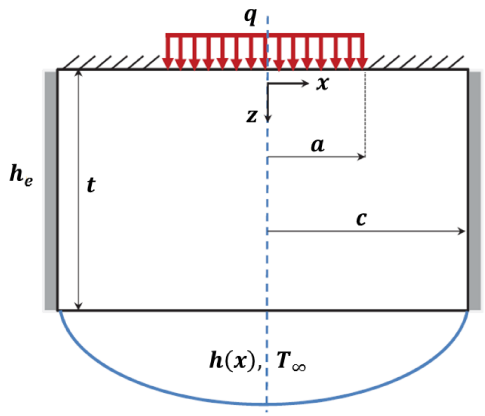

(b)

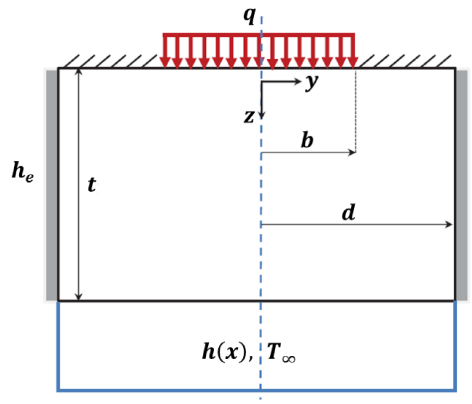

(c)

Figure 2.2: Schematic view of a 3D flux channel layout. (a) Top view. (b) Cross-sectional view in the xz-plane. (c) Cross-sectional view in the yz-plane.

boundary condition is given by:

$$-k \left.\frac{\partial \theta}{\partial z}\right|_{z=0} = \begin{cases} q, & \text{inside source region,} \\ 0, & \text{outside source region.} \end{cases} \tag{2.3}$$

Convective cooling boundary conditions are taken along the lateral edges of the system. However, since the symmetry of the system is considered, only a quarter model is required to be solved; therefore, the boundary conditions along the planes $x = c$ and $y = d$ are given by:

$$\left.\frac{\partial \theta}{\partial x}\right|_{x=c} = -\frac{h_e}{k}\theta(c, y, z), \tag{2.4}$$

$$\left.\frac{\partial \theta}{\partial y}\right|_{y=d} = -\frac{h_e}{k}\theta(x, d, z). \tag{2.5}$$

These convective cooling boundary conditions can be turned to adiabatic conditions when $h_e \to 0$. The boundary conditions along the center planes of the system ($x = 0$ and $y = 0$) are as follows:

$$\left.\frac{\partial \theta}{\partial x}\right|_{x=0} = 0, \qquad \left.\frac{\partial \theta}{\partial y}\right|_{y=0} = 0. \tag{2.6}$$

Along the sink plane, a variable heat transfer coefficient varying in the x-direction exists, and the boundary condition is given by:

$$\left.\frac{\partial \theta}{\partial z}\right|_{z=t} = -\frac{h(x)}{k}\theta(x, y, t). \tag{2.7}$$

To define the variable heat transfer coefficient $h(x)$, a modeling function changing in the x-direction is used to define a wide variety of different conductance distributions

along the sink plane:

$$h(x) = h_0 \left[1 - \left(\frac{x}{c}\right)^p\right], \tag{2.8}$$

where h_0 is a reference conductance representing the maximum heat transfer coefficient in the central region of the sink plane (when $x = 0$). To change the configuration of the conductance along the sink plane, the power in the sink-conductance function p has to be changed. Different conductance profiles can be obtained by changing the value of the power p, which would vary the conductance profile from intense cooling in the central region for $p < 1$, a linear profile when $p = 1$ or a parabolic profile for $p = 2$ up to uniform conductance when $p \to \infty$. It is clear from Eq. (2.8) that the total conductance (averaged along the sink plane) depends on the value of p, while the maximum conductance in the central region h_0 is the same for all values of p. However, it is more appropriate and meaningful to present the system with a constant total conductance for all values of p in order to study the effect of the different conductance distributions with the same total conductance. This can be done by integrating and averaging the conductance in Eq. (2.8) over half of the flux channel and then presenting h_0 in terms of the total averaged conductance $\bar{h}_s$:

$$\bar{h}_s = \frac{1}{c}\int_0^c h(x)dx = \frac{p\ h_0}{p+1}. \tag{2.9}$$

Hence, the conductance function in Eq. (2.8) can be rewritten as:

$$h(x) = \frac{(p+1)\ \bar{h}_s}{p}\left[1 - \left(\frac{x}{c}\right)^p\right]. \tag{2.10}$$

Figure 2.3 shows different nonuniform heat transfer coefficient distributions along the sink plane for different values of the parameter p with same total averaged conductance as defined in Eq. (2.10).

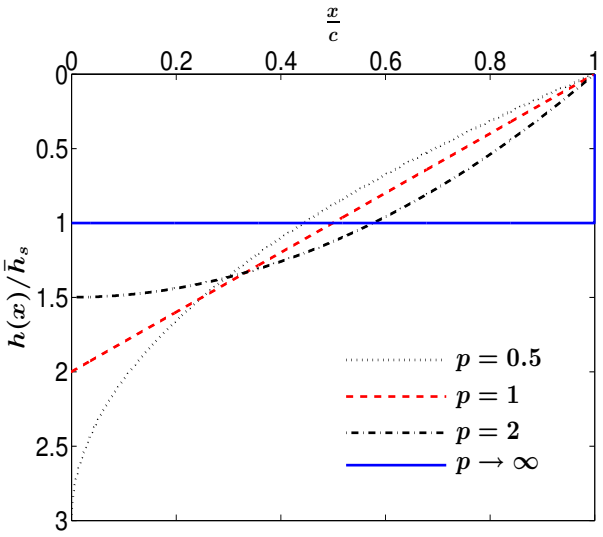

Figure 2.3: Variable heat transfer coefficient function along half of the sink plane for different values of p.

2.2.2 General Solution

The general solution of Laplace's equation given in Eq. (2.2) may be found by using the method of separation of variables, where the solution is assumed to have the form $\theta(x, y, z) = X(x) \cdot Y(y) \cdot Z(z)$ [20–22]. Applying the method of separation of variables and using the boundary conditions along the planes $(x = 0,\ x = c)$ and $(y = 0,\ y = d)$ yield the following general solution:

$$\theta(x, y, z) = \sum_{m=1}^{\infty} \sum_{n=1}^{\infty} \cos(\lambda_m x) \cos(\delta_n y) \left[C_{mn} \cosh(\beta_{mn} z) + D_{mn} \sinh(\beta_{mn} z) \right], \quad (2.11)$$

where λ_m and δ_n are the eigenvalues in the x- and y-directions, respectively, which can be obtained by solving the following transcendental equations numerically:

$$\lambda_m \sin(\lambda_m c) = \frac{h_e}{k} \cos(\lambda_m c), \qquad m = 1, 2, \ldots \quad (2.12)$$

$$\delta_n \sin(\delta_n d) = \frac{h_e}{k} \cos(\delta_n d), \qquad n = 1, 2, \ldots \quad (2.13)$$

whereas β_{mn} is defined by $\beta_{mn} = \sqrt{\lambda_m^2 + \delta_n^2}$. The following result is obtained for the Fourier coefficients when the boundary condition at the sink plane is applied Eq. (2.7):

$$D_{mn} = -\phi_{mn}(x) C_{mn}, \tag{2.14}$$

where $\phi_{mn}(x)$ is the spreading function defined by:

$$\phi_{mn}(x) = \frac{\beta_{mn} \tanh(\beta_{mn} t) + [h(x)/k]}{\beta_{mn} + [h(x)/k] \tanh(\beta_{mn} t)}. \tag{2.15}$$

Thus, the general solution can be rewritten as:

$$\theta(x, y, z) = \sum_{m=1}^{\infty} \sum_{n=1}^{\infty} C_{mn} \cos(\lambda_m x) \cos(\delta_n y) \left[\cosh(\beta_{mn} z) - \phi_{mn}(x) \sinh(\beta_{mn} z)\right]. \tag{2.16}$$

Finally, the boundary condition at the source plane given by Eq. (2.3) is considered in order to find the Fourier coefficients C_{mn}. Usually, when solving flux channel problems with a constant heat transfer coefficient, the Fourier coefficients are obtained directly by taking the Fourier series expansions of the boundary condition at the source plane ($z = 0$) and using the orthogonality of the eigenfunctions. However, since the heat transfer coefficient $h(x)$ depends on the variable x and so does the spreading function $\phi_{mn}(x)$, then the use of the orthogonality of the eigenfunctions in the x-direction is prevented when following the same procedure for the constant heat transfer coefficient. Instead, the method of least squares is used to obtain the Fourier coefficients C_{mn}. The general approximate solution for finite M, N can be written as:

$$\theta(x, y, z) = \sum_{m=1}^{M} \sum_{n=1}^{N} C_{mn} \cos(\lambda_m x) \cos(\delta_n y) \left[\cosh(\beta_{mn} z) - \phi_{mn}(x) \sinh(\beta_{mn} z)\right]. \tag{2.17}$$

The method of least squares can be applied to the general solution given in Eq. (2.17).

Hence, the following integral (which represents the residual) is defined:

$$I_{MN} = \int_0^c \int_0^d \left[- \left. \frac{\partial \theta}{\partial z} \right|_{z=0} - \ S(x,y) \right]^2 dydx, \tag{2.18}$$

where $S(x,y)$ is the function defining the boundary condition at the source plane given by:

$$S(x,y) = \begin{cases} q/k, & 0 < x < a \ \text{ and } \ 0 < y < b \\ 0, & a < x < c \quad \text{or} \quad b < y < d. \end{cases} \tag{2.19}$$

The first derivative of the general solution Eq. (2.17) with respect to z at the source plane (at $z = 0$) is:

$$\left. \frac{\partial \theta}{\partial z} \right|_{z=0} = - \sum_{m=1}^{M} \sum_{n=1}^{N} C_{mn} \beta_{mn} \phi_{mn}(x) \cos(\lambda_m x) \cos(\delta_n y). \tag{2.20}$$

Hence, the residual integral in Eq. (2.18) can be rewritten as:

$$I_{MN} = \int_0^c \int_0^d \left[\sum_{m=1}^{M} \sum_{n=1}^{N} C_{mn} \beta_{mn} \phi_{mn}(x) \cos(\lambda_m x) \cos(\delta_n y) - S(x,y) \right]^2 dydx. \tag{2.21}$$

The Fourier coefficients are obtained to minimize the residual I_{MN} by using [23]:

$$\frac{\partial I_{MN}}{\partial C_{ij}} = 0, \qquad i = 1, 2, \ldots, M, \ j = 1, 2, \ldots, N. \tag{2.22}$$

The application of Eq. (2.22) yields:

$$\int_0^c \int_0^d \left[\sum_{m=1}^{M} \sum_{n=1}^{N} C_{mn} \beta_{mn} \phi_{mn}(x) \cos(\lambda_m x) \cos(\delta_n y) - S(x,y) \right] \cdot \phi_{ij}(x) \cos(\lambda_i x) \cos(\delta_j y) \ dydx = 0. \tag{2.23}$$

Equation (2.23) can be simplified by using the orthogonality of the eigenfunctions in the y-direction to get:

$$\sum_{m=1}^{M} C_{mj}\beta_{mj} \int_0^c \phi_{mj}(x)\phi_{ij}(x)\cos(\lambda_m x)\cos(\lambda_i x)\,dx = \frac{q\sin(\delta_j b)}{k\delta_j N(\delta_j)} \int_0^a \phi_{ij}(x)\cos(\lambda_i x)\,dx, \tag{2.24}$$

where $N(\delta_j)$ is the norm of the y-direction eigenfunctions which depends on the specific nature of the y-direction eigenvalues:

$$N(\delta_j) = \int_0^d \cos^2(\delta_j y)\,dy = \frac{1}{2}\left[d + \frac{h_e/k}{\delta_j^2 + (h_e/k)^2}\right]. \tag{2.25}$$

Thus, in order to find the Fourier coefficients C_{ij}, a linear system has to be solved for every j (i.e., for every eigenvalue in the y-direction). The linear system is as follows:

$$\mathbf{A}^j\mathbf{C}^j = \mathbf{b}^j, \tag{2.26}$$

where $\mathbf{A}^j = [a_{im}^j]$ is an $M \times M$ matrix whose entries (represented by row i and column m) are given by:

$$a_{im}^j = \beta_{mj} \int_0^c \phi_{mj}(x)\phi_{ij}(x)\cos(\lambda_m x)\cos(\lambda_i x)\,dx. \tag{2.27}$$

$\mathbf{C}^j = [C_{1j}\ \ C_{2j}\ \ \ldots\ \ C_{Mj}]^t$ is the unknown Fourier coefficients vector, and $\mathbf{b}^j = [b_1^j\ \ b_2^j\ \ \ldots\ \ b_M^j]^t$ represents the right-hand-side vector whose components are given by:

$$b_i^j = \frac{q\sin(\delta_j b)}{k\delta_j N(\delta_j)} \int_0^a \phi_{ij}(x)\cos(\lambda_i x)\,dx. \tag{2.28}$$

It is important to note that the full set of Fourier coefficients C_{ij} can be obtained

by solving N-linear systems using any mathematical software package (for example, MATLAB) in which numerical integration is used to evaluate the entries of each system.

2.2.3 Total Thermal Resistance

For a single heat source spreading heat to a larger extended sink area, the total thermal resistance of the system can be defined as [18, 24]:

$$R_t = \frac{\overline{T}_c - T_\infty}{Q} = \frac{\bar{\theta}_c}{Q}, \tag{2.29}$$

where $\overline{T}_c$ is the mean temperature over the heat-source area, $\bar{\theta}_c$ is the mean heat-source temperature excess, and $Q = 4qab$ is the total heat input of the flux channel. The mean source temperature excess is given by:

$$\bar{\theta}_c = \frac{1}{A_c} \iint_{A_c} \theta(x, y, 0)\, dA_c, \tag{2.30}$$

where A_c is the heat-source area. The application of Eq. (2.30) yields:

$$\begin{aligned} \bar{\theta}_c &= \frac{1}{4ab} \int_{-a}^{a} \int_{-b}^{b} \sum_{m=1}^{M} \sum_{n=1}^{N} C_{mn} \cos(\lambda_m x) \cos(\delta_n y)\, dydx \\ &= \frac{1}{ab} \sum_{m=1}^{M} \sum_{n=1}^{N} \frac{C_{mn}}{\lambda_m \delta_n} \sin(\lambda_m a) \sin(\delta_n b). \end{aligned} \tag{2.31}$$

Hence, the total thermal resistance can be obtained by using Eq. (2.29) to get:

$$R_t = \frac{1}{4a^2b^2q} \sum_{m=1}^{M} \sum_{n=1}^{N} \frac{C_{mn}}{\lambda_m\ \delta_n} \sin(\lambda_m a) \sin(\delta_n b). \tag{2.32}$$

2.2.4 Aspect Ratios and Dimensionless Resistance

Before beginning to present and analyze the results of the problem, it is clear that the problem depends on a large number of parameters: the heat-source dimensions $a,\ b$; the cross-sectional dimensions $c,\ d$; the channel thickness t; the thermal conductivity k; the magnitude of the heat flux q; heat transfer coefficient of the lateral edges h_e; and the average heat transfer coefficient at the sink plane $\bar{h}_s$. Thus, it is more convenient to present and study the total thermal resistance in a nondimensional form as a function of some aspect ratios of the channel dimensions and some Biot numbers, which are represented by: the aspect ratio between the heat-source length and the cross-sectional length $\epsilon_x = a/c$, the aspect ratio between the heat-source width and the cross-sectional width $\epsilon_y = b/d$, the aspect ratio between the channel thickness and the cross-sectional length $\tau_x = t/c$, the aspect ratio between the channel thickness and the cross-sectional width $\tau_y = t/d$, the Biot number in the x-direction $Bi_{e,x} = h_e c/k$, the Biot number in the y-direction $Bi_{e,y} = h_e d/k$ and the z-direction Biot number $\overline{Bi}_s = \bar{h}_s t/k$. This can be done by defining the following nondimensional variables:

$$x^* = \frac{x}{c}, \qquad y^* = \frac{y}{d}, \qquad z^* = \frac{z}{t}. \tag{2.33}$$

Hence, the general solution in Eq. (2.17) can be rewritten as:

$$\theta(x^*, y^*, z^*) = \sum_{m=1}^{M}\sum_{n=1}^{N} C_{mn}\cos(\lambda_m^* x^*)\cos(\delta_n^* y^*)\left[\cosh(\beta_{mn}^* z^*) - \phi_{mn}^*(x^*)\sinh(\beta_{mn}^* z^*)\right], \tag{2.34}$$

where $\lambda_m^* = \lambda_m c$ and $\delta_n^* = \delta_n d$ are the dimensionless eigenvalues that can be obtained by solving the following transcendental equations numerically:

$$\lambda_m^* \sin(\lambda_m^*) = Bi_{e,x}\cos(\lambda_m^*), \qquad m = 1, 2, \ldots M$$

$$\delta_n^* \sin(\delta_n^*) = Bi_{e,y} \cos(\delta_n^*), \qquad n = 1, 2, \ldots N \tag{2.35}$$

while β_{mn}^* is defined by $\beta_{mn}^* = \beta_{mn} t = \sqrt{(\lambda_m^* \tau_x)^2 + (\delta_n^* \tau_y)^2}$ and the spreading function $\phi_{mn}^*(x^*)$ is given by:

$$\phi_{mn}^*(x^*) = \frac{\beta_{mn}^* \tanh(\beta_{mn}^*) + Bi_s(x^*)}{\beta_{mn}^* + Bi_s(x^*) \tanh(\beta_{mn}^*)}, \tag{2.36}$$

where

$$Bi_s(x^*) = \overline{Bi}_s \frac{(p+1)}{p} \left[1 - (x^*)^p\right]. \tag{2.37}$$

To find the Fourier coefficients C_{mn} based on the aspect ratio factors, the general equation for the linear systems given in Eq. (2.24) can be written as:

$$\sum_{m=1}^{M} \hat{C}_{mj} \beta_{mj}^* \int_0^1 \phi_{mj}^*(x^*) \phi_{ij}^*(x^*) \cos(\lambda_m^* x^*) \cos(\lambda_i^* x^*)\, dx^* = \frac{\sin(\delta_j^* \epsilon_y)}{\delta_j^* N^*(\delta_j^*)} \int_0^{\epsilon_x} \phi_{ij}^*(x^*) \cos(\lambda_i^* x^*)\, dx^*, \tag{2.38}$$

where

$$N^*(\delta_j^*) = \frac{1}{2} \left[1 + \frac{Bi_{e,y}}{\delta_j^{*2} + Bi_{e,y}^2}\right]. \tag{2.39}$$

It is important to note that in the linear systems included in Eq. (2.38) we solve for the modified Fourier coefficients $\hat{C}_{mn}$, which are related to the actual Fourier coefficient C_{mn} by $\hat{C}_{mn} = C_{mn}/\alpha$, where $\alpha = qt/k$.

Finally, the total thermal resistance R_t is nondimensionalized by using the thermal conductivity k and an intrinsic length scale, which is taken to be $\sqrt{ab}$ (i.e., $\sqrt{A_c}/2$):

$$R_t^* = k\sqrt{ab} R_t. \tag{2.40}$$

Thus, the nondimensional total thermal resistance can be expressed as a function of the aspect ratio factors as follows:

$$R_t^* = \frac{\sqrt{\tau_x \tau_y}}{4(\epsilon_x \epsilon_y)^{3/2}} \sum_{m=1}^{M} \sum_{n=1}^{N} \frac{\hat{C}_{mn}}{\lambda_m^* \delta_n^*} \sin(\lambda_m^* \epsilon_x) \sin(\delta_n^* \epsilon_y). \tag{2.41}$$

2.3 Results and Discussions

In modeling heat-sink cooling systems, it is desirable to minimize the total thermal resistance of the system. We will focus on studying the thermal resistance for flux channels with different conductance profiles along the sink plane as it gives an index of the effectiveness of the heat-sink cooling systems and the results can be useful in thermal design analysis for heat-sink sizing and optimization. In this section, the dimensionless thermal resistance of the 3D flux channel for different aspect ratios and different conductance distribution profiles along the sink plane is calculated and analyzed. First, in order to show the accuracy of the developed analytical solution, a solution validation study is presented in which the analytical solution is compared to results obtained by solving the problem numerically. Second, different parametric studies are then conducted to study the effect of the different conductance distribution profiles along the sink plane on total thermal resistance for different values of the Biot number. Third, a dimensional study is then presented to study the effect of the different conductance profiles on the temperature rise of the flux channel. For the analytical solution results, MATLAB (version 2013b) software is used to carry out the results [25], while the numerical results have been conducted with the finite element method (FEM) using the ANSYS commercial software package [26].

2.3.1 Solution Validation Study

To demonstrate the accuracy and computational efficiency of the developed analytical solution, a test study is conducted and compared to the results obtained by solving the problem numerically with the FEM. The results of the test case study are obtained based on solving a flux channel problem that has the following aspect ratios and properties: $\epsilon_x = \epsilon_y = 0.2$, $\tau_x = \tau_y = 0.1$, $Bi_{e,x} = Bi_{e,y} = 0.5$, and $\overline{Bi}_s = 0.1$. For the variable heat transfer coefficient at the sink plane, a linear profile is considered with $p = 1$. The dimensionless total thermal resistance is calculated and compared both for the analytical and the FEM solutions. The FEM results are obtained with a tetrahedral mesh and the convergence is checked by refining the mesh, especially around the heat-source region. The system with a tetrahedral mesh consisting of 183351 elements converged with three digits of precision for the dimensionless thermal resistance, which is shown in Table 2.1. Regarding the analytical solution results, the number of terms for each summation in Eq. (2.41) is chosen to be the same, $M = N$, and the convergence is checked by increasing the number of terms in the summations. It can be seen from Table 2.1 that with $M = N = 25$, the nondimensional thermal resistance agrees well with the FEM results with an approximately relative error of 0.1% compared to the finest mesh result. Furthermore, increasing the the number of terms in the summations will increase accuracy. For example, with $M = N = 40$, the relative error decreases to approximately 0.03%.

2.3.2 Model Parametric Analysis

In this part, the proposed analytical solution is used to find and analyze the dimensionless total thermal resistance of a 3D flux channel and to study the effect of the different conductance profiles on thermal resistance for different aspect ratios and Biot

FEM		Analytical	
Number of Elements	R_t^*	$M = N$	R_t^*
286	0.258199	5	0.264356
636	0.262854	10	0.269531
9822	0.269025	20	0.270850
49109	0.270851	25	0.271011
183351	0.271153	30	0.271112
282386	0.271214	40	0.271206

Table 2.1: Test study dimensionless thermal resistance for FEM and analytical results

numbers. In order to only consider the effect of the variable heat transfer coefficient along the sink plane, the lateral edges of the channel are assumed to be adiabatic by assigning the x- and y-direction Biot numbers a very small value, which is taken in the rest of this analysis as $Bi_{e,x} = Bi_{e,y} = 0.001$. Hence, the dimensionless thermal resistance is now represented as a function of five parameters: ϵ_x, ϵ_y, τ_x, τ_y, and $\overline{Bi}_s$. First, a flux channel of equal aspect ratios is considered, i.e., $\epsilon_x = \epsilon_y = \epsilon$ and $\tau_x = \tau_y = \tau$. Different variable heat transfer coefficient profiles along the sink plane are considered, including the concave profile $p = 0.5$, the linear profile $p = 1$, the parabolic profile $p = 2$, and the uniform heat transfer coefficient $p \longrightarrow \infty$. The dimensionless thermal resistance is calculated for different values of the Biot number, $\overline{Bi}_s = 0.1,\ 1,\ 5,\ 10$ and with thickness aspect ratio $\tau = 0.1$. For calculating the dimensionless thermal resistance, the number of terms in Eq. (2.41) is taken the same for both the x and y summations, i.e., $M = N$, starting from $M = N = 15$ and then the number of terms is incremented until the following stopping criteria are satisfied

$$\left| \frac{R_t^{*M+1} - R_t^{*M}}{R_t^{*M+1}} \right| \leq 10^{-4}, \tag{2.42}$$

where R_t^{*M+1} represents the dimensionless resistance R_t^* calculated by using $M + 1$ and $N + 1$ terms in the summations. Figures 2.4-2.7 show the dimensionless thermal resistance R_t^* versus the aspect ratio ϵ (ϵ is taken to vary from 0.1 to 1) for the different

Biot numbers. Moreover, the numerical solution results are obtained using the FEM for different values of ϵ to validate the analytical results, where both analytical and FEM results are shown on the same plots. For the FEM numerical results, the results can be obtained by considering any model that satisfies the nondimensional parameters. For example, considering a flux channel model of $a = b = 0.01$ m, $c = d = 0.1$ m, $t = 0.01$ m, $k = 10$ W/m·K, $h_e = 0.1$ W/m^2·K, and $\bar{h}_s = 100$ W/m^2·K will give the same value of the dimensionless thermal resistance if we consider the following different model of $a = b = 0.001$ m, $c = d = 0.01$ m, $t = 0.001$ m, $k = 5$ W/m·K, $h_e = 0.5$ W/m^2·K, and $\bar{h}_s = 500$ W/m^2·K, since both the models have the same nondimensional parameters of $\epsilon = 0.1$, $\tau = 0.1$, $Bi_{e,x} = Bi_{e,y} = 0.001$, and $\overline{Bi}_s = 0.1$. However, we used the first model in our numerical simulations and all the results are obtained by changing the source dimensions a, b and the averaged heat transfer coefficient $\bar{h}_s$ according to the nondimensional parameters. For the analytical results, the number of terms used to satisfy Eq. (2.42) varied approximately between $M = N = 16$ and $M = N = 30$ depending on the aspect ratio value ϵ, the Biot number value $\overline{Bi}_s$ and the conductance distribution profile along the sink plane determined by the value of p. In general, using $M = N = 30$ for all the analytical results is found to be sufficient to satisfy Eq. (2.42) and keep the relative error of less than 0.2% compared to the FEM results, as shown in Table 2.2.

In the set of nondimensional parameters, the nondimensional Biot number $\overline{Bi}_s$ is of particular physical significance as it represents the ratio between the one-dimensional (1D) conduction resistance inside the channel, defined by $t/(kcd)$, and the convection resistance along the sink plane based on the averaged heat transfer coefficient $\bar{h}_s$, given by $1/(\bar{h}_s cd)$.

It can be seen from Figs. 2.4-2.7 that the order of magnitude for the dimensionless thermal resistance decreases by increasing the Biot number, because the Biot number

is defined as $\overline{Bi}_s = \bar{h}_s t/k$ and for a fixed-thickness aspect ratio system with fixed material properties, increasing the Biot number is equivalent to increasing the averaged heat transfer coefficient value $\bar{h}_s$. Hence, more heat can be removed from the system, so the total thermal resistance is decreased. Moreover, the effect of the different conductance profiles along the sink plane on thermal resistance is obvious for the different Biot numbers. In particular, for $\overline{Bi}_s < 5$, the dimensionless thermal resistance depends strongly on the source-size aspect ratio ϵ and the shape of the conductance profile represented by the value of the power p. As seen from Figs. 2.4 and 2.5 when the aspect ratio ϵ has small values, the dimensionless thermal resistance gets smaller by decreasing the value of p. However, for large values of ϵ, the dimensionless thermal resistance gets larger by decreasing the value of p. The reason behind this is that for small aspect ratios ϵ (and small thickness ratio τ), the heat flow will reach the sink plane concentrated in the central area of the sink plane, and by decreasing the value of p, the intense cooling is concentrated in that area as well, which would decrease the thermal resistance. On the other hand, for a large aspect ratio ϵ, the heat flow will constrict to go through the intense cooling area which would increase the effort, and therefore the thermal resistance by decreasing the value of p.

In Fig. 2.4, which shows the dimensionless thermal resistance profiles for $\overline{Bi}_s = 0.1$, one can see the significant difference between the different profiles. For the concave conductance distribution ($p = 0.5$), the profile has the minimum values of the dimensionless thermal resistance when $\epsilon < 0.6$ compared to the other three profiles. For the linear conductance distribution ($p = 1$), the dimensionless thermal resistance profile shows lower values when $\epsilon < 0.7$ compared to using the parabolic conductance distribution ($p = 2$) and the uniform conductance distribution ($p \to \infty$). Moreover, when considering the parabolic conductance distribution ($p = 2$), the dimensionless thermal resistance profile shows lower values when $\epsilon < 0.87$ compared to using the

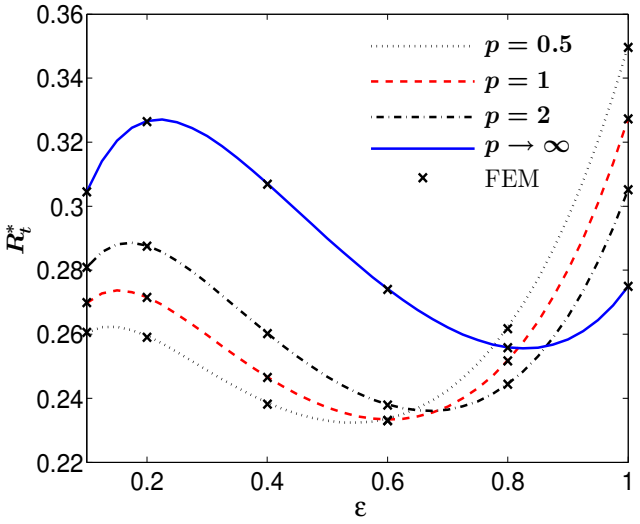

Figure 2.4: Dimensionless thermal resistance for $\overline{Bi}_s = 0.1$ and $\tau = 0.1$.

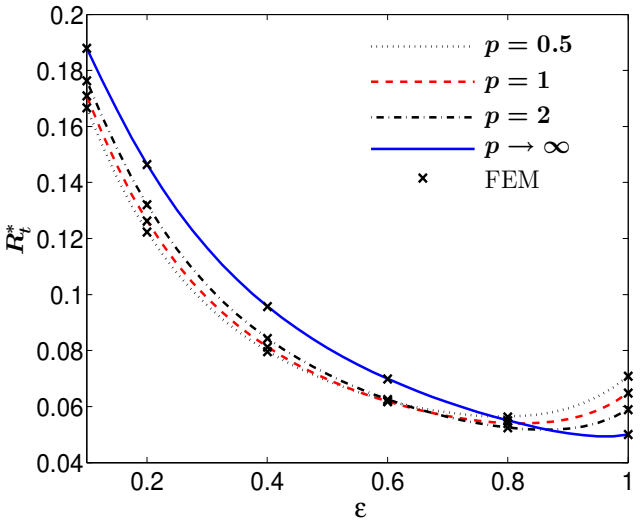

Figure 2.5: Dimensionless thermal resistance for $\overline{Bi}_s = 1$ and $\tau = 0.1$.

uniform conductance distribution. The effect of the different conductance profiles along the sink plane on thermal resistance gets weaker by increasing the value of the Biot number, as shown in Figs. 2.6 and 2.7. One can note from Figs. 2.5-2.7 a sudden increase in the dimensionless thermal resistance for the nonuniform conductance distributions when $\epsilon > 0.8$ compared to using the uniform conductance distribution.

ϵ	R_t^* (Analytical)	R_t^* (FEM)	Relative Error(%)
0.1	0.176285	0.176325	0.03%
0.2	0.132151	0.132038	0.09%
0.4	0.084396	0.084317	0.1%
0.6	0.062567	0.062476	0.15%
0.8	0.052503	0.052424	0.15%
1	0.059053	0.058995	0.1%

Table 2.2: Relative error of dimensionless thermal resistance between analytical and FEM results for $\overline{Bi}_s = 1$, $\tau = 0.1$ and $p = 2$.

The reason behind this is that when considering the uniform conductance distribution with the uniform heat transfer coefficient along the sink plane, as the source-size aspect ratio gets closer to 1, i.e., $\epsilon \to 1$, the heat flow becomes of 1D nature and so does the thermal resistance (spreading resistance gets weaker). However, this is not the case when considering the nonuniform conductance distributions, where the heat flow and the thermal resistance are always multidimensional for all the values of ϵ, and as the source aspect ratio approaches 1, the thermal resistance increases since the cooling is concentrated in the central area of the sink plane for the nonuniform conductance distributions under study. It is important to note that for a fixed p, the behavior (increasing/decreasing intervals) of the dimensionless thermal resistance profile R_t^* with respect to ϵ is not necessarily representing the same behavior for the dimensional thermal resistance profile R_t, since $\sqrt{ab}$ is used to nondimensionalize the thermal resistance and hence the dimensional value of the resistance depends on the value of ϵ.

The effect of the thickness aspect ratio τ on thermal resistance is also studied for the different conductance profiles. Figure 2.8 shows the dimensionless thermal resistance profiles for $\epsilon = 0.2$ and $\overline{Bi}_s = 1$ versus the thickness aspect ratios τ (τ was taken to vary from 0.1 to 2). It can be seen that the behavior of the dimensionless thermal resistance for the different conductance profiles is dependent on the value of

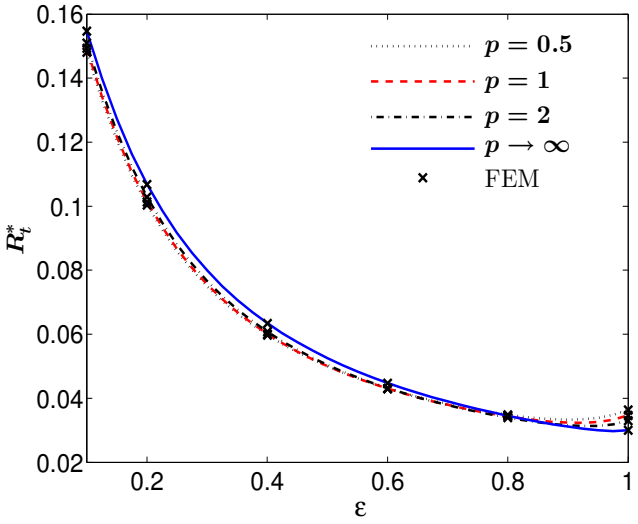

Figure 2.6: Dimensionless thermal resistance for $\overline{Bi}_s = 5$ and $\tau = 0.1$.

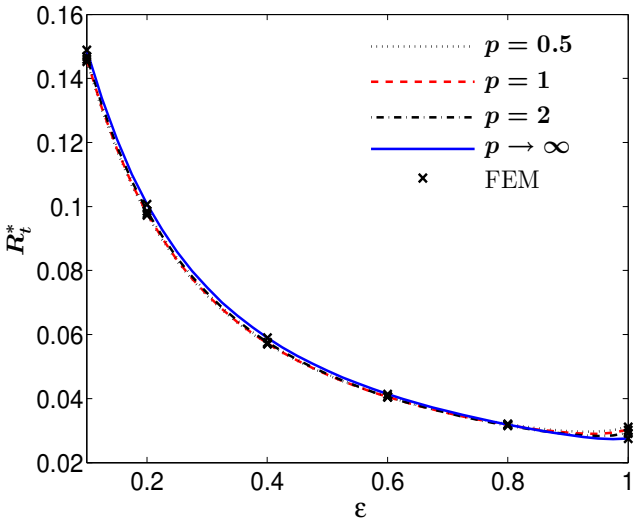

Figure 2.7: Dimensionless thermal resistance for $\overline{Bi}_s = 10$ and $\tau = 0.1$.

the thickness aspect ratio τ, where for $\tau < 0.75$, the dimensionless thermal resistance decreases when the value of p decreases, and this agrees with the previous results shown in Fig. 2.5 for the small source-size aspect ratio ϵ. However, as the thickness aspect ratio becomes larger than 0.75, i.e., $\tau > 0.75$, the dimensionless thermal resistance increases when the value of p decreases. The reason is that for this relatively small fixed value of Biot number $\overline{Bi}_s = 1$, when the thickness aspect ratio gets larger,

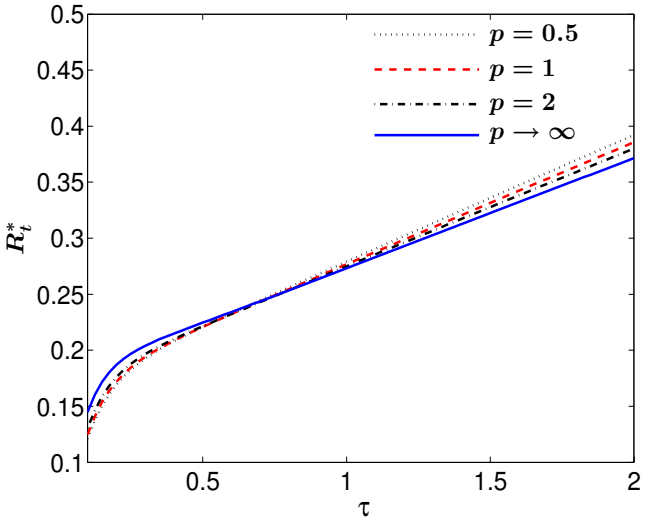

Figure 2.8: Dimensionless thermal resistance for $\overline{Bi}_s = 1$ and $\epsilon = 0.2$.

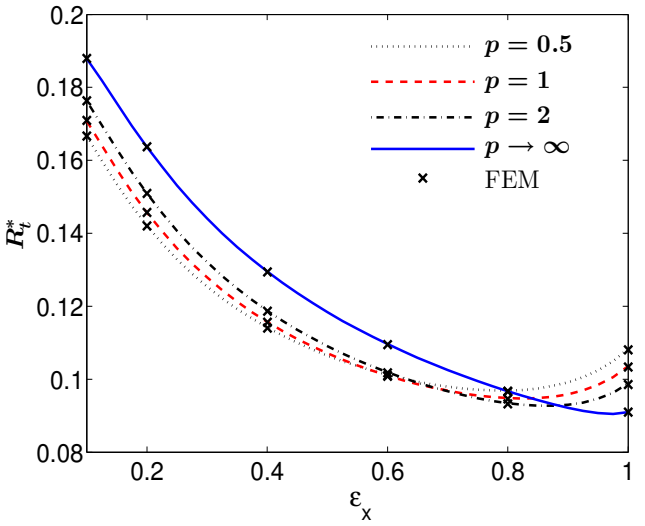

Figure 2.9: Dimensionless thermal resistance for $\epsilon_y = 0.1$, $\tau = 0.1$ and $\overline{Bi}_s = 1$.

the value of the averaged heat transfer coefficient $\bar{h}_s$ gets smaller, and thus the dependency of thermal resistance on the conductance profile becomes stronger, where for smaller values of p, heat flow should constrict to go through the heat sink, and this would increase the thermal resistance.

Furthermore, the effect of changing one of the heat-source-size aspect ratios (ϵ_x or ϵ_y) while fixing the other one is considered. Figure 2.9 shows the dimensionless thermal

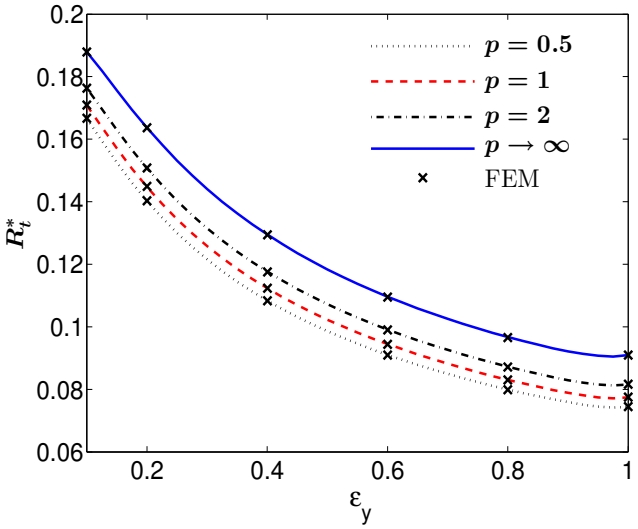

Figure 2.10: Dimensionless thermal resistance for $\epsilon_x = 0.1$, $\tau = 0.1$ and $\overline{Bi}_s = 1$.

resistance profiles for $\tau = 0.1$ and $\overline{Bi}_s = 1$ versus the heat-source-length aspect ratio ϵ_x with a fixed heat-source-width aspect ratio $\epsilon_y = 0.1$. Meanwhile, Fig. 2.10 shows the dimensionless thermal resistance profiles versus the heat-source-width aspect ratio ϵ_y with fixed heat-source-length aspect ratio $\epsilon_x = 0.1$ for the same Biot number and thickness aspect ratio. It is clear from Figs. 2.9 and 2.10 that the effect of changing the length aspect ratio ϵ_x is the one responsible for changing the pattern of the the dimensionless thermal resistance of the different conductance profiles.

In the previous discussion, the dimensionless thermal resistance is studied for flux channels with different properties and parameters. However, the dimensional analytical solution of the temperature distribution presented in Section 2.2.2 can be used to obtain the temperature distribution in the flux channel if desired. A dimensional study is conducted to study the effect of the different conductance distributions on the temperature rise. A 3D square flux channel with side dimensions of $c = d = 0.1$ m and thickness $t = 0.01$ m is considered. The heat-source dimensions are $a = b = 0.02$ m. The thermal conductivity of the system is $k = 10$ W/m·K. A uniform heat flux of $q = 10^4$ W/m^2 is applied in the source region. The conductance along the lateral edges

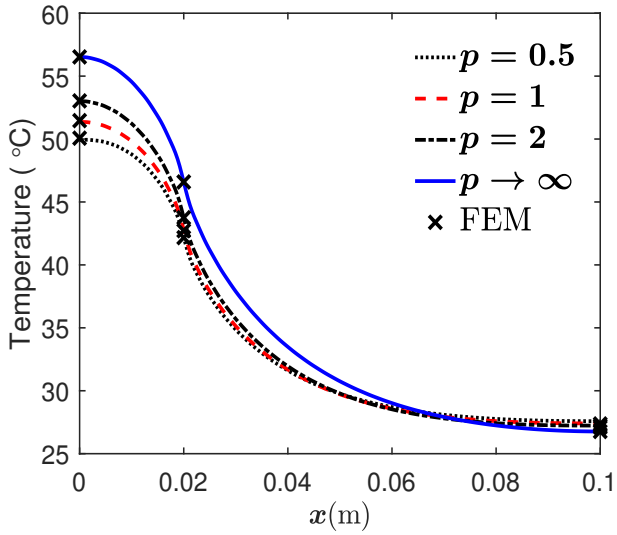

Figure 2.11: Temperature profiles along half of the source plane (along the x-axis when $y = 0$) for the different conductance distributions.

is $h_e = 0.1$ W/m^2·K, and the average conductance along the sink plane is $\bar{h}_s = 100$ W/m^2·K. The ambient temperature is chosen of 25° C. Figure 2.11 shows the source-plane temperature profile along the x-axis when $y = 0$ for the different conductance distributions in which the effect of the different conductance distributions along the sink plane on the temperature rise along the source plane is clear.

2.4 Conclusion

In this chapter, an analytical solution of a 3D flux channel with a nonuniform heat transfer coefficient along the sink plane was presented by using the method of separation of variables combined with the method of least squares. The nonuniform heat transfer coefficient along the sink plane has been modeled by using a conductance function changing in the x-direction, which can define a wide variety of different conductance distributions along the sink plane. The proposed analytical solution was used to find and analyze the dimensionless total thermal resistance, where the thermal

resistance was presented in a nondimensional form as a function of the heat-source-size aspect ratios, channel-thickness aspect ratios, and Biot numbers. The solution was validated by comparing the developed analytical solution results with results obtained by solving the problem numerically using the FEM in which excellent agreement has been observed, and then, the solution was used to study the effect of different conductance distributions on the dimensionless total thermal resistance of the channel and the temperature rise.

References

[1] B. Al-Khamaiseh, M. Razavi, Y. S. Muzychka, and S. Kocabiyik, "Thermal resistance of a 3D flux channel with nonuniform heat convection in the sink plane," *IEEE Trans. Compon., Packag., Manuf. Technol.*, 2017, advance online publication. doi:10.1109/TCPMT.2017.2776601.

[2] D. P. Kennedy, "Spreading resistance in cylindrical semiconductor devices," *J. Appl. Phys.*, vol. 31, no. 8, pp. 1490–1497, 1960.

[3] G. Ellison, "Extensions of a closed form method for substrate thermal analyzers to include thermal resistances from source-to-substrate and source-to-ambient," in *7th IEEE Semi-Therm Symp.*, Feb. 1991, pp. 140–148.

[4] ——, "Thermal analysis of microelectric packages and printed circuit boards using an analytic solution to the heat conduction equation," *Adv. Eng. Softw.*, vol. 22, no. 2, pp. 99–111, 1994.

[5] ——, "Thermal analysis of circuit boards and microelectronic components using an analytical solution to the heat conduction equation," in *20th IEEE Semi-Therm Symp.*, Mar. 1996, pp. 144–150.

[6] M. M. Yovanovich, "General expression for constriction resistances due to arbitrary flux distribution at non-symmetric, coaxial contacts," in *AIAA 13th Aerosp. Sci. Meeting*, Pasadena, CA, USA, 1975, pp. 381–396.

[7] ——, "Thermal constriction resistance of contacts on a half-space: Integral formulation," in *AIAA Prog. in Astron. Aeronautics, Radiat. Transf. Thermal Control*, vol. 49, New York, NY, USA, 1976, pp. 397–418.

[8] ——, "Constriction resistance of planar isoflux heat sources within semi-infinite conductors: Image method," in *4th ASME/JSME Thermal Eng. Joint Conf.*, Maui, HI, USA, Mar. 1995, pp. 19–24.

[9] ——, "Four decades of research on thermal contact, gap and joint resistance in microelectronics," *IEEE Trans. Compon. Packag. Technol.*, vol. 28, no. 2, pp. 182–206, Jun. 2005.

[10] T. F. Lemczyk and M. M. Yovanovich, "Thermal constriction resistance with convective boundary conditions, part 1: Half-space contacts," *Int. J. Heat Mass Transf.*, vol. 31, no. 9, pp. 1861–1872, 1988.

[11] ——, "Thermal constriction resistance with convective boundary conditions, part 2: Layered half-space contacts," *Int. J. Heat Mass Transf.*, vol. 31, no. 9, pp. 1873–1883, 1988.

[12] Y. S. Muzychka, J. R. Culham, and M. M. Yovanovich, "Thermal spreading resistance of eccentric heat sources on rectangular flux channels," *J. Electron. Packag.*, vol. 125, no. 2, pp. 178–185, Jun. 2003.

[13] Y. S. Muzychka, M. M. Yovanovich, and J. R. Culham, "Influence of geometry and edge cooling on thermal spreading resistance," *J. Thermophys. Heat Transf.*, vol. 20, no. 2, pp. 247–255, 2006.

[14] Y. S. Muzychka, K. R. Bagnall, and E. N. Wang, "Thermal spreading resistance and heat source temperature in compound orthotropic systems with interfacial resistance," *IEEE Trans. Compon., Packag., Manuf. Technol.*, vol. 3, no. 11, pp. 1826–1841, Nov. 2013.

[15] Y. S. Muzychka, "Spreading resistance in compound orthotropic flux tubes and channels with interfacial resistance," *J. Thermophys. Heat Transf.*, vol. 28, no. 2, pp. 313–319, Mar. 2014.

[16] ——, "Influence coefficient method for calculating discrete heat source temperature on finite convectively cooled substrates," *IEEE Trans. Compon. Packag. Technol.*, vol. 29, no. 3, pp. 636–643, Sep. 2006.

[17] K. R. Bagnall, Y. S. Muzychka, and E. N. Wang, "Application of the Kirchhoff transform to thermal spreading problems with convection boundary conditions," *IEEE Trans. Compon., Packag., Manuf. Technol.*, vol. 4, no. 3, pp. 408–420, Mar. 2014.

[18] ——, "Analytical solution for temperature rise in complex, multilayer structures with discrete heat sources," *IEEE Trans. Compon., Packag., Manuf. Technol.*, vol. 4, no. 5, pp. 817–830, May 2014.

[19] M. Razavi, Y. S. Muzychka, and S. Kocabiyik, "Thermal resistance in a rectangular flux channel with nonuniform heat convection in the sink plane," *J. Heat Transf.*, vol. 137, no. 11, pp. 111 401–1–111 401–9, Nov. 2015.

[20] V. S. Arpaci, *Conduction Heat Transfer*. New York, NY, USA: Addison-Wesley, 1966.

[21] M. N. Özisik, *Boundary Value Problems of Heat Conduction*. Scranton, PA, USA: International Textbook, 1968.

[22] S. Kakac and Y. Yener, *Heat Conduction, 3rd ed.* Malabar, FL, USA: Taylor & Francis, 1993.

[23] R. B. Kelman, "Least squares Fourier series solutions to boundary value problems," *Soc. Ind. Appl. Math.*, vol. 21, no. 3, pp. 329–338, Jul. 1979.

[24] M. M. Yovanovich, Y. S. Muzychka, and J. R. Culham, "Spreading resistance in isoflux rectangles and strips on compound flux channels," *J. Thermophys. Heat Transf.*, vol. 13, no. 4, pp. 495–500, 1999.

[25] MATLAB Release 2013b, The MathWorks, Inc., Natick, MA, USA, 2013.

[26] ANSYS® Release 16.2, ANSYS, Inc., Canonsburg, PA, USA, 2015.

Statement of co-authorship

This statement describes the authors' research contributions in the following journal manuscript.

Title: **Thermal Resistance of a 3D Flux Channel with Eccentric Source and 2D Variable Heat Convection**
Located in Chapter 3.

The following people contributed to the conception of this paper:
Author 1: Belal Al-Khamaiseh
Author 2: Dr. Yuri S. Muzychka
Author 3: Dr. Serpil Kocabiyik

Belal Al-Khamaiseh was the primary author of this research. He played a major role in constructing the mathematical model of the problem, developing the analytical solutions, conducting the computational part, analyzing the results, and comparing the analytical results with numerical results for verification purposes. Dr. Yuri S. Muzychka played a significant role in presenting the idea of the research and together he and Dr. Serpil Kocabiyik contributed to the conception and design of this research. They also guided it's analytical and computational components.

Chapter 3

Thermal Resistance of a 3D Flux Channel with Eccentric Source and 2D Variable Heat Convection

3.1 Introduction

Thermal management of microelectronic devices is considered as a key factor in the development of microelectronic systems for better performance and device reliability. In most applications, microelectronic systems are modeled as rectangular flux channels, where heat is generated in a small heat-source area and flows by conduction through the system to spread the heat into a larger convective heat-sink area where the generated heat is then transferred into an ambient fluid. The heat convection along the sink plane depends strongly on the sink configuration, where sometimes a nonuniform heat transfer coefficient along the sink plane might be present. For

Submitted to the ASME-Journal of Heat Transfer.

example, when considering nonuniformly distributed extended surfaces with different lengths or a nonuniform nature of the moving ambient fluid, the heat transfer coefficient along the sink plane becomes nonuniform.

Many relevant studies can be found in the literature on thermal analysis of flux channels. In particular, many analytical solutions for the temperature distribution and thermal spreading resistance in flux channels have been studied comprehensively [1–9]. Kadambi and Abuaf [1] obtained analytical solutions for the temperature field in rectangular flux channels. Yovanovich et al. [2] obtained general analytical solutions for temperature field and spreading resistance in compound flux channels. Muzychka et al. [3–7] have conducted comprehensive research on different spreading resistance problems including different geometries, boundaries, and properties. Bagnall et al. [8] obtained analytical solutions for the temperature rise and thermal spreading resistance in multilayered flux channels. However, in most of the existing work, attention has been focused on problems with a uniform heat transfer coefficient along the sink plane. Recently, Razavi et al. [10] studied thermal resistance of a two-dimensional (2D) flux channel with a concentric heat source in the source plane and a nonuniform heat transfer coefficient along the sink plane.

In this chapter, general analytical solutions for the temperature field and thermal resistance of a three-dimensional (3D) flux channel with eccentric heat source and a variable heat transfer coefficient that varies in the two horizontal dimensions are developed by using the method of separation of variables combined with the method of least squares. These solutions can be used to find the optimal configuration of the heat sink for many applications.

3.2 Mathematical Theory

In this section, the mathematical model of the problem under consideration is presented along with the governing equation of the temperature distribution and the appropriate boundary conditions. The analytical solutions for the temperature field and total thermal resistance are then obtained using the method of separation of variables and the method of least squares, in which the two methods are used to construct a mathematical algorithm for finding the Fourier coefficients. Finally, a nondimensional total thermal resistance is introduced in terms of some aspect ratio factors.

3.2.1 Mathematical model

The system under study is a 3D rectangular flux channel in which heat enters the system through an eccentric heat source and flows by conduction to a larger convective heat sink with variable heat transfer coefficient $h(x, y)$ varying in the two horizontal dimensions. The system is modeled in Cartesian coordinates such that the origin is at the left corner of the source plane, as shown in Fig. 3.1.

The steady-state heat conduction equation of the temperature excess $\theta = T - T_\infty$ is governed by Laplace's equation:

$$\frac{\partial^2 \theta}{\partial x^2} + \frac{\partial^2 \theta}{\partial y^2} + \frac{\partial^2 \theta}{\partial z^2} = 0, \tag{3.1}$$

with respect to the following boundary conditions: in the source plane, a uniform heat flux q is specified over the heat-source region, where the heat source is considered as a rectangular shape with dimensions a and b in the x- and y-directions, respectively,

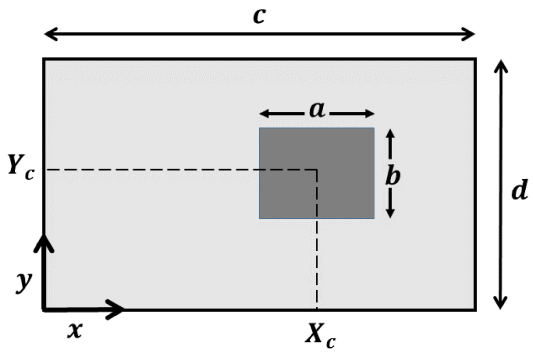

(a)

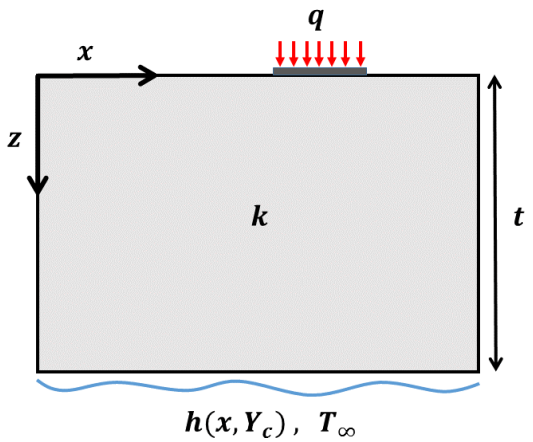

(b)

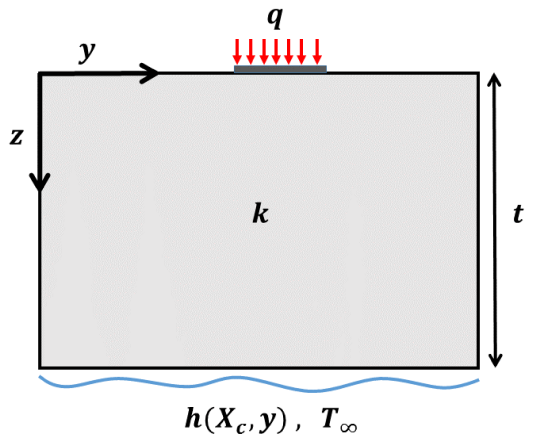

(c)

Figure 3.1: Schematic view of a 3D flux channel layout. (a) Top view. (b) Vertical cross-sectional view in the xz-plane at $y = Y_c$. (c) Vertical cross-sectional view in the yz-plane at $x = X_c$.

while the remainder of the source plane is considered as adiabatic. Hence, the source-plane boundary condition is given by:

$$-k \left.\frac{\partial \theta}{\partial z}\right|_{z=0} = \begin{cases} q, & \text{inside source region,} \\ 0, & \text{outside source region.} \end{cases} \tag{3.2}$$

The lateral edges of the system are assumed to be adiabatic. Thus, the lateral-edge boundary conditions are:

$$\left.\frac{\partial \theta}{\partial x}\right|_{x\,=\,0,\,c} = 0, \qquad \left.\frac{\partial \theta}{\partial y}\right|_{y\,=\,0,\,d} = 0. \tag{3.3}$$

Along the sink plane, a variable heat transfer coefficient varying in the x- and y-directions exists and the boundary condition is addressed by:

$$\left.\frac{\partial \theta}{\partial z}\right|_{z=t} = -\frac{h(x,y)}{k}\theta(x,y,t). \tag{3.4}$$

The variable heat transfer coefficient function $h(x,y)$ might present along the sink plane in different distributions according to the sink configuration when considering a nonuniform distribution of the extended surfaces (fins or bins) or according to a nonuniform nature of the moving ambient fluid over the sink region. Thus, the heat transfer coefficient function depends on the specific problem under study. However, the general solution for the temperature distribution and thermal resistance can be obtained in the same manner for any heat transfer coefficient distribution. In this study, we will consider two heat transfer coefficient distributions that are of opposite nature in distributing the convective cooling along the sink plane, defined by:

$$h_1(x,y) = h_0 \sin\left(\frac{x\pi}{c}\right) \sin\left(\frac{y\pi}{d}\right), \tag{3.5}$$

$$h_2(x,y) = h_0 \left[1 - \sin\left(\frac{x\pi}{c}\right) \sin\left(\frac{y\pi}{d}\right)\right], \tag{3.6}$$

where h_0 is a reference conductance representing the maximum value of the heat transfer coefficient in the sink region. It can be seen that the first distribution function $h_1(x,y)$ has the maximum conductance in the central region of the sink plane and the conductance decreases when moving away from the central region, whereas in the second distribution function $h_2(x,y)$, the maximum value of the conductance is along the sink boundaries and the conductance decreases when moving towards the central region. Figures 3.2 and 3.3 show two samples of flux channels with extended surfaces distributed along the sink plane based on the heat transfer coefficient functions given by Eqs. (3.5) and (3.6). For the purpose of comparing the effect of the different conductance distribution functions on the temperature field and the thermal resistance of the channel, it is more appropriate to present the distributions with the same total average conductance. This can be done by integrating the conductance distributions along the sink plane and finding the average total conductance $\bar{h}_s$ as:

$$\bar{h}_s = \frac{1}{cd} \int_0^c \int_0^d h(x,y) dy dx. \tag{3.7}$$

Hence, the two conductance functions in Eqs. (3.5) and (3.6) can be rewritten to have the same average conductance as:

$$h_1(x,y) = \frac{\pi^2 \bar{h}_s}{4} \sin\left(\frac{x\pi}{c}\right) \sin\left(\frac{y\pi}{d}\right), \tag{3.8}$$

$$h_2(x,y) = \frac{\pi^2 \bar{h}_s}{\pi^2 - 4} \left[1 - \sin\left(\frac{x\pi}{c}\right) \sin\left(\frac{y\pi}{d}\right)\right]. \tag{3.9}$$

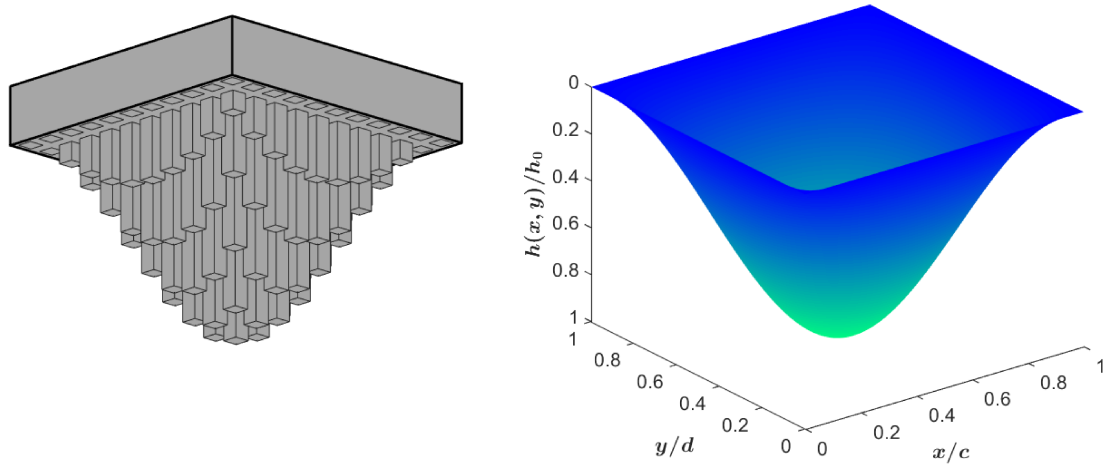

Figure 3.2: Flux channel with $h_1(x, y)$ as the conductance function along the sink plane. Extended surfaces sample (left). Function's surface plot (right).

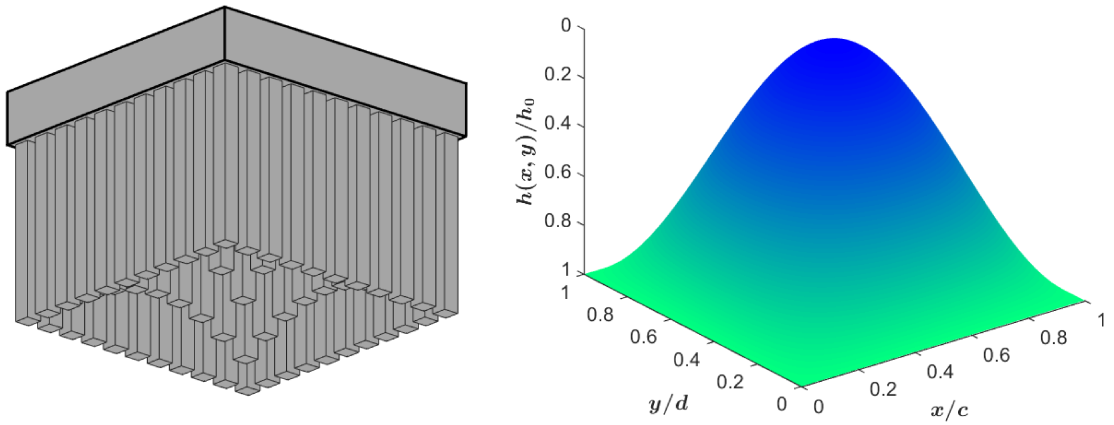

Figure 3.3: Flux channel with $h_2(x, y)$ as the conductance function along the sink plane. Extended surfaces sample (left). Function's surface plot (right).

3.2.2 General Solution

The general solution of temperature excess can be obtained by solving the Laplace equation (3.1) with respect to the set of boundary conditions given in Eqs. (3.2)-(3.4). The method of separation of variables can be used to obtain the general solution in

the form of an infinite Fourier series solution. The solution is assumed to have the form $\theta(x, y, z) = X(x) \cdot Y(y) \cdot Z(z)$ [11–14]. Applying the method of separation of variables and making use of the lateral-edge boundary conditions along the planes ($x = 0$, $x = c$, $y = 0$, and $y = d$) yields the following general solution:

$$\begin{aligned}\theta(x, y, z) = C_{00} + D_{00}z \\ + \sum_{m=1}^{\infty} \cos(\lambda_m x) \left[C_{m0} \cosh(\lambda_m z) + D_{m0} \sinh(\lambda_m z)\right] \\ + \sum_{n=1}^{\infty} \cos(\delta_n y) \left[C_{0n} \cosh(\delta_n z) + D_{0n} \sinh(\delta_n z)\right] \\ + \sum_{m=1}^{\infty} \sum_{n=1}^{\infty} \cos(\lambda_m x) \cos(\delta_n y) \left[C_{mn} \cosh(\beta_{mn} z) + D_{mn} \sinh(\beta_{mn} z)\right], \quad (3.10)\end{aligned}$$

where $\lambda_m = m\pi/c$ and $\delta_n = n\pi/d$ are the eigenvalues in the x- and y-directions, respectively, and $\beta_{mn} = \sqrt{{\lambda_m}^2 + {\delta_n}^2}$ $(m, n > 0)$ are the double Fourier expansion eigenvalues. The relationship between the Fourier coefficients C_{mn} and D_{mn} can be obtained by applying the sink boundary condition in Eq. (3.4), where the following result can be obtained:

$$D_{mn} = -\phi_{mn}(x, y) C_{mn}, \quad (3.11)$$

where $\phi_{mn}(x, y)$ is given by:

$$\phi_{mn}(x, y) = \begin{cases} \dfrac{h(x, y)}{k + h(x, y)t}, & \text{for } m = n = 0, \\ \dfrac{\gamma \tanh(\gamma t) + [h(x, y)/k]}{\gamma + [h(x, y)/k] \tanh(\gamma t)}, & \text{otherwise,} \end{cases} \quad (3.12)$$

where γ refers to any of the corresponding eigenvalues λ_m, δ_n, or β_{mn}.

Finally, the source-plane boundary condition is used to find the Fourier coefficients C_{mn} by means of the method of least squares. The method of least squares is used

to find the Fourier coefficients because of the existence of the variable conductance function $h(x, y)$ in the general solution. The general solution in Eq. (3.10) is presented in an infinite series form; however, in practical applications we consider a finite number of terms to calculate the results provided that the number of terms is sufficient to represent the solution without loss of accuracy. The general approximate solution for finite M and N eigenvalues in the x- and y-directions, respectively, can be rewritten after making use of Eq. (3.11) as:

$$\begin{aligned}\theta(x,y,z) = {} & C_{00}\left[1-\phi_{00}(x,y)z\right] \\ & + \sum_{m=1}^{M-1} C_{m0}\cos(\lambda_m x)\left[\cosh(\lambda_m z) - \phi_{m0}(x,y)\sinh(\lambda_m z)\right] \\ & + \sum_{n=1}^{N-1} C_{0n}\cos(\delta_n y)\left[\cosh(\delta_n z) - \phi_{0n}(x,y)\sinh(\delta_n z)\right] \\ & + \sum_{m=1}^{M-1}\sum_{n=1}^{N-1} C_{mn}\cos(\lambda_m x)\cos(\delta_n y)\left[\cosh(\beta_{mn} z) - \phi_{mn}(x,y)\sinh(\beta_{mn} z)\right].\end{aligned} \tag{3.13}$$

The method of least squares can be applied to the general solution given in Eq. (3.13) by considering the source-plane boundary condition in Eq. (3.2). This can be done by defining the least squares integral [15, 16]:

$$I_{MN} = \int_0^c \int_0^d \left[-\left.\frac{\partial\theta}{\partial z}\right|_{z=0} - S(x,y)\right]^2 dydx, \tag{3.14}$$

where $S(x, y)$ is the function defining the boundary condition at the source plane given by:

$$S(x,y) = \begin{cases} q/k, & \text{inside source region,} \\ 0, & \text{outside source region.} \end{cases} \tag{3.15}$$

To simplify the least squares integral, the first derivative of the general solution in Eq. (3.13) with respect to z at the source plane (at $z = 0$) can be found as:

$$\begin{aligned}\left.\frac{\partial\theta}{\partial z}\right|_{z=0} = & -C_{00}\phi_{00}(x,y) - \sum_{m=1}^{M-1} C_{m0}\lambda_m\phi_{m0}(x,y)\cos(\lambda_m x) \\ & - \sum_{n=1}^{N-1} C_{0n}\delta_n\phi_{0n}(x,y)\cos(\delta_n y) - \sum_{m=1}^{M-1}\sum_{n=1}^{N-1} C_{mn}\beta_{mn}\phi_{mn}(x,y)\cos(\lambda_m x)\cos(\delta_n y).\end{aligned} \tag{3.16}$$

Thus, the least square integral in Eq. (3.14) can be rewritten in a compact form as:

$$I_{MN} = \int_0^c \int_0^d \left[\sum_{m=0}^{M-1}\sum_{n=0}^{N-1} C_{mn}\psi_{mn}(x,y) - S(x,y)\right]^2 dydx, \tag{3.17}$$

where $\psi_{mn}(x,y)$ is the Fourier coefficient's corresponding function given by:

$$\psi_{mn}(x,y) = \begin{cases} \phi_{00}(x,y), & \text{for } m = n = 0, \\ \lambda_m\phi_{m0}(x,y)\cos(\lambda_m x), & \text{for } m \neq 0,\ n = 0, \\ \delta_n\phi_{0n}(x,y)\cos(\delta_n y), & \text{for } m = 0,\ n \neq 0, \\ \beta_{mn}\phi_{mn}(x,y)\cos(\lambda_m x)\cos(\delta_n y), & \text{for } m \neq 0,\ n \neq 0. \end{cases} \tag{3.18}$$

The least squares Fourier coefficients are obtained to minimize the least squares integral I_{MN} using [17, 18]:

$$\frac{\partial I_{MN}}{\partial C_{ij}} = 0, \qquad i = 0, 1, \ldots, M-1,\ j = 0, 1, \ldots, N-1. \tag{3.19}$$

The application of Eq. (3.19) yields:

$$\int_0^c \int_0^d \left[\sum_{m=0}^{M-1} \sum_{n=0}^{N-1} C_{mn} \psi_{mn}(x,y) - S(x,y) \right] \psi_{ij}(x,y) dy dx = 0, \tag{3.20}$$

which can be simplified to:

$$\sum_{m=0}^{M-1} \sum_{n=0}^{N-1} C_{mn} \int_0^c \int_0^d \psi_{mn}(x,y) \psi_{ij}(x,y) dy dx = \frac{q}{k} \int_{X_c - a/2}^{X_c + a/2} \int_{Y_c - b/2}^{Y_c + b/2} \psi_{ij}(x,y) dy dx. \tag{3.21}$$

Equation (3.21) represents a system of MN linear equations, where each equation is obtained by considering different values of i and j for $i = 0, 1, \ldots, M-1$ and $j = 0, 1, \ldots, N-1$. The system of linear equations has to be solved for the Fourier coefficients which can be represented in a matrix form as:

$$\mathbf{AC} = \mathbf{b}, \tag{3.22}$$

where $\mathbf{A}$ is an $MN \times MN$ matrix whose components are represented by definite integrals, which can defined by:

$$\mathbf{A} = \int_0^c \int_0^d \Psi^t(x,y) \Psi(x,y) dy dx, \tag{3.23}$$

where $\Psi(x,y)$ is vector-valued function of MN components given by:

$$\Psi(x,y) = [\psi_{00}\ \psi_{01} \ldots \psi_{0N-1}\ \psi_{10}\ \psi_{11} \ldots \psi_{1N-1} \ldots\ldots \psi_{M-1N-1}], \tag{3.24}$$

$\mathbf{C}$ is the unknown Fourier coefficients vector defined as:

$$\mathbf{C} = [C_{00}\ C_{01} \ldots C_{0N-1}\ C_{10}\ C_{11} \ldots C_{1N-1} \ldots\ldots C_{M-1N-1}]^t, \tag{3.25}$$

and $\mathbf{b}$ is the right-hand-side vector given by:

$$\mathbf{b} = \frac{q}{k} \int_{X_c - a/2}^{X_c + a/2} \int_{Y_c - b/2}^{Y_c + b/2} \Psi^t(x, y) dy dx. \tag{3.26}$$

It is worth mentioning that the linear system matrix $\mathbf{A}$ and the right-hand-side vector $\mathbf{b}$ are presented in the form of definite integrals of a matrix-valued function and vector-valued function, respectively, where the integrals are applied componentwise to the component functions. Thus, numerical integration can be used to evaluate the entries of the linear system using any mathematical software package (e.g., MATLAB) and then the Fourier coefficients C_{mn} can be obtained by solving the resultant linear system.

From the previous discussion, the general solution of the temperature excess θ is illustrated along with a mathematical linear system that has to be solved for the Fourier coefficients. The solution in the source plane $z = 0$ is of most interest for finding the maximum temperature and the total thermal resistance of the flux channel, and is given by:

$$\theta(x, y, 0) = C_{00} + \sum_{m=1}^{M-1} C_{m0} \cos(\lambda_m x) + \sum_{n=1}^{N-1} C_{0n} \cos(\delta_n y) + \sum_{m=1}^{M-1} \sum_{n=1}^{N-1} C_{mn} \cos(\lambda_m x) \cos(\delta_n y). \tag{3.27}$$

3.2.3 Total Thermal Resistance

The total thermal resistance of the system under consideration can be properly defined as [3, 6]:

$$R_t = \frac{\overline{T}_c - T_\infty}{Q} = \frac{\bar{\theta}_c}{Q}, \tag{3.28}$$

where $\overline{T}_c$ and $\bar{\theta}_c$ are the mean temperature over the heat-source area and the mean heat-source temperature excess, respectively, and $Q = abq$ is the total heat flow rate

into the flux channel. The mean source temperature excess is addressed by:

$$\bar{\theta}_c = \frac{1}{A_c} \iint_{A_c} \theta(x, y, 0)\, dA_c = \frac{1}{ab} \int_{X_c - a/2}^{X_c + a/2} \int_{Y_c - b/2}^{Y_c + b/2} \theta(x, y, 0) dy dx. \tag{3.29}$$

The application of Eq. (3.29) to the source-plane solution in Eq. (3.27) yields:

$$\begin{aligned} \bar{\theta}_c = \; & C_{00} + 2 \sum_{m=1}^{M-1} C_{m0} \frac{\cos(\lambda_m X_c) \sin(\frac{1}{2}\lambda_m a)}{a \lambda_m} + 2 \sum_{n=1}^{N-1} C_{0n} \frac{\cos(\delta_n Y_c) \sin(\frac{1}{2}\delta_n b)}{b \delta_n} \\ & + 4 \sum_{m=1}^{M-1} \sum_{n=1}^{N-1} C_{mn} \frac{\cos(\lambda_m X_c) \sin(\frac{1}{2}\lambda_m a) \cos(\delta_n Y_c) \sin(\frac{1}{2}\delta_n b)}{a \lambda_m b \delta_n}. \end{aligned} \tag{3.30}$$

3.2.4 Dimensionless Resistance

As the general expression of the thermal resistance depends on a large number of parameters, it is more appropriate to present the results in a general dimensionless form in terms of some aspect ratio factors. This can be done by considering the following nondimensional variables:

$$x^* = \frac{x}{c}, \qquad y^* = \frac{y}{d}, \qquad z^* = \frac{z}{t}, \tag{3.31}$$

which leads to the following effective nondimensional parameters:

$$\epsilon_x = a/c, \qquad \epsilon_y = b/d, \qquad \tau_x = t/c, \qquad \tau_y = t/d, \qquad \overline{Bi}_s = \bar{h}_s t/k, \tag{3.32}$$

where ϵ_x and ϵ_y are the aspect ratios between the heat-source dimensions and the horizontal cross-sectional dimensions. τ_x and τ_y are the aspect ratios between the channel thickness and the horizontal cross-sectional dimensions in the x- and y-directions, respectively, while $\overline{Bi}_s$ represents the Biot number based on the total average heat transfer coefficient. Thus, the general solution in Eq. (3.13) can be rewritten in terms

of the nondimensional variables as:

$$\begin{aligned}\theta(x^*,y^*,z^*) = \; & C_{00}\left[1-\phi^*_{00}(x^*,y^*)z^*\right] \\ & + \sum_{m=1}^{M-1} C_{m0}\cos(\lambda^*_m x^*)\left[\cosh(\tau_x\lambda^*_m z^*) - \phi^*_{m0}(x^*,y^*)\sinh(\tau_x\lambda^*_m z^*)\right] \\ & + \sum_{n=1}^{N-1} C_{0n}\cos(\delta^*_n y^*)\left[\cosh(\tau_y\delta^*_n z^*) - \phi^*_{0n}(x^*,y^*)\sinh(\tau_y\delta^*_n z^*)\right] + \\ & \sum_{m=1}^{M-1}\sum_{n=1}^{N-1} C_{mn}\cos(\lambda^*_m x^*)\cos(\delta^*_n y^*)\left[\cosh(\beta^*_{mn} z^*) - \phi^*_{mn}(x^*,y^*)\sinh(\beta^*_{mn} z^*)\right],\end{aligned} \tag{3.33}$$

where $\lambda^*_m = \lambda_m c = m\pi$ and $\delta^*_n = \delta_n d = n\pi$ are the dimensionless eigenvalues in the x- and y-directions, respectively, and $\beta^*_{mn} = \beta_{mn}t = \sqrt{(\lambda^*_m\tau_x)^2 + (\delta^*_n\tau_y)^2}$ are the dimensionless double Fourier expansion eigenvalues. The Fourier coefficients function $\phi^*_{mn}(x^*,y^*)$ is rewritten as:

$$\phi^*_{mn}(x^*,y^*) = \begin{cases} \dfrac{Bi(x^*,y^*)}{1+Bi(x^*,y^*)}, & \text{for } \; m=n=0, \\ \dfrac{\gamma^*\tanh(\gamma^*\tau_\gamma) + [Bi(x^*,y^*)/\tau_\gamma]}{\gamma^* + [Bi(x^*,y^*)/\tau_\gamma]\tanh(\gamma^*\tau_\gamma)}, & \text{otherwise,} \end{cases} \tag{3.34}$$

where γ^* refers to any of the corresponding dimensionless eigenvalues λ^*_m, δ^*_n, or β^*_{mn} and τ_γ is the corresponding thickness-aspect ratio, i.e., $\tau_\gamma = \tau_x$ for λ^*_m, $\tau_\gamma = \tau_y$ for δ^*_n, and $\tau_\gamma = 1$ for β^*_{mn}. The function $Bi(x^*,y^*)$ represents the nondimensional heat transfer coefficient function $h(x,y)$, where the two functions considered in this study given by Eqs. (3.8) and (3.9) can be represented as:

$$Bi_1(x^*,y^*) = \overline{Bi}_s\frac{\pi^2}{4}\sin(x^*\pi)\sin(y^*\pi), \tag{3.35}$$

$$Bi_2(x^*, y^*) = \overline{Bi}_s \frac{\pi^2}{\pi^2 - 4} \left[1 - \sin(x^*\pi)\sin(y^*\pi)\right]. \tag{3.36}$$

To find the Fourier coefficients C_{mn} based on the nondimensional representation, the general equation of the linear system in Eq. (3.21) can be rewritten as:

$$\sum_{m=0}^{M-1}\sum_{n=0}^{N-1} \hat{C}_{mn} \int_0^1 \int_0^1 \psi^*_{mn}(x^*, y^*)\psi^*_{ij}(x^*, y^*)dy^*dx^* = \int_{X_c^*-\epsilon_x/2}^{X_c^*+\epsilon_x/2} \int_{Y_c^*-\epsilon_y/2}^{Y_c^*+\epsilon_y/2} \psi^*_{ij}(x^*, y^*)dy^*dx^*, \tag{3.37}$$

where

$$\psi_{mn}(x, y) = \begin{cases} \phi^*_{00}(x^*, y^*), & \text{for } m = n = 0, \\ \lambda^*_m \phi^*_{m0}(x^*, y^*)\cos(\lambda^*_m x^*), & \text{for } m \neq 0,\ n = 0, \\ \delta^*_n \phi^*_{0n}(x^*, y^*)\cos(\delta^*_n y^*), & \text{for } m = 0,\ n \neq 0, \\ \beta^*_{mn}\phi^*_{mn}(x^*, y^*)\cos(\lambda^*_m x^*)\cos(\delta^*_n y^*), & \text{for } m \neq 0,\ n \neq 0. \end{cases} \tag{3.38}$$

It is important to note that the nondimensional linear system equation (3.37) is presented in terms of the modified Fourier coefficients that can be related to the actual Fourier coefficients as $\hat{C}_{00} = C_{00}k/qt$, $\hat{C}_{m0} = C_{m0}k/qc$, $\hat{C}_{0n} = C_{0n}k/qd$, and $\hat{C}_{mn} = C_{mn}k/qt$ for both $m \neq 0$ and $n \neq 0$.

Finally, the total thermal resistance R_t is nondimensionalized by using the thermal conductivity k and an intrinsic length scale which is taken to be $\sqrt{ab}$ (i.e., $\sqrt{A_c}$) to get:

$$R^*_t = k\sqrt{ab}R_t. \tag{3.39}$$

Thus, once the linear system is solved for the modified Fourier coefficients $\hat{C}_{mn}$, the nondimensional total thermal resistance can be expressed in terms of the aspect ratio factors as:

$$R_t^* = \frac{\sqrt{\tau_x \tau_y}}{\sqrt{\epsilon_x \epsilon_y}} \left[\hat{C}_{00} + \frac{2}{\epsilon_x \tau_x} \sum_{m=1}^{M-1} \hat{C}_{m0} \frac{\cos(\lambda_m^* X_c^*) \sin(\frac{1}{2}\lambda_m^* \epsilon_x)}{\lambda_m^*} + \frac{2}{\epsilon_y \tau_y} \sum_{n=1}^{N-1} \hat{C}_{0n} \frac{\cos(\delta_n^* Y_c^*) \sin(\frac{1}{2}\delta_n^* \epsilon_y)}{\delta_n^*} + \frac{4}{\epsilon_x \epsilon_y} \sum_{m=1}^{M-1} \sum_{n=1}^{N-1} \hat{C}_{mn} \frac{\cos(\lambda_m^* X_c^*) \sin(\frac{1}{2}\lambda_m^* \epsilon_x) \cos(\delta_n^* Y_c^*) \sin(\frac{1}{2}\delta_n^* \epsilon_y)}{\lambda_m^* \delta_n^*} \right]. \quad (3.40)$$

3.3 Results and Discussions

In this section, different parametric studies are conducted to validate the analytical solution and to study the effect of the different conductance distribution profiles along the sink plane on the thermal resistance and temperature rise. First, the analytical solution is used to calculate and study the dimensionless thermal resistance of a 3D flux channel for different aspect ratios and different values of the Biot number where the results are compared with numerical simulation results. One parametric dimensional study is then presented to see the effect of the different conductance profiles on the temperature distribution along the source plane. For the analytical solution results, MATLAB (version 2016b) software is used to carry out the results [19], while the numerical results are conducted based on the finite element method (FEM) using the ANSYS commercial software package [20].

3.3.1 Dimensionless Parametric Analysis

We start our investigation by considering the developed analytical solution to evaluate the dimensionless total thermal resistance of a 3D flux channel and to study the effect of the different conductance profiles on the thermal resistance for different aspect ratios and different Biot numbers. The analytical dimensionless thermal resistance presented in Eq. (3.40) can be seen as a function of seven parameters: X_c^*, Y_c^*, ϵ_x,

ϵ_y, τ_x, τ_y, and $\overline{Bi}_s$. In this study, we consider a channel flux of equal aspect ratios, i.e., $\epsilon_x = \epsilon_y = \epsilon$ and $\tau_x = \tau_y = \tau$, and a centered heat source of $X_c^* = Y_c^* = 0.5$. The two variable heat transfer coefficient profiles along the sink plane given by Eqs. (3.8) and (3.9) are considered and compared with using a uniform heat transfer coefficient along the sink plane $\bar{h}_s$. The dimensionless thermal resistance is calculated for different values of the Biot number: $\overline{Bi}_s = 0.1,\ 1,\ 10$ and with a thickness-aspect ratio fixed as $\tau = 0.1$. The dimensionless total thermal resistance is calculated for different values of the aspect ratio ϵ (ϵ is taken to vary from 0.1 to 1) and the analytical results are compared to the FEM numerical solution results. Regarding the analytical solution results, the number of terms for each summation in Eq. (3.40) is taken the same, i.e., $M = N$, and the convergence is checked by increasing the number of terms in the summations starting from $M = N = 10$ and then the number of terms is incremented until the following stopping criteria are satisfied [21]:

$$\left| \frac{R_t^{*M+1} - R_t^{*M}}{R_t^{*M+1}} \right| \leq 10^{-3}, \tag{3.41}$$

where R_t^{*M+1} represents the dimensionless resistance R_t^* calculated by using $M + 1$ and $N + 1$ terms in the summations. Moreover, the FEM results are obtained with a tetrahedral mesh and the convergence is checked by refining the mesh. In particular, most of the refinement is required around the heat-source region. Table 3.1 shows the convergence of the analytical and the numerical dimensionless thermal resistance of one sample of the conducted studies for $\epsilon = 0.4$ and $\overline{Bi}_s = 0.1$ when considering $h_1(x, y)$ as the heat transfer coefficient along the sink plane. It can be seen that with $M = N = 20$, the dimensionless thermal resistance has very good agreement with the FEM results with a relative error of approximately 0.1% compared to the finest mesh result.

FEM		Analytical	
Number of Elements	R_t^*	$M = N$	R_t^*
14842	0.619830	5	0.619728
34443	0.631640	10	0.636532
43882	0.636269	15	0.640422
119160	0.639505	20	0.641298
282386	0.641478	25	0.641519
482386	0.641934	30	0.641675

Table 3.1: Convergence study of the dimensionless thermal resistance for the analytical and the FEM results with $\overline{Bi}_s = 0.1$, and $\epsilon = 0.4$ when considering $h_1(x, y)$.

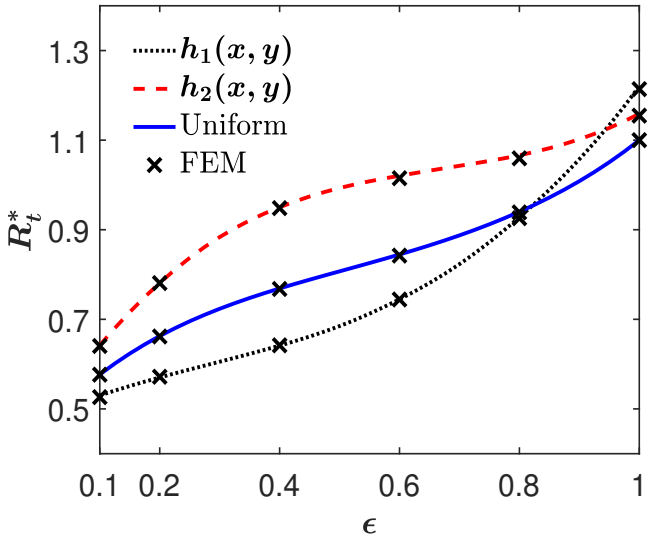

Figure 3.4: Dimensionless thermal resistance for $\overline{Bi}_s = 0.1$ and $\tau = 0.1$.

Figures 3.4-3.6 show the dimensionless thermal resistance R_t^* as a function of the aspect ratio ϵ for the different values of the Biot numbers where both of the analytical and the FEM results are shown on the same plots. For the analytical results, the number of terms used to satisfy Eq. (3.41) is found to be varying between $M = N = 15$ and $M = N = 30$ depending on the aspect ratio value ϵ where more terms are required for the smaller values of ϵ. It is important to note that the behavior (increasing/decreasing intervals) of the dimensionless thermal resistance profile R_t^* with respect to ϵ is not necessarily representing the same behavior of the dimensional thermal resistance profile R_t since $\sqrt{ab}$ is used to nondimensionalize the

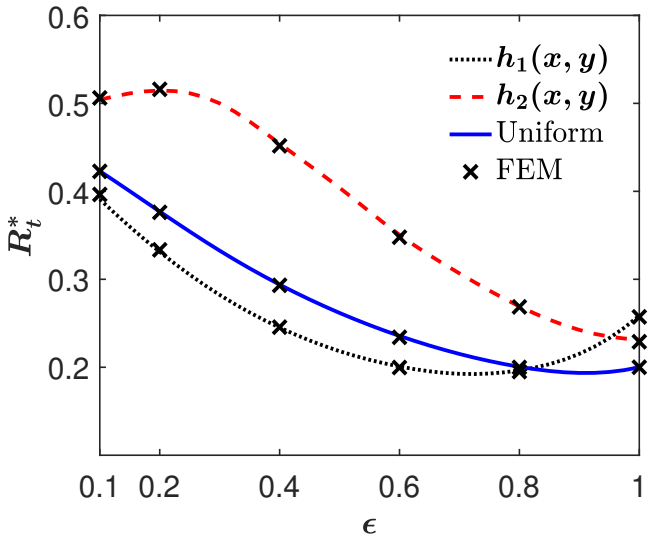

Figure 3.5: Dimensionless thermal resistance for $\overline{Bi}_s = 1$ and $\tau = 0.1$.

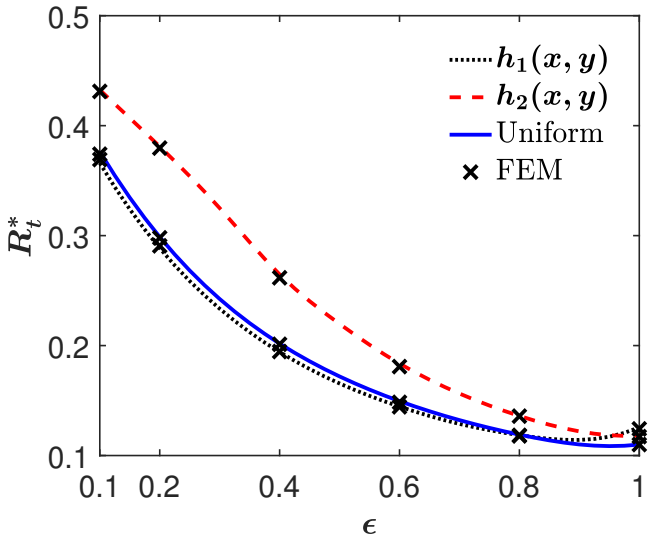

Figure 3.6: Dimensionless thermal resistance for $\overline{Bi}_s = 10$ and $\tau = 0.1$.

thermal resistance; hence, the dimensional value of the resistance depends on the value of ϵ.

One can see from Figs. 3.4-3.6 that the order of magnitude for the dimensionless thermal resistance decreases when the Biot number increases. Furthermore, the effect of the different conductance profiles along the sink plane on the thermal resistance is obvious for the different Biot numbers. Although the total average conductance of the

different conductance profiles is the same and equals to the uniform conductance value $\bar{h}_s$, the thermal resistance is strongly dependent on the distribution of the conductance profile along the sink plane. In particular, for $\epsilon < 0.8$, the thermal resistance has minimum values when using $h_1(x, y)$ as the conductance profile compared with using uniform conductance along the entire sink plane or $h_2(x, y)$. The reason behind this is that by considering the distribution of $h_1(x, y)$, the intense cooling area is located directly under the heat-source region. However, for the larger values of the aspect ratio, i.e., $\epsilon > 0.8$, the thermal resistance has minimum values when using the uniform conductance profile. It is worth mentioning that the heat flow mechanism through the channel is different for the three conductance distributions. For example, when considering the uniform conductance along the sink plane, as the heat-source aspect ratio ϵ increases to cover the source-plane area, i.e., $\epsilon = 1$, the nature of the heat flow becomes one-dimensional (1D). However, this is not the case when considering the two other distributions $h_1(x, y)$ and $h_2(x, y)$ where the flow is always multidimensional for all the values of ϵ, as we will see in the next section.

3.3.2 Source-Plane Temperature

In this part, a dimensional study is conducted to see the impact of the variable heat transfer coefficients on the temperature distribution along the source plane. A 3D square flux channel with side dimensions of $c = d = 0.1$ m and thickness $t = 0.01$ m ($\tau = 0.1$) is considered. In the source plane, the heat-source center is located at the point $(X_c, Y_c) = (0.05 \text{ m}, 0.05 \text{ m})$ where two different dimensions of the heat source are considered. First, we consider a small heat source of dimensions $a = b = 0.02$ m ($\epsilon = 0.2$). Then a large heat source that covers the whole source plane of dimensions $a = b = 0.1$ m ($\epsilon = 1.0$) is considered. The thermal conductivity is $k = 10$ W/m·K. A uniform heat flux of $q = 10^4$ W/m^2 is applied in the source region. Along the

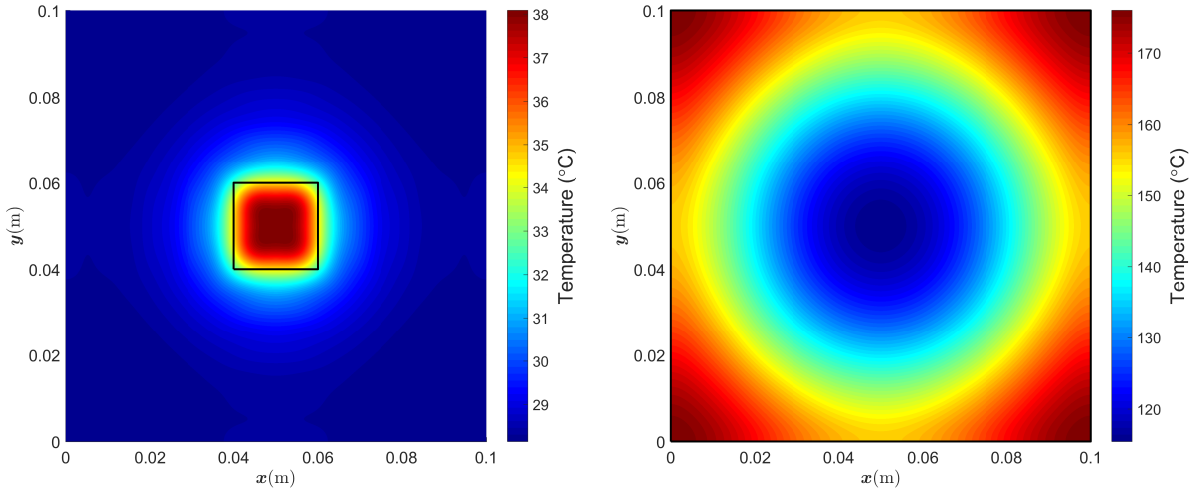

(a) (b)

Figure 3.7: Color-map plots of the temperature distribution along the source plane when considering $h_1(x, y)$ as the heat transfer coefficient. (a) $\epsilon = 0.2$. (b) $\epsilon = 1.0$.

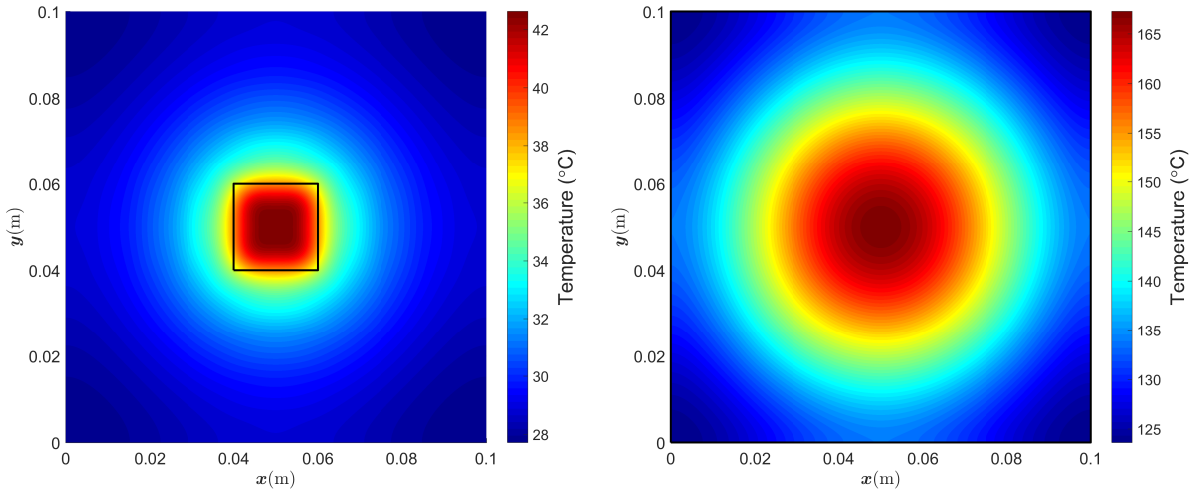

(a) (b)

Figure 3.8: Color-map plots of the temperature distribution along the source plane when considering $h_2(x, y)$ as the heat transfer coefficient. (a) $\epsilon = 0.2$. (b) $\epsilon = 1.0$.

sink plane, the different heat transfer coefficients represented by $h_1(x, y)$, $h_2(x, y)$ and the uniform heat transfer coefficient $\bar{h}_s$ are considered with average conductance of $\bar{h}_s = 100$ W/m^2·K ($\overline{Bi}_s = 0.1$). The ambient temperature is chosen as 25° C.

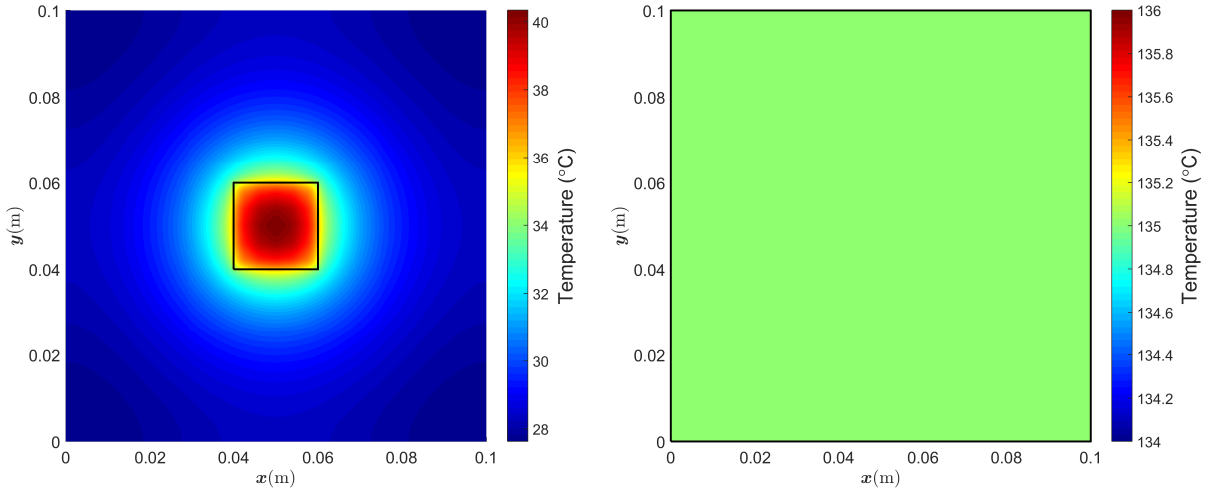

(a) (b)

Figure 3.9: Color-map plots of the temperature distribution along the source plane when considering a uniform heat transfer coefficient $\bar{h}_s$. (a) $\epsilon = 0.2$. (b) $\epsilon = 1.0$.

The developed analytical solution is used to evaluate the temperature distribution along the source plane for the different conductance functions. Figures 3.7-3.9 show the source-plane temperature distributions for the different conductance functions. One can observe how the different conductance profiles along the sink plane affect the temperature distributions along the source plane. In particular, for the small heat-source case, i.e., $\epsilon = 0.2$, the temperature rise inside the heat-source area records the minimum values when considering $h_1(x, y)$ as the conductance profile. On the other hand, for the large heat-source case, i.e., $\epsilon = 1.0$, the nature of the temperature distributions is significantly different for the three conductance profiles. When considering $h_1(x, y)$ as the conductance profile, the temperature distribution records the minimum values in the central region (intense cooling region) and the maximum values along the corners of the source plane, whereas the temperature distribution records the maximum values in the central region of the source plane when considering $h_2(x, y)$. However, the temperature distribution has a uniform value along the

source plane when considering the uniform heat transfer coefficient $\bar{h}_s$.

3.4 Conclusion

In this chapter, analytical solutions for the temperature field and thermal resistance of a 3D flux channel with eccentric heat source and a variable heat transfer coefficient that varies in the two horizontal dimensions were developed by using the method of separation of variables combined with the method of least squares. Two different variable heat transfer coefficients were considered in this chapter to study the effect of the variable conductance distribution along the sink plane on the temperature distribution and the thermal resistance of the flux channel compared with using uniformly distributed conductance along the sink plane. The thermal resistance was presented in a general dimensionless form as a function of the heat-source aspect ratios, the channel-thickness aspect ratios, and the Biot number. The analytical solution results were validated by comparing the developed analytical solution results with the results obtained by solving the problem numerically based on the FEM using the ANSYS commercial software package [20] where very good agreement was found. Different parametric studies were conducted to study the effect of the different conductance distributions on the dimensionless total thermal resistance of the channel and the temperature distribution along the source plane. It was observed that although the total average conductance of the different conductance profiles are considered to be the same, the temperature distribution and the thermal resistance are strongly dependent on the distribution of the conductance profile along the sink plane.

References

[1] V. Kadambi and N. Abuaf, "An analysis of thermal response for power chip packages," *IEEE Trans. Electron Devices*, vol. 32, no. 6, pp. 1024–1033, Jun. 1985.

[2] M. M. Yovanovich, Y. S. Muzychka, and J. R. Culham, "Spreading resistance in isoflux rectangles and strips on compound flux channels," *J. Thermophys. Heat Transf.*, vol. 13, no. 4, pp. 495–500, 1999.

[3] Y. S. Muzychka, J. R. Culham, and M. M. Yovanovich, "Thermal spreading resistance of eccentric heat sources on rectangular flux channels," *J. Electron. Packag.*, vol. 125, no. 2, pp. 178–185, Jun. 2003.

[4] Y. S. Muzychka, M. M. Yovanovich, and J. R. Culham, "Influence of geometry and edge cooling on thermal spreading resistance," *J. Thermophys. Heat Transf.*, vol. 20, no. 2, pp. 247–255, 2006.

[5] Y. S. Muzychka, "Influence coefficient method for calculating discrete heat source temperature on finite convectively cooled substrates," *IEEE Trans. Compon. Packag. Technol.*, vol. 29, no. 3, pp. 636–643, Sep. 2006.

[6] Y. S. Muzychka, K. R. Bagnall, and E. N. Wang, "Thermal spreading resistance and heat source temperature in compound orthotropic systems with interfacial

resistance," *IEEE Trans. Compon., Packag., Manuf. Technol.*, vol. 3, no. 11, pp. 1826–1841, Nov. 2013.

[7] Y. S. Muzychka, "Spreading resistance in compound orthotropic flux tubes and channels with interfacial resistance," *J. Thermophys. Heat Transf.*, vol. 28, no. 2, pp. 313–319, Mar. 2014.

[8] K. R. Bagnall, Y. S. Muzychka, and E. N. Wang, "Analytical solution for temperature rise in complex, multilayer structures with discrete heat sources," *IEEE Trans. Compon., Packag., Manuf. Technol.*, vol. 4, no. 5, pp. 817–830, May 2014.

[9] A. Gholami and M. Bahrami, "Thermal spreading resistance inside anisotropic plates with arbitrarily located hotspots," *J. Thermophys. Heat Transf.*, vol. 28, no. 4, pp. 679–686, Oct.-Dec. 2014.

[10] M. Razavi, Y. S. Muzychka, and S. Kocabiyik, "Thermal resistance in a rectangular flux channel with nonuniform heat convection in the sink plane," *J. Heat Transf.*, vol. 137, no. 11, pp. 111 401–1–111 401–9, Nov. 2015.

[11] S. Kakac and Y. Yener, *Heat Conduction, 3rd ed.* Malabar, FL, USA: Taylor & Francis, 1993.

[12] M. N. Özisik, *Boundary Value Problems of Heat Conduction.* Scranton, PA, USA: International Textbook, 1968.

[13] D. W. Hahn and M. N. Özisik, *Heat Conduction.* Hoboken, NJ, USA: Wiley, 2012.

[14] V. S. Arpaci, *Conduction Heat Transfer.* New York, NY, USA: Addison-Wesley, 1966.

[15] R. L. Burden and J. D. Faires, *Numerical Analysis, 9th ed.* Boston, MA, USA: Brooks/Cole, 2011.

[16] W. Gautschi, *Numerical Analysis.* New York, NY, USA: Springer, 2012.

[17] R. B. Kelman, "Least squares fourier series solutions to boundary value problems," *Soc. Ind. Appl. Math.*, vol. 21, no. 3, pp. 329–338, Jul. 1979.

[18] Q. Wang, K. Wang, and S. Chen, "Least squares approximation method for the solution of Volterra-Fredholm integral equations," *J. Comput. Appl. Math.*, vol. 272, pp. 141–147, Dec. 2014.

[19] MATLAB Release 2016b, The MathWorks, Inc., Natick, MA, USA, 2016.

[20] ANSYS® Release 16.2, ANSYS, Inc., Canonsburg, PA, USA, 2015.

[21] Y. Rahmani, M. G. Bandpy, and D. D. Ganji, "Numerical study of thermal spreading resistance in body-fitted curvilinear coordinates," *Int. J. Appl. Comput. Math.*, vol. 3, no. 4, pp. 2873–2888, Dec. 2017.

Statement of co-authorship

This statement describes the authors' research contributions in the following journal manuscript.

Title: **Effect of Temperature-Dependent Thermal Conductivity on Spreading Resistance in Flux Channels**
Located in Chapter 4.

The following people contributed to the conception of this paper:
Author 1: Belal Al-Khamaiseh
Author 2: Dr. Yuri S. Muzychka
Author 3: Dr. Serpil Kocabiyik

Belal Al-Khamaiseh was the primary author of this research. He played a major role in conducting an extensive literature search, developing the analytical solutions, conducting the computational part, analyzing the results, and comparing the analytical results with numerical results for verification purposes. Dr. Yuri S. Muzychka played a significant role in presenting the idea of the research and together he and Dr. Serpil Kocabiyik contributed to the conception and design of this research. They also guided it's analytical and computational components.

Chapter 4

Effect of Temperature-Dependent Thermal Conductivity on Spreading Resistance in Flux Channels

4.1 Introduction

Accurate thermal analysis of microelectronic devices is considered as a key factor in the development of electronic systems for better performance and device reliability. In many materials used in the microelectronics industry, the thermal properties vary with temperature. In particular, the thermal conductivity of most of the materials are temperature dependent, and the assumption of constant thermal conductivity within

Accepted for publication in the AIAA-Journal of Thermophysics and Heat Transfer.

the whole temperature variation interval when considering thermal management may lead to unacceptable errors in the temperature distribution field, and so, in thermal analysis [1, 2]. Therefore, a good understanding of the effects of the material's properties used for designing the device on the temperature rise and thermal resistance is essential to design a durable device. Most electronic systems are modeled as rectangular flux channels or cylindrical flux tubes, where heat enters the channel through small region(s) and flows by conduction through the system to spread the heat out into a larger heat-sink area, which gives rise to thermal spreading resistance.

The temperature-dependent thermal conductivity produces a nonlinearity in the heat conduction governing equation and this makes the problem complicated to be solved directly. Usually, numerical methods are used to solve nonlinear conduction problems; however, in most applications, the numerical methods are computationally expensive and less flexible for the optimization studies of the device layout to reduce thermal resistance. The Kirchhoff transform method is an attractive technique for dealing with nonlinear conduction problems with temperature-dependent thermal conductivity since it provides a convenient way to linearize the governing equation and then the solution of the linearized system can be transformed back to the solution of the nonlinear problem in an exact manner [3–6]. The Kirchhoff transform was introduced by Kirchhoff in 1894, and since its introduction it has been widely used to solve heat conduction problems in which the thermal conductivity of the materials depends on temperature [7]. Although the Kirchhoff transform is considered a powerful technique in solving nonlinear conduction problems, its applicability has some restrictions. In particular, when the boundary conditions of the problem are Dirichlet (first kind) or Neumann (second kind), the Kirchhoff transform will transform the boundary conditions to linear boundary conditions that can be used directly to solve the transformed linear system. However, this is not the case when considering

convective boundary conditions (third kind or Robin), as the transformed boundary conditions become nonlinear boundary conditions, and this produces a difficulty when trying to solve the transformed linear problem [3, 4].

Many relevant studies can be found in the literature on thermal analysis of flux channels. In most of the existing work, attention has been focused on problems with constant thermal conductivities. Yovanovich studied different spreading resistance problems for more than forty years, and he summarized the most important models of thermal spreading resistance in a review paper about contact, gap and joint resistance in [8]. Muzychka et al. [9–14] have done comprehensive research on different aspects of thermal spreading resistance problems including different geometries, boundaries, and properties. Bagnall et al. [15] developed an analytical solution for the spreading resistance in multilayered flux channels with isotropic and transversely isotropic properties. Bonani and Ghoine [1] applied the Kirchhoff transform to a composite medium with temperature-dependent and piecewise inhomogeneous thermal conductivity for a fixed-sink-temperature boundary condition. Ditri [16] studied a single-layer flux channel with orthotropic temperature-dependent thermal conductivities and a fixed-temperature boundary condition along the sink plane. A review of the literature reveals that analytical solutions for the temperature field and thermal spreading resistance for flux channels with temperature-dependent thermal conductivities and convective boundary conditions are limited. Recently, Bagnall et al. [7] applied the Kirchhoff transform to problems with convection boundary conditions to study the temperature rise.

In this chapter, the Kirchhoff transform is used to study the effect of the temperature-dependent thermal conductivity on the temperature rise and thermal resistance of a three-dimensional (3D) flux channel for different conductivity functions. The Kirchhoff transform is used to transform the nonlinear conduction problem into a linear

problem, after which the solution of the linear problem is presented and used to find the solution of the original nonlinear problem by means of the inverse Kirchhoff transform. Moreover, explicit approximation of the total thermal resistance of the nonlinear problem is developed.

4.2 Mathematical Theory

The model under consideration is a 3D rectangular flux channel in which heat enters the system through an eccentric heat source and flows by conduction to a larger convective heat sink, as shown in Fig. 4.1. This model represents the general layout of many applications including heat spreaders, semiconductors and microelectronic devices.

In many applications, the thermal conductivity of the used materials is temperature dependent and can be represented by a functional relationship $k(T)$. Hence, the steady-state heat conduction is governed by the following nonlinear heat equation:

$$\nabla \cdot k(T) \nabla T = 0, \tag{4.1}$$

with respect to the following boundary conditions (see Fig. 4.1). In the source plane, a uniform heat flux is specified over the heat-source region, where the heat source is considered as of rectangular shape with dimensions a and b in the x- and y-directions, respectively, whereas outside the heat-source region is considered as adiabatic. Hence, the source-plane boundary condition is given by:

$$-k(T) \frac{\partial T}{\partial z}\bigg|_{z\,=\,0} = \begin{cases} q, & \text{inside source region,} \\ 0, & \text{outside source region.} \end{cases} \tag{4.2}$$

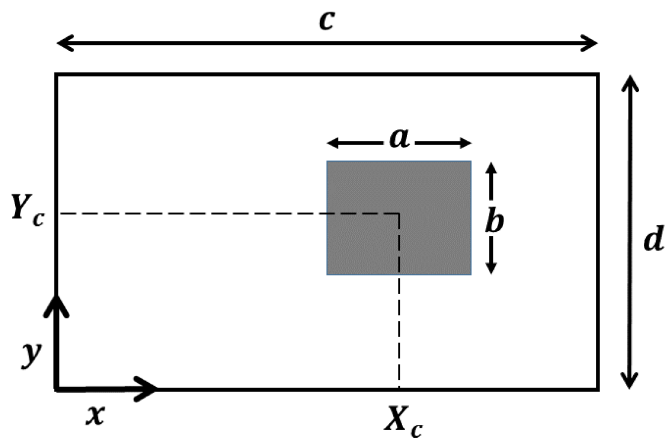

(a)

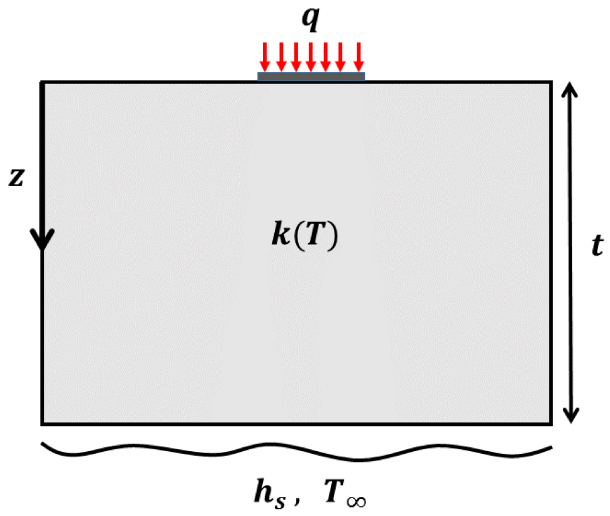

(b)

Figure 4.1: Schematic view of a 3D flux channel layout. (a) Top view. (b) Vertical cross-sectional view.

Along the sink plane, a convective boundary condition with uniform heat transfer coefficient h_s exists and the boundary condition is given by:

$$-k(T)\frac{\partial T}{\partial z}\bigg|_{z=t} = h_s\left(T(x,y,t) - T_\infty\right). \tag{4.3}$$

The lateral edges of the system are assumed to be adiabatic. The lateral-edge boundary conditions are:

$$\left.\frac{\partial T}{\partial x}\right|_{x\,=\,0,\,c} = 0, \qquad \left.\frac{\partial T}{\partial y}\right|_{y\,=\,0,\,d} = 0. \tag{4.4}$$

The problem statement is illustrated along with the nonlinear governing equation and boundary conditions. It is important to note that the nonlinearity of the problem makes it difficult to be solved analytically. However, this problem can be linearized and solved by means of the Kirchhoff transform.

4.2.1 Kirchhoff Transform

The Kirchhoff transform is considered a convenient method for solving heat conduction problems with temperature-dependent properties, which can be applied for solving nonlinear steady-state and transient problems [3]. However, the method is more attractive for solving steady-state problems in the context of obtaining fully exact solutions without considering any assumptions or approximations.

The Kirchhoff transform can be used to linearize the nonlinear heat conduction equation in Eq. (4.1) by transforming the nonlinear system with the temperature-dependent thermal conductivity into another linear system with a constant thermal conductivity. This can be done by introducing a new variable θ, which can be defined in its general form as:

$$\theta = K\{T\} = A + \frac{1}{C}\int_{B}^{T} k(\tau)d\tau, \tag{4.5}$$

where A, B, and C are constants that can be chosen arbitrarily. Kirchhoff originally introduced the transform in 1894 of the form:

$$U = \frac{1}{k_0}\int_{0}^{T} k(\tau)d\tau, \tag{4.6}$$

with k_0 as the thermal conductivity evaluated at 0, i.e., $k_0 = k(0)$. However, the

general form in Eq. (4.5) can be seen as a result of applying the so-called Hopf-Cole transformation [17]. The Hopf-Cole transformation was originally presented to linearize the viscous Burgers' equation into a linear diffusion equation, by introducing new variables that would eliminate the nonlinear terms when the equation is presented in terms of the new transformed variables. By following the Holf-Cole method, the nonlinear heat conduction equation given by Eq. (4.1) can be rewritten as:

$$k(T)\nabla^2 T + \frac{dk}{dT}\underbrace{\left(\left(\frac{\partial T}{\partial x}\right)^2 + \left(\frac{\partial T}{\partial y}\right)^2 + \left(\frac{\partial T}{\partial z}\right)^2\right)}_{(\nabla T\cdot\nabla T)} = 0, \tag{4.7}$$

which shows the nonlinearity clearly. It is desirable to introduce a transformation of the form:

$$T = \psi(\theta), \tag{4.8}$$

such that the nonlinear term represented by the second term in Eq. (4.7) is eliminated when using the new variable θ. It follows from Eq. (4.8) that,

$$\nabla T = \psi'\nabla\theta, \qquad \nabla^2 T = \psi'\nabla^2\theta + \psi''\nabla\theta\cdot\nabla\theta, \tag{4.9}$$

where the derivatives of ψ are with respect to the new variable θ, i.e., $\psi' = d\psi/d\theta$ and $\psi'' = d^2\psi/d\theta^2$. Thus, the nonlinear conduction equation in Eq. (4.7) is transformed under the new variable θ to:

$$k(\psi)\psi'\nabla^2\theta + \left[k(\psi)\psi'' + \frac{dk}{d\psi}\psi'^2\right]\nabla\theta\cdot\nabla\theta = 0. \tag{4.10}$$

It can be seen that the second nonlinear term in Eq. (4.10) corresponds to $\nabla\theta\cdot\nabla\theta$

vanishes when

$$\left[k(\psi)\psi'' + \frac{dk}{d\psi}\psi'^2\right] = 0, \tag{4.11}$$

which can be rewritten as:

$$\frac{d}{d\theta}\left[k(\psi)\frac{d\psi}{d\theta}\right] = 0. \tag{4.12}$$

Integrating Eq. (4.12) with respect to θ yields:

$$k(\psi)\frac{d\psi}{d\theta} = C, \tag{4.13}$$

where C is the integration constant. Furthermore, the result in Eq. (4.13) implies that the coefficient of the Laplacian term $\nabla^2\theta$ in Eq. (4.10) is constant, i.e., $k(\psi)\psi'\nabla^2\theta = C\nabla^2\theta$. Equation (4.13) can be rewritten in a separable form and integrated from θ_0 to θ to get the general formula of the new variable θ as:

$$\theta = \theta_0 + \frac{1}{C}\int_{\psi(\theta_0)}^{\psi(\theta)} k(\dot{\psi})d\dot{\psi}, \tag{4.14}$$

where θ_0 and $\psi(\theta_0)$ can be chosen to be any arbitrary constants. Hence, the general formula in Eq. (4.14) can be written as:

$$\theta = A + \frac{1}{C}\int_{B}^{T} k(\tau)d\tau, \tag{4.15}$$

which is the general form of the Kirchhoff transform presented in Eq. (4.5) where ψ is just the inverse Kirchhoff transform, i.e., $\psi = K^{-1}$. As a convenient choice and to give the new variable θ the dimension of temperature, in order to keep the physical meaning of the problem, the constants can be chosen as $A = B = T_0$, where T_0 is a convenient reference temperature depending on the problem to be investigated and

$C = k(T_0) = k_0$ is the thermal conductivity evaluated at T_0. Therefore, the new variable θ (usually referred to as the apparent temperature) can be written as:

$$\theta = K\{T\} = T_0 + \frac{1}{k_0}\int_{T_0}^{T} k(\tau)d\tau. \tag{4.16}$$

As a result, when applying the Kirchhoff transform given by Eq. (4.16) to the nonlinear heat conduction equation in Eq. (4.1), the nonlinear equation is transformed into the linear Laplace's equation:

$$\nabla^2\theta = 0. \tag{4.17}$$

From the previous discussion on the Kirchhoff transform, one can see the importance of this transform for solving nonlinear heat conduction problems by transforming them into linear problems in terms of the new variable θ. The linearized problem can be solved using the existing analytical methods for solving linear problems provided that the boundary conditions can be transformed into linear boundary conditions.

In heat conduction problems, the linear boundary conditions are of three main kinds: prescribed temperature (Dirichlet or first kind) boundary conditions, prescribed heat flux (Neumann or second kind) boundary conditions, and convective (Robin or third kind) boundary conditions. For boundary conditions of the first and second kinds, the boundary conditions can be transformed directly through the Kirchhoff transform into linear boundary conditions in terms of the new variable θ. This can be seen by considering the following boundary conditions:

$$T|_{boundary} = T_b, \qquad \text{(prescribed temperature)}, \tag{4.18}$$

which can be transformed through the Kirchhoff transform into:

$$\theta|_{boundary} = K\{T_b\} = T_0 + \frac{1}{k_0}\int_{T_0}^{T_b} k(\tau)d\tau = \theta_b, \tag{4.19}$$

which is again a prescribed temperature boundary condition after evaluating the definite integral. The boundary condition of the second kind in the form:

$$k(T)\frac{\partial T}{\partial n}\bigg|_{boundary} = q, \qquad \text{(prescribed heat flux)}, \tag{4.20}$$

can be transformed through the Kirchhoff transform into (using Eq. (4.13))

$$k_0\frac{\partial \theta}{\partial n}\bigg|_{boundary} = q, \tag{4.21}$$

where $\partial/\partial n$ denotes the derivative along the outward normal at the boundary surface. More details about the transformations of the boundary conditions of the first and second kinds can be found in [3].

Although the boundary conditions of the first and second kinds can be transformed easily into linear boundary conditions through the Kirchhoff transform, in general, this is not the case when considering a boundary condition of the third kind which has the form:

$$-k(T)\frac{\partial T}{\partial n}\bigg|_{boundary} = h_s(T|_{boundary} - T_\infty), \tag{4.22}$$

and when the Kirchhoff transform is considered, the boundary condition is transformed to:

$$-k_0\frac{\partial \theta}{\partial n}\bigg|_{boundary} = h_s(K^{-1}\{\theta|_{boundary}\} - T_\infty), \tag{4.23}$$

which is a nonlinear boundary condition since, in general, $K^{-1}\{\theta\}$ is a nonlinear function of θ ($K^{-1}\{\theta\} \neq \theta$). However, for some cases when the temperature distribution at the boundary can be approximated prior to using the Kirchhoff transform, the

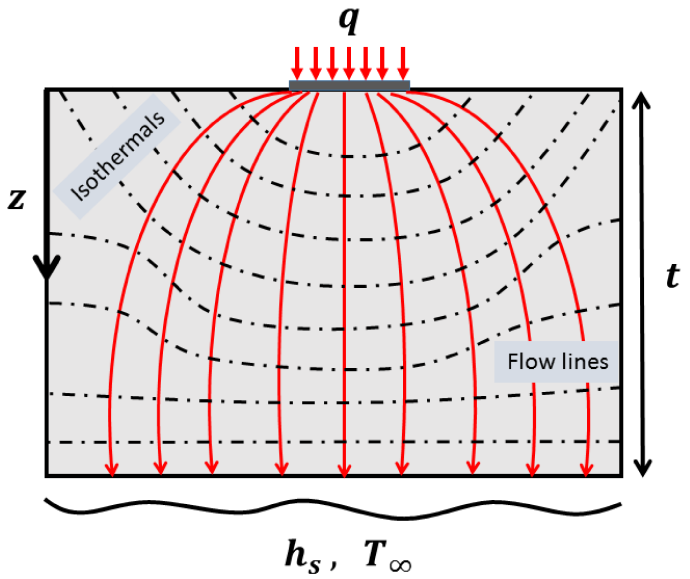

Figure 4.2: Isothermal lines and flow lines in spreading flux channel.

transform can be applied for convective boundary conditions to get linear transformed boundary conditions. By considering the problem under study given in Fig. 4.1, the heat enters the flux channel through the small heat-source region and flows by conduction to spread the heat out from the heat-source area into the larger heat-sink area. Hence, the temperature profile along the sink plane can be approximated from a physical point of view (conservation of energy) by [7]:

$$T|_{z=t} \approx \overline{T}|_{z=t} = \frac{1}{h_s}\frac{Q}{cd} + T_\infty. \tag{4.24}$$

Furthermore, when the channel thickness is adequate to spread the heat through the whole channel, the heat distribution along the sink plane will be approximately uniform. Thus, the approximate sink temperature in Eq. (4.24) becomes exact, as shown in Fig. 4.2. Now, when the approximated temperature along the sink plane is used as the reference temperature T_0 in the Kirchhoff transform Eq. (4.16), the convective boundary condition in Eq. (4.22) can be transformed into the following

linear boundary condition:

$$-k_0 \frac{\partial \theta}{\partial n}\bigg|_{z=t} = h_s(\theta|_{z=t} - T_\infty). \tag{4.25}$$

This can be seen as a result of considering the approximate sink temperature as a reference temperature in the Kirchhoff transform, where the following relation is obtained:

$$\theta|_{z=t} \approx T|_{z=t}. \tag{4.26}$$

To summarize, by using the Kirchhoff transform given in Eq. (4.16) with a reference temperature T_0 defined by:

$$T_0 = \frac{1}{h_s}\frac{Q}{cd} + T_\infty, \tag{4.27}$$

the nonlinear system gevin in Eqs. (4.1)-(4.4) is transformed to the following linear system in terms of the apparent temperature θ:

$$\nabla^2 \theta = 0, \tag{4.28}$$

with respect to the following boundary conditions:

$$-k_0 \frac{\partial \theta}{\partial z}\bigg|_{z\,=\,0} = \begin{cases} q, & \text{inside source region,} \\ 0, & \text{outside source region.} \end{cases} \tag{4.29}$$

in the source plane, and

$$-k_0 \frac{\partial \theta}{\partial z}\bigg|_{z\,=\,t} = h_s\left(\theta(x,y,t) - T_\infty\right), \tag{4.30}$$

along the sink plane, while the lateral-edge boundary conditions are transformed to:

$$\left.\frac{\partial\theta}{\partial x}\right|_{x\,=\,0,\,c} = 0, \qquad \left.\frac{\partial\theta}{\partial y}\right|_{y\,=\,0,\,d} = 0. \tag{4.31}$$

Once the solution of the new linear problem is obtained for θ, this solution can be transformed easily to the actual temperature of the nonlinear problem T by employing the inverse Kirchhoff transform, where the inverse Kirchhoff $K^{-1}\{\theta\}$ is not defined explicitly in general. However, the actual temperature can be obtained after finding the relationship between θ and T (once the thermal conductivity is specified) by using Eq. (4.16).

4.2.2 Linear System Solution

The general solution of the linearized system given by Eqs. (4.28)-(4.31) can be obtained by using the method of separation of variables. By defining $\theta' = \theta - T_\infty$, the linear system of θ' is the same as the linear system of θ but with homogenous boundary condition at the sink plane. The solution of θ' is assumed to have the form $\theta'(x,y,z) = X(x)\cdot Y(y)\cdot Z(z)$. Applying the method of separation of variables and using the boundary conditions along the planes $(x=0,\ x=c)$ and $(y=0,\ y=d)$ yield the following general solution:

$$\begin{aligned}\theta'(x,y,z) = {} & A_{00} + B_{00}z \\ & + \sum_{m=1}^{\infty} \cos(\lambda_m x)\left[A_{m0}\cosh(\lambda_m z) + B_{m0}\sinh(\lambda_m z)\right] \\ & + \sum_{n=1}^{\infty} \cos(\delta_n y)\left[A_{0n}\cosh(\delta_n z) + B_{0n}\sinh(\delta_n z)\right] \\ & + \sum_{m=1}^{\infty}\sum_{n=1}^{\infty} \cos(\lambda_m x)\cos(\delta_n y)\left[A_{mn}\cosh(\beta_{mn} z) + B_{mn}\sinh(\beta_{mn} z)\right],\end{aligned} \tag{4.32}$$

where $\lambda_m = m\pi/c$ and $\delta_n = n\pi/d$ are the eigenvalues in the x- and y-directions, respectively, and $\beta_{mn} = \sqrt{{\lambda_m}^2 + {\delta_n}^2}$ are the double Fourier expansion eigenvalues. The general solution contains four components: a uniform flow solution, and three spreading solutions represented by the series components that vanish when the heat flux is covering the whole source-plane surface ($z = 0$). For m, n not both equal to zero, the application of the sink-plane boundary condition leads to the following relationship between the Fourier coefficients:

$$\phi(\gamma) = -\frac{B_{mn}}{A_{mn}} = \frac{(\gamma k_0/h_s)\tanh(\gamma t) + 1}{(\gamma k_0/h_s) + \tanh(\gamma t)}, \tag{4.33}$$

where ϕ is the spreading function and γ refers to any of the eigenvalues λ_m, δ_n, or β_{mn}. In the limit of $h_s \longrightarrow \infty$, i.e., fixed-sink temperature, the spreading function becomes $\phi(\gamma) = \coth(\gamma t)$.

Finally, the boundary condition at the source plane ($z = 0$) is considered to find the Fourier coefficients A_{mn} after making use of $B_{mn} = -\phi(\gamma)A_{mn}$. This can be done by taking Fourier series expansions of the boundary condition at the source plane and using the orthogonality of the eigenfunctions to get:

$$A_{m0} = \frac{4Q\cos(\lambda_m X_c)\sin(\frac{1}{2}\lambda_m a)}{acdk_0{\lambda_m}^2\phi(\lambda_m)}, \tag{4.34}$$

and

$$A_{0n} = \frac{4Q\cos(\delta_n Y_c)\sin(\frac{1}{2}\delta_n b)}{bcdk_0{\delta_n}^2\phi(\delta_n)}, \tag{4.35}$$

and

$$A_{mn} = \frac{16Q\cos(\lambda_m X_c)\sin(\frac{1}{2}\lambda_m a)\cos(\delta_n Y_c)\sin(\frac{1}{2}\delta_n b)}{abcdk_0\beta_{mn}\lambda_m\delta_n\phi(\beta_{mn})}, \tag{4.36}$$

where $Q = abq$ is the total heat input of the flux channel. Now, when m, n are both

zeros, the zeroth-order Fourier coefficients A_{00} and B_{00} can be found by applying the sink-plane boundary condition and taking the Fourier expansion in the source plane to get:

$$A_{00} = \frac{Q}{cd}\left[\frac{t}{k_0} + \frac{1}{h_s}\right],$$
$$B_{00} = -\frac{Q}{cdk_0}. \tag{4.37}$$

The general solution of θ' is illustrated along with the Fourier coefficients; hence, the general solution of θ can be written as $\theta = \theta' + T_\infty$. The solution in the source plane ($z = 0$) is of most interest for finding the maximum temperature and the total thermal resistance of the flux channel which is addressed by:

$$\theta(x, y, 0) = T_\infty + A_{00} + \sum_{m=1}^{\infty} A_{m0}\cos(\lambda_m x) + \sum_{n=1}^{\infty} A_{0n}\cos(\delta_n y) + \sum_{m=1}^{\infty}\sum_{n=1}^{\infty} A_{mn}\cos(\lambda_m x)\cos(\delta_n y). \tag{4.38}$$

4.2.3 Temperature-Dependent Thermal Conductivity

The thermal conductivity of most materials is temperature dependent, and varies with temperature according to specific functional relationships between the thermal conductivity and the temperature $k(T)$. In some materials, the thermal conductivity increases with increasing the temperature (e.g., Aluminum), while in other materials, the thermal conductivity decreases with increasing the temperature (e.g., Silicon). Different dependency functions of the thermal conductivity on temperature can be found in the literature explicitly or can be obtained by considering the best curve fitting of experimental data. In this study, we will focus on three general forms of the

thermal conductivity functions given by [7, 17, 18]:

$$k_1(T) = k_0(1 + \omega_1(T - T_0))^p, \tag{4.39}$$

$$k_2(T) = k_0 \exp[\omega_2(T - T_0)], \tag{4.40}$$

$$k_3(T) = k_0 \left(\frac{T_0}{T}\right)^s, \tag{4.41}$$

where k_0 is a reference constant thermal conductivity; ω_1, ω_2 are constants called the temperature coefficients of the thermal conductivity [19]; and p, s are real numbers representing the exponents in the corresponding functions. It is important to note that the reference temperature T_0 is included in the definition of the temperature-dependent thermal conductivities in order to get the same reference thermal conductivity at T_0, i.e., $k_i(T_0) = k_0$, for comparison reasons.

Considering the Kirchhoff transform in Eq. (4.16), the functional relationship between the apparent temperature θ and the actual temperature T that corresponds to each of the three general forms of thermal conductivity functions given in Eqs. (4.39)-(4.41) can be obtained explicitly, and then by solving these relationships for T, the actual temperature T can be obtained in terms of the apparent temperature θ as:

$$T = K_1^{-1}\{\theta\} = \begin{cases} T_0 + \dfrac{1}{\omega_1}\left\{\exp[\omega_1(\theta - T_0)] - 1\right\}, & p = -1 \\ T_0 + \dfrac{1}{\omega_1}\left[(\omega_1(p+1)(\theta - T_0) + 1)^{1/(p+1)} - 1\right], & p \neq -1 \end{cases} \tag{4.42}$$

$$T = K_2^{-1}\{\theta\} = T_0 + \frac{1}{\omega_2}\ln(1 + \omega_2(\theta - T_0)), \tag{4.43}$$

$$T = K_3^{-1}\{\theta\} = \begin{cases} T_0 \exp(\theta/T_0 - 1), & s = 1 \\ T_0\left[\dfrac{(1-s)\theta}{T_0} + s\right]^{1/(1-s)}, & s \neq 1 \end{cases} \tag{4.44}$$

4.2.4 Total Thermal Resistance

For a single heat source spreading heat to a much larger sink area, the total thermal resistance can be defined by [9, 13, 20]:

$$R_t = \frac{\bar{T}_c - T_\infty}{Q}, \tag{4.45}$$

where $\bar{T}_c$ is the mean temperature over the heat-source contact area that can be defined by:

$$\bar{T}_c = \frac{1}{A_c} \iint_{A_c} T(x, y, 0)\, dA_c, \tag{4.46}$$

where $A_c = ab$ is the heat-source area. It is important to note that it is complicated to integrate the solution for T explicitly over the heat-source area because of the non-linearity of the inverse Kirchhoff transform functions. Thus, numerical integration can be used to evaluate the integrals in Eq. (4.46). However, since the mean temperature $\bar{T}_c$ requires only evaluation of the integrals over the small heat-source area, a good approximation of the temperature field $T(x, y, 0)$ is the first-order Taylor series approximation of the functional relationships between the actual temperature T and the apparent temperature θ ($T = K_1^{-1}\{\theta\} = \psi(\theta)$) around the centroidal temperature of the linear solution $\hat{\theta} = \theta(X_c, Y_c, 0)$. Thus, the solution in the heat-source region can be approximated by:

$$T(x, y, 0) = \psi(\hat{\theta}) + \psi'(\hat{\theta})(\theta(x, y, 0) - \hat{\theta}). \tag{4.47}$$

Hence, the mean source temperature $\bar{T}_c$ can be approximated explicitly by:

$$\bar{T}_c(\text{approx.}) = \psi(\hat{\theta}) + \psi'(\hat{\theta})(\bar{\theta}_c - \hat{\theta}),$$

$$= \psi(\hat{\theta}) + (A_{00} + T_\infty - \hat{\theta})\psi'(\hat{\theta}) + \psi'(\hat{\theta}) \left[2\sum_{m=1}^{\infty} A_{m0} \frac{\cos(\lambda_m X_c)\sin(\frac{1}{2}\lambda_m a)}{a\lambda_m} + 2\sum_{n=1}^{\infty} A_{0n} \frac{\cos(\delta_n Y_c)\sin(\frac{1}{2}\delta_n b)}{b\delta_n} + 4\sum_{m=1}^{\infty}\sum_{n=1}^{\infty} A_{mn} \frac{\cos(\lambda_m X_c)\sin(\frac{1}{2}\lambda_m a)\cos(\delta_n Y_c)\sin(\frac{1}{2}\delta_n b)}{a\lambda_m b\delta_n} \right], \quad (4.48)$$

where ψ' is the derivative of any of the inverse Kirchhoff functional relationships given in Eqs. (4.42)-(4.44) with respect to θ that can be addressed by:

$$\psi_1'(\theta) = K_1^{'-1}\{\theta\} = \begin{cases} \exp[\omega_1(\theta - T_0)], & p = -1 \\ (\omega_1(p+1)(\theta - T_0) + 1)^{-p/(p+1)}, & p \neq -1 \end{cases} \quad (4.49)$$

$$\psi_2'(\theta) = K_2^{'-1}\{\theta\} = \frac{1}{1 + \omega_2(\theta - T_0)}, \quad (4.50)$$

$$\psi_3'(\theta) = K_3^{'-1}\{\theta\} = \begin{cases} \exp(\theta/T_0 - 1), & s = 1 \\ \left[\dfrac{(1-s)\theta}{T_0} + s\right]^{s/(1-s)}, & s \neq 1. \end{cases} \quad (4.51)$$

4.3 Results and discussion

In this section, different parametric studies are considered to illustrate the influence of the temperature-dependent thermal conductivity on the temperature rise and total thermal resistance in flux channels with different configurations. For the purpose of verifying and demonstrating the computational efficiency of the analytical solutions, numerical analysis has been conducted by solving the problems numerically based on the finite element method (FEM) and comparing the numerical results to the analytical results. For the analytical results, MATLAB (version 2016b) software is used to carry out the results [21], while the numerical simulations are performed based on the FEM using the ANSYS commercial software package [22].

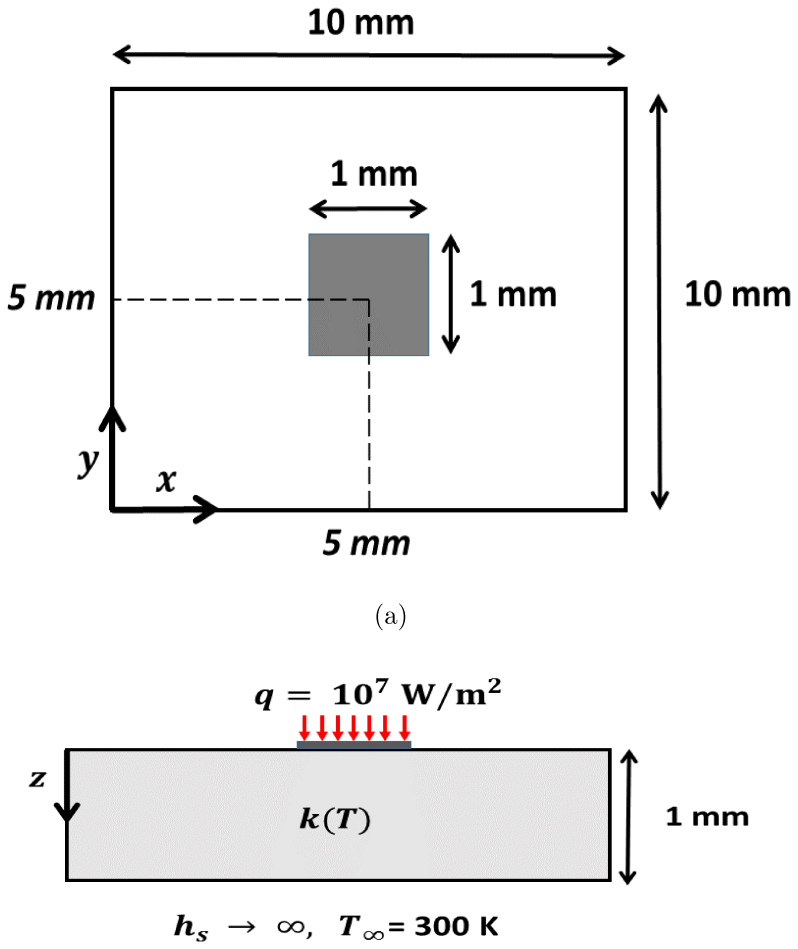

Figure 4.3: Schematic view of the fixed-sink-temperature flux channel layout. (a) Top view. (b) Vertical cross-sectional view.

4.3.1 Fixed-Sink Temperature ($h_s \longrightarrow \infty$)

We start our investigation by considering a system of 3D square flux channel with a fixed-temperature boundary condition at the base of the channel of 300 K. By considering the fixed-sink temperature, the analytical solution by means of the Kirchhoff transform is introduced as an exact solution of the problem without using any restrictions or assumptions since all the boundary conditions become of the first and second kinds. The system has side dimensions of $c = d = 10$ mm, whereas the heat-source

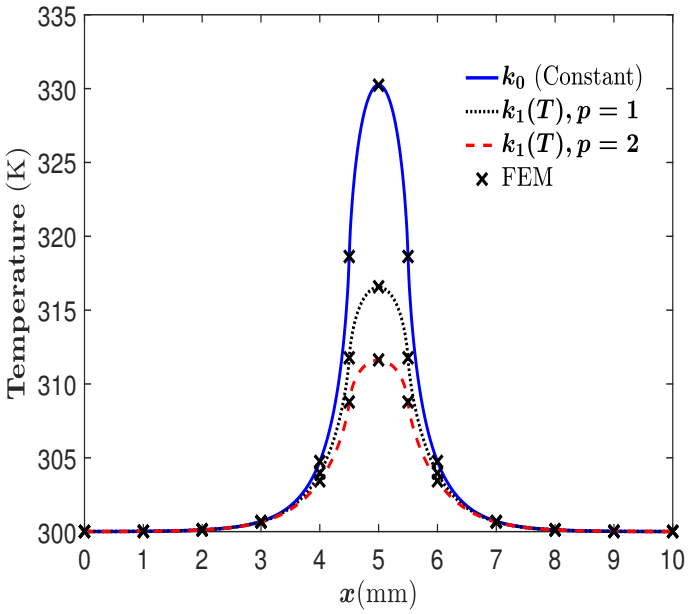

Figure 4.4: Temperature profile along x-axis in the source plane (at $y = Y_c$) by considering $k_1(T)$ with $\omega_1 = 0.1$ for the fixed-sink-temperature study.

dimensions are $a = b = 1$ mm. The center of the heat source is located at the point $(X_c, Y_c) = (5, 5)$ mm and the thickness of the channel is $t = 1$ mm, as shown in Fig. 4.3. The different thermal conductivity functions given in Eqs. (4.39)-(4.41) are considered with a reference thermal conductivity of $k_0 = 150$ W/m·K. In the source region, a uniform heat flux of $q = 10^7$ W/m^2 is applied. The analytical solution is used to compute the temperature profile along the source plane including the centroidal temperature of the heat source ($\hat{T} = T(X_c, Y_c, 0)$), and the source mean temperature $\overline{T}_c$ that can be used to obtain the total thermal resistance of the flux channel using Eq. (4.45). The source mean temperature is computed in two ways. First, by using numerical integration to evaluate the source mean temperature $\overline{T}_c$. Second, using the result in Eq. (4.48) by approximating the source mean temperature using the first-order Taylor series approximation to get $\overline{T}_c$(approx.). Furthermore, all the results are compared to numerical results obtained by solving the system numerically using the FEM.

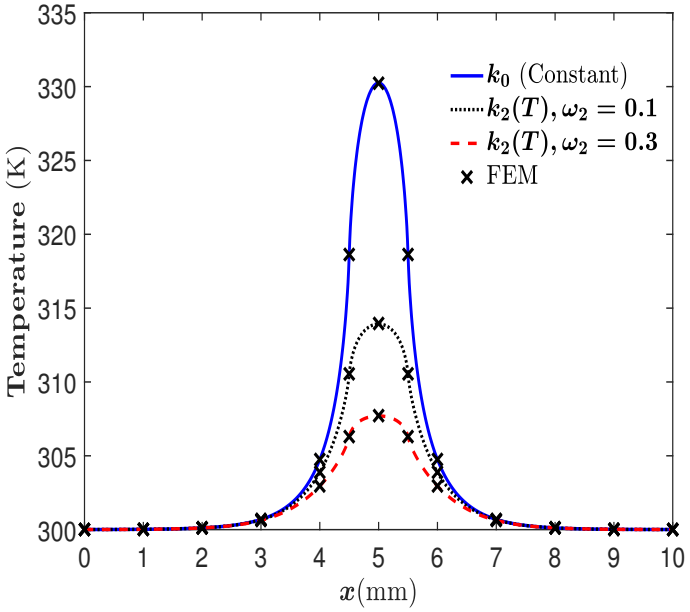

Figure 4.5: Temperature profile along x-axis in the source plane (at $y = Y_c$) by considering $k_2(T)$ for the fixed-sink-temperature study.

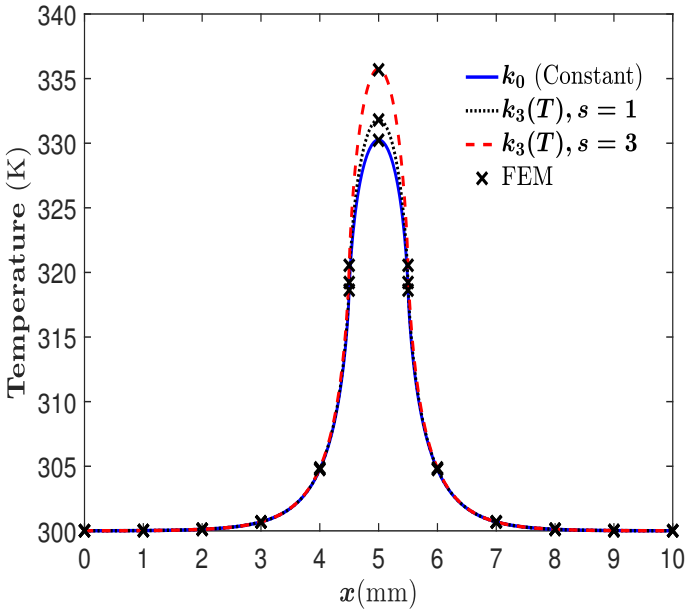

Figure 4.6: Temperature profile along x-axis in the source plane (at $y = Y_c$) by considering $k_3(T)$ for the fixed-sink-temperature study.

In the analytical solution, the number of terms used in the infinite Fourier series summation of the linear system solution is 500 in each of the summations and then

	Analytical			**FEM**	
$k(T)$ (W/m·K)	$\hat{T}$ (K)	$\overline{T}_c$ (K)	$\overline{T}_c$(approx.) (K)	$\hat{T}$ (K)	$\overline{T}_c$ (K)
k_0	330.249	324.549	324.549	330.23	324.349
$k_1(T), p = 1$	316.552	314.255	314.405	316.58	314.193
$k_1(T), p = 2$	311.598	310.254	310.376	311.63	310.225
$k_2(T), \omega_2 = 0.1$	313.925	312.332	312.509	313.96	312.299
$k_2(T), \omega_2 = 0.3$	307.700	307.046	307.134	307.72	307.033
$k_3(T), s = 1$	331.827	325.604	325.522	331.80	325.380
$k_3(T), s = 3$	335.759	328.156	327.768	335.68	327.869

Table 4.1: Source temperatures for the different thermal conductivity functions with $h_s \longrightarrow \infty$ and $T_\infty = 300$ K.

the inverse Kirchhoff transform is used to obtain the actual temperature (T). A sensitivity study on the number of terms in the series is performed by increasing the number of terms in the linear solution to 1000 in each summation and it is found that the change in the results is very small of a relative error less than 0.01%. The computational time required to find the temperature of any point in the source plane is approximately 0.03 s. Furthermore, the FEM numerical results are obtained with a tetrahedral mesh and the convergence is checked by refining the mesh. In particular, most of the refinement is required around the heat-source region due to the rapid change in temperature. The system with a tetrahedral mesh consisting of approximately 9.2×10^4 elements is found to be sufficient to solve the problem with a very small loss in accuracy (relative error of less than 0.05% compared to using approximately 1.5×10^5 elements). Figures 4.4-4.6 show the source plane temperature profiles along the x-axis when $y = Y_c$ for the three different conductivity functions with different parameters. In each of the figures, the effect of the temperature-dependent thermal conductivity on the temperature rise is obvious compared to using the constant thermal conductivity, where for the case of considering $k_1(T)$ or $k_2(T)$ with the specified parameters, it is clear that the thermal conductivity is an increasing function with respect to temperature; hence, the temperature rise around the heat-source area

is less in magnitude than the temperature rise when considering the constant thermal conductivity, as shown in Figs. 4.4 and 4.5. However, for the case of considering $k_3(T)$, the thermal conductivity is a decreasing function of temperature. Thus, the magnitude of the temperature rise is higher than the case of the constant thermal conductivity, as shown in Fig. 4.6. Moreover, it can be seen from Figs. 4.4-4.6 that the temperature distribution in the source plane is highly localized at and around the source region, while the surface temperature away from the heat source is at or near 300 K, which is the temperature of the sink plane. The reason behind this is the large value of the heat transfer coefficient along the sink plane (in the limit of $h_s \longrightarrow \infty$) [23]. For the flux channel configuration shown in Fig. 4.3 with $k_0 = 150$ W/m·K, increasing the heat transfer coefficient leads to less spreading of the heat flow. On the other hand, decreasing the heat transfer coefficient leads to a wider spreading through the channel. Hence, the surface temperature becomes of a different nature as we will see in the next convective-sink study. Furthermore, the centroidal and the mean source temperature of the analytical and the numerical results for the different thermal conductivity functions are given in Table 4.1 for comparison. The agreement between the analytical and the FEM results is considerably very good with a relative error of less than 0.1% for all the results. It is worth mentioning that in computing the mean source temperature, the closed-form analytical approximate average $\overline{T}_c$(approx.) presented in Eq. (4.48) has a very good agreement with the mean source temperature $\overline{T}_c$ obtained by using the numerical integration with a relative error of less than 0.1%. The most important advantage of this closed-form analytical approximation for the mean source temperature is the shorter computational time compared with using the numerical integration. For example, the computational time required to compute the mean source temperature using Eq. (4.48) is found to be approximately 0.05 s, while the computational time when using the numerical integration is found to be more

than 10 s for some cases.

4.3.2 Convective Sink

In the second study, the analytical solution is used to study the influence of the temperature-dependent thermal conductivity for flux channels with a uniform heat transfer coefficient along the sink plane. The same previous flux channel shown in Fig. 4.3 with the same channel's configuration is considered but by assuming a uniform heat transfer coefficient along the sink plane $h_s = 500$ W/m^2·K. For this flux channel, the average sink-plane reference temperature can be obtained using Eq. (4.27) as $T_0 = 500$ K which has been used as the reference temperature in the Kirchhoff transform. In the analytical solution, the number of terms used in the infinite Fourier series summations for the linear system solution is taken the same as the previous study of 500 terms in each of the summations without any loss in accuracy and the computational time required to compute the temperature at any point in the source plane is of approximately 0.03 s. Further, the FEM results are obtained with a tetrahedral mesh consisting of approximately 9.2×10^4 elements. Figures 4.7-4.9 show the source plane temperature profiles along the x-axis when $y = Y_c$ for the three different conductivity functions with different parameters, where the effect of the temperature-dependent thermal conductivity on the temperature rise can be seen.

The accuracy of the analytical solution by using the average sink plane as a reference temperature in the Kirchhoff transform can be seen in Table 4.2. The results show very good agreement between the analytical and FEM results of a relative error within 0.2% for all the results. However, it is more advantageous to consider the analytical solutions since the numerical solutions are time consuming and less flexible for optimization studies compared to using the closed-form analytical solution.

Although the previous study shows the use of the Kirchhoff transform for solving

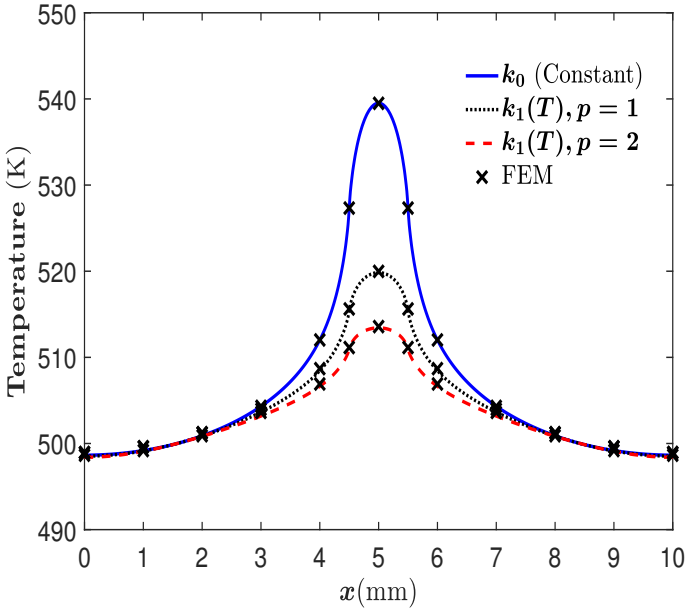

Figure 4.7: Temperature profile along x-axis in the source plane (at $y = Y_c$) by considering $k_1(T)$ with $\omega_1 = 0.1$ for the convective-sink study with $h_s = 500$ W/m^2·K.

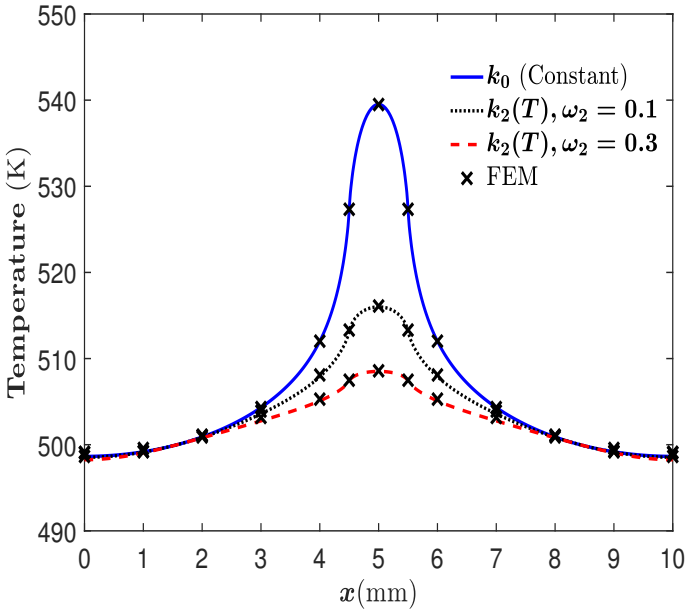

Figure 4.8: Temperature profile along x-axis in the source plane (at $y = Y_c$) by considering $k_2(T)$ for the convective-sink study with $h_s = 500$ W/m^2·K.

spreading heat problems with convective-sink boundary conditions, the applicability of the method may have larger errors for some cases, such as extremely thin flux

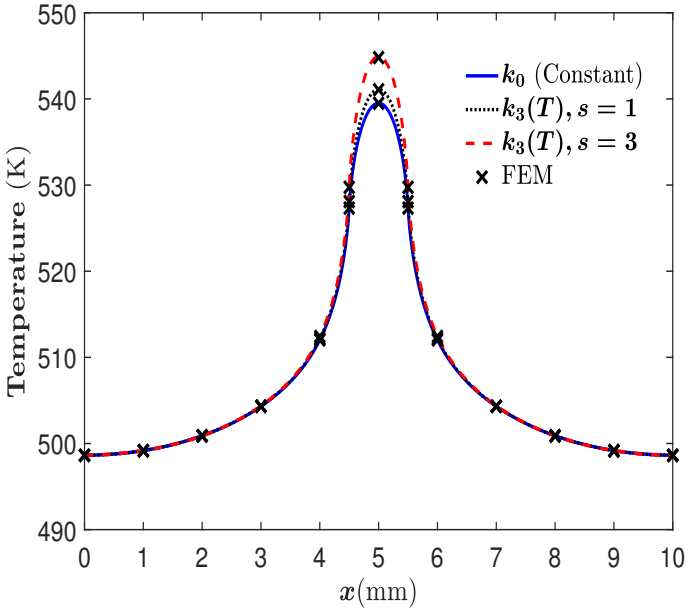

Figure 4.9: Temperature profile along x-axis in the source plane (at $y = Y_c$) by considering $k_3(T)$ for the convective-sink study with $h_s = 500$ W/m^2·K.

	Analytical			**FEM**	
$k(T)$ (W/m·K)	$\hat{T}$ (K)	$\bar{T}_c$ (K)	$\bar{T}_c$(approx.) (K)	$\hat{T}$ (K)	$\bar{T}_c$ (K)
k_0	539.506	533.435	533.435	539.49	533.22
$k_1(T), p = 1$	519.835	517.684	517.799	519.98	517.778
$k_1(T), p = 2$	513.424	512.228	512.317	513.57	512.347
$k_2(T), \omega_2 = 0.1$	515.995	514.640	514.769	516.1	514.708
$k_2(T), \omega_2 = 0.3$	508.512	507.981	508.039	508.58	508.039
$k_3(T), s = 1$	541.109	534.590	534.538	541.07	534.349
$k_3(T), s = 3$	544.904	537.276	537.0455	544.8	536.956

Table 4.2: Source temperatures for the different thermal conductivity functions with $h_s = 500$ W/m^2·K and $T_\infty = 300$ K.

channels and weak conduction/convection effects, where the sink-plane temperature distribution becomes highly nonuniform. Hence, the use of the approximate uniform average sink temperature in the definition of the Kirchhoff transform may produce unreliable results. To examine this, one study is conducted to see the effect of changing the thickness of the channel on the analytical results. The same previous channel's

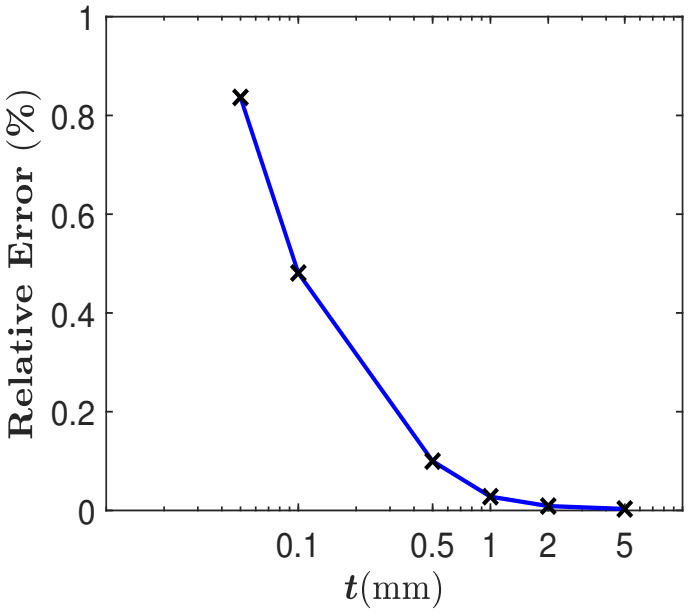

Figure 4.10: Relative error of the centroidal temperature between analytical and FEM results by considering $k_1(T)$ with $\omega_1 = 0.1$, and $p = 1$.

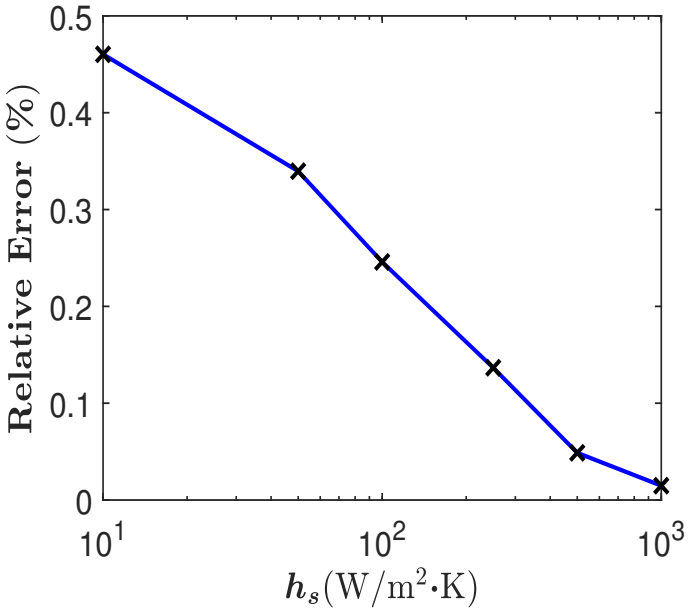

Figure 4.11: Relative error of the centroidal temperature between analytical and FEM results by considering $k_3(T)$ with $s = 3$.

configuration of the convective-sink example is considered but with varying the thickness of the channel as $0.05 \leq t \leq 5$ mm. Figure 4.10 show the relative error of the

centroidal temperature between the analytical and numerical results for different values of the thickness t by considering the thermal conductivity function $k_1(T)$. One can see that the relative error of the centroidal temperature between the analytical and FEM results increases as the thickness of the channel decreases.

Another study is conducted to see the effects of the heat-source position and the weak conduction/convection on the analytical results. The configuration shown in Fig. 4.3 is considered with the same heat source dimensions but the center is located at the point $(X_c, Y_c) = (2, 5)$ mm. The effects of the weak conduction/convection on the centroidal temperature of the heat source are examined. The heat transfer coefficient along the sink plane is varied as $10 \leq h_s \leq 10^3$ W/m^2·K, whereas the ratio between the heat transfer coefficient h_s and the reference thermal conductivity k_0 is kept fixed ($k_0/h_s = 0.3$). Figure 4.11 shows the relative error of the centroidal temperature between the analytical and numerical results for different values of the heat transfer coefficient by considering the thermal conductivity function $k_3(T)$ with $s = 3$. One can see that the relative error of the centroidal temperature between the analytical and FEM results increases as the heat transfer coefficient (and the reference thermal conductivity) decreases.

4.4 Conclusion

In this chapter, the effects of temperature-dependent thermal conductivities on the temperature rise and thermal resistance of a 3D flux channel was studied analytically by means of the Kirchhoff transform for different thermal conductivity functions. A significant change in the temperature rise and thermal resistance has been observed when considering different thermal conductivity functions compared to using a constant thermal conductivity. The results were validated by comparing the analytical

results with results obtained by solving the problem numerically based on the FEM using the ANSYS commercial software package [22] in which a very good agreement has been shown. In addition, the computational efficiency of using the analytical solution was illustrated in comparison with using the numerical solutions. Moreover, a closed-form analytical approximation of the mean source temperature that can be used in computing the total thermal resistance was presented and found to approximate the actual mean source temperature with good accuracy and less computational time.

References

[1] F. Bonani and G. Ghione, "On the application of the Kirchhoff transformation to the steady-state thermal analysis of semiconductor devices with temperature-dependent and piecewise inhomogenous thermal conductivity," *Solid-State Electron.*, vol. 38, no. 7, pp. 1409–1412, 1995.

[2] A. Karageorghis and D. Lesnic, "Steady-state nonlinear heat conduction in composite materials using the method of fundamental solutions," *Comput. Methods in Appl. Mech. Eng.*, vol. 197, pp. 3122 –3137, Jun. 2008.

[3] M. N. Özisik, *Boundary Value Problems of Heat Conduction.* Scranton, PA, USA: International Textbook, 1968.

[4] H. S. Carslaw and J. C. Jaeger, *Conduction of Heat in Solids.* UK: Oxford Univ. Press, 1959.

[5] V. S. Arpaci, *Conduction Heat Transfer.* New York, NY, USA: Addison-Wesley, 1966.

[6] J. H. Knight and J. R. Philip, "Exact solutions in nonlinear diffusion," *J. Eng. Math.*, vol. 8, no. 3, pp. 219–227, Jul. 1974.

[7] K. R. Bagnall, Y. S. Muzychka, and E. N. Wang, "Application of the Kirchhoff transform to thermal spreading problems with convection boundary conditions,"

IEEE Trans. Compon., Packag., Manuf. Technol., vol. 4, no. 3, pp. 408–420, Mar. 2014.

[8] M. M. Yovanovich, "Four decades of research on thermal contact, gap and joint resistance in microelectronics," *IEEE Trans. Compon. Packag. Technol.*, vol. 28, no. 2, pp. 182–206, Jun. 2005.

[9] Y. S. Muzychka, J. R. Culham, and M. M. Yovanovich, "Thermal spreading resistance of eccentric heat sources on rectangular flux channels," *J. Electron. Packag.*, vol. 125, no. 2, pp. 178–185, Jun. 2003.

[10] Y. S. Muzychka, M. M. Yovanovich, and J. R. Culham, "Thermal spreading resistance in compound and orthotropic systems," *J. Thermophys. Heat Transf.*, vol. 18, no. 1, pp. 45–51, Jan.-Mar. 2004.

[11] ——, "Influence of geometry and edge cooling on thermal spreading resistance," *J. Thermophys. Heat Transf.*, vol. 20, no. 2, pp. 247–255, 2006.

[12] Y. S. Muzychka, "Influence coefficient method for calculating discrete heat source temperature on finite convectively cooled substrates," *IEEE Trans. Compon. Packag. Technol.*, vol. 29, no. 3, pp. 636–643, Sep. 2006.

[13] Y. S. Muzychka, K. R. Bagnall, and E. N. Wang, "Thermal spreading resistance and heat source temperature in compound orthotropic systems with interfacial resistance," *IEEE Trans. Compon., Packag., Manuf. Technol.*, vol. 3, no. 11, pp. 1826–1841, Nov. 2013.

[14] Y. S. Muzychka, "Spreading resistance in compound orthotropic flux tubes and channels with interfacial resistance," *J. Thermophys. Heat Transf.*, vol. 28, no. 2, pp. 313–319, Mar. 2014.

[15] K. R. Bagnall, Y. S. Muzychka, and E. N. Wang, "Analytical solution for temperature rise in complex, multilayer structures with discrete heat sources," *IEEE Trans. Compon., Packag., Manuf. Technol.*, vol. 4, no. 5, pp. 817–830, May 2014.

[16] J. Ditri, "Heat conduction in microwave devices with orthotropic and temperature-dependent thermal conductivity," *IEEE Trans. Microwave Theory Tech.*, vol. 55, no. 3, pp. 555–560, Mar. 2007.

[17] P. Vadasz, "Analytical solution to nonlinear thermal diffusion: Kirchhoff versus Cole-Hopf transformations," *J. Heat Transf.*, vol. 132, no. 12, pp. 121 302–1–121 302–6, Dec. 2010.

[18] L. M. Jiji, *Heat Conduction.* Berlin, Germany: Springer, 2009.

[19] S. Kakac and Y. Yener, *Heat Conduction, 3rd ed.* Malabar, FL, USA: Taylor & Francis, 1993.

[20] M. M. Yovanovich, Y. S. Muzychka, and J. R. Culham, "Spreading resistance in isoflux rectangles and strips on compound flux channels," *J. Thermophys. Heat Transf.*, vol. 13, no. 4, pp. 495–500, 1999.

[21] MATLAB Release 2016b, The MathWorks, Inc., Natick, MA, USA, 2016.

[22] ANSYS® Release 16.2, ANSYS, Inc., Canonsburg, PA, USA, 2015.

[23] B. Vermeersch and G. De Mey, "Dependency of thermal spreading resistance on convective heat transfer coefficient," *Microelectron. Reliab.*, vol. 48, no. 5, pp. 734–738, May 2008.

Statement of co-authorship

This statement describes the authors' research contributions in the following journal manuscript.

Title: **Spreading Resistance in Multilayered Orthotropic Flux Channels with Different Conductivities in the Three Spatial Directions**
Located in Chapter 5.

The following people contributed to the conception of this paper:
Author 1: Belal Al-Khamaiseh
Author 2: Dr. Yuri S. Muzychka
Author 3: Dr. Serpil Kocabiyik

Belal Al-Khamaiseh was the primary author of this research. He played a major role in conducting an extensive literature search, constructing the mathematical model, developing the analytical solutions, conducting the computational part, analyzing the results, and comparing the analytical results with numerical results for verification purposes. Dr. Yuri S. Muzychka played a significant role in presenting the idea of the research and together he and Dr. Serpil Kocabiyik contributed to the conception, design, and revised versions of this paper. They also guided the analytical and computational components of this research.

Chapter 5

Spreading Resistance in Multilayered Orthotropic Flux Channels with Different Conductivities in the Three Spatial Directions

5.1 Introduction

Thermal management is considered as a key factor in the development of power devices and microelectronic systems for better performance and device functionality. A good understanding of the effects of materials' properties used for designing the device on

Published in the ASME-Journal of Heat Transfer [1].

temperature rise and thermal resistance is essential to design a durable device. Thermal spreading resistance, which occurs when heat enters the system through small region(s) and flows by conduction through the system to spread the heat out into a larger heat-sink area, is an increasingly important topic in thermal management. There have been some interesting and new materials that have emerged recently in the development of microelectronic devices due to their superior properties. These materials include β-Gallium-oxide (β-Ga_2O_3) [2], Black Phosphorus (BP) [3–5], and Tungsten telluride (WTe_2) [6], which are known to have anisotropic thermal conductivity tensors. In particular, β-Ga_2O_3 is considered an attractive material for high-power device applications, such as field-effect transistors (FETs) and light-emitting diodes (LEDs), due to its superior material properties [2, 7, 8]. Despite the fact that β-Ga_2O_3 has excellent electrical properties, it has relatively low thermal conductivities that range from 11 W/m·K to 27 W/m·K at room temperature along the three principal directions [7]. Hence, thermal management in β-Ga_2O_3-based power devices is essential. Black Phosphorus has also attracted much attention in the development of microelectronic devices and is considered a promising semiconducting material for the new generation of smaller and flexible devices.

Different analytical and numerical studies have been conducted to study the temperature rise and thermal resistance for different heat spreading problems. However, numerical methods are less efficient for most problems compared to using a closed-form analytical solution since they are time consuming and are less flexible for the optimization of the device layout to reduce thermal resistance [9].

Many relevant studies can be found in the literature on this topic. Kennedy [10] started the research on thermal spreading resistance of cylindrical shaped semiconductor devices. Kokkas [11] studied thermal analysis in multilayered rectangular

structures with isotropic materials. Yovanovich [12–14] studied different spreading resistance problems including flux channels and flux tubes with finite and semi-infinite geometries. He summarized the most important models of thermal spreading resistance for more than forty years in a review paper [15]. Muzychka et al. [16–21] have done extensive research on different thermal spreading resistance problems, including different geometries, boundaries, and properties. In most of the existing work, attention has been focused on problems with isotropic materials. Gholami and Bahrami [22] obtained analytical solution for the spreading resistance of a single-layer flux channel with orthotropic properties. Recently, Muzychka et al. [19] analytically modeled the thermal spreading resistance for compound transversely isotropic two-layer systems with equal thermal conductivities in the in-plane directions that are different than the through-plane thermal conductivity (i.e., $k_x = k_y \neq k_z$). Bagnall et al. [23] developed an analytical solution for the thermal spreading resistance in multilayered flux channels with isotropic and transversely isotropic properties.

In this chapter, general analytical solutions for the temperature distribution and thermal resistance in a multilayered orthotropic flux channel consisting of N-layers with different thermal conductivities in the three spatial directions (i.e., $k_x \neq k_y \neq k_z$) in each layer are obtained. The solutions account for the effect of interfacial resistance or contact conductance between the adjacent layers. Moreover, an extension of the problem to consider multiple eccentric heat sources in the source plane is also considered.

5.2 Mathematical Theory

In this section, the problem statement is mathematically illustrated by the governing equations of temperature distributions along with the appropriate boundary conditions, then the analytical solution of the problem is presented after applying special transformations on the governing equations. The total thermal resistance is then introduced based on the analytical solution of the temperature distribution. Then the solution is extended to account for multiple heat sources in the source plane.

5.2.1 Mathematical Formulation of the Problem

The problem under consideration is a three-dimensional (3D) rectangular flux channel consisting of N-layers with an eccentric heat source in the source plane and a convective cooling along the sink plane, whereas all the lateral edges are assumed to be adiabatic. Each layer is assumed to be orthotropic with different thermal conductivities in the three spatial directions (x, y, z). An interfacial contact conductance h_{c_i} is considered between the adjacent layers (layer i and $i+1$) to model the effects of surface roughness, imperfect contact, or the intrinsic phonon mismatch between dissimilar materials, as shown in Fig. 5.1. The system is modeled using a local system of coordinates for each layer in which the xy-plane have the same coordinates in all the layers with $0 < x < c$ and $0 < y < d$, while the through-plane direction (z) is different for each layer. This approach is used as it facilitates the stretched coordinate transformations and produces a convenient form of the general solution [19].

By defining the temperature excess $\theta = T - T_\infty$ relative to the ambient temperature (T_∞), the governing equation in each layer is Laplace's equation. Hence, the following system of equations represents the governing equations for the N-layers:

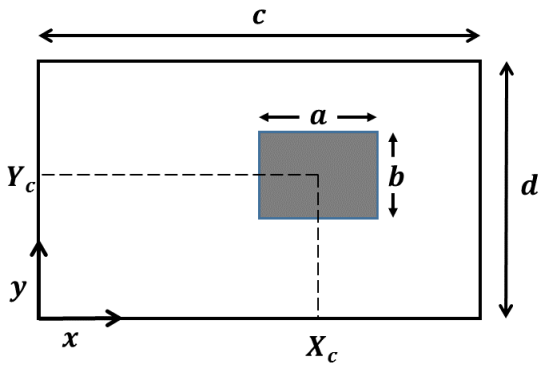

(a)

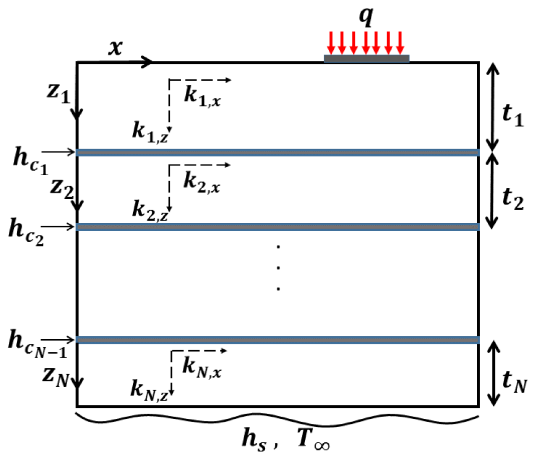

(b)

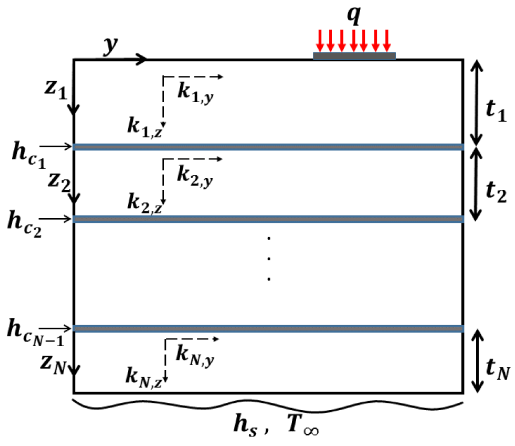

(c)

Figure 5.1: Schematic view of a 3D flux channel layout. (a) Top view. (b) Cross-sectional view in the xz-plane. (c) Cross-sectional view in the yz-plane.

$$
\begin{aligned}
k_{1,x}\frac{\partial^2\theta_1}{\partial x^2} + \;& k_{1,y}\frac{\partial^2\theta_1}{\partial y^2} + \;& k_{1,z}\frac{\partial^2\theta_1}{\partial z_1^2} = 0, \quad & 0 < z_1 < t_1, \\
k_{2,x}\frac{\partial^2\theta_2}{\partial x^2} + \;& k_{2,y}\frac{\partial^2\theta_2}{\partial y^2} + \;& k_{2,z}\frac{\partial^2\theta_2}{\partial z_2^2} = 0, \quad & 0 < z_2 < t_2, \\
& \vdots & & \vdots \\
k_{N,x}\frac{\partial^2\theta_N}{\partial x^2} + & k_{N,y}\frac{\partial^2\theta_N}{\partial y^2} + & k_{N,z}\frac{\partial^2\theta_N}{\partial z_N^2} = 0, \quad & 0 < z_N < t_N,
\end{aligned} \tag{5.1}
$$

with different thermal conductivities in each direction, *i.e.*, $k_x \neq k_y \neq k_z$ for each layer. The following boundary conditions based on the configuration shown in Fig. 5.1 are considered. In the source plane, a uniform heat flux is specified over the heat-source region where the heat source is considered as of rectangular shape with dimensions a and b in the x- and y-directions, respectively, while the remainder of the source plane is considered as adiabatic. Hence, the source-plane boundary condition is given by:

$$
-k_{1,z}\frac{\partial\theta_1}{\partial z_1}\bigg|_{z_1\,=\,0} = \begin{cases} q, & \text{inside source region,} \\ 0, & \text{outside source region.} \end{cases} \tag{5.2}
$$

At the interface between the adjacent layers, the following conditions are considered (for $i = 1, 2, \ldots, N-1$), representing the continuity of heat flux and the temperature drop due to the interfacial conductance, respectively:

$$
k_{i,z}\frac{\partial\theta_i}{\partial z_i}\bigg|_{z_i\,=\,t_i} = k_{i+1,z}\frac{\partial\theta_{i+1}}{\partial z_{i+1}}\bigg|_{z_{i+1}\,=\,0}, \tag{5.3}
$$

$$
-k_{i,z}\frac{\partial\theta_i}{\partial z_i}\bigg|_{z_i\,=\,t_i} = h_{c_i}\left[\theta_i(x,y,t_i) - \theta_{i+1}(x,y,0)\right]. \tag{5.4}
$$

The temperature drop condition in Eq. (5.4) might be replaced by the following condition in the case of a high value of the interfacial conductance $h_{c_i} \longrightarrow \infty$ (continuity

of temperature excess):

$$\theta_i(x, y, t_i) = \theta_{i+1}(x, y, 0). \tag{5.5}$$

Along the sink plane, a uniform heat transfer coefficient h_s exists and the boundary condition is given by:

$$-k_{N,z}\frac{\partial \theta_N}{\partial z_N}\bigg|_{z_N\,=\,t_N} = h_s\theta_N(x, y, t_N). \tag{5.6}$$

The lateral edges of the system are assumed to be adiabatic. The lateral-edge boundary conditions are:

$$\frac{\partial \theta_i}{\partial x}\bigg|_{x\,=\,0,\,c} = 0, \quad \frac{\partial \theta_i}{\partial y}\bigg|_{y\,=\,0,\,d} = 0, \quad i = 1, 2, \ldots, N. \tag{5.7}$$

The problem statement along with the governing equations and boundary conditions is now completely illustrated. We then proceed to apply stretched coordinate transformations in order to present the problem in a simpler solvable form.

5.2.2 Transformations (Stretched Coordinates)

Stretched coordinate transformations can be used as a powerful technique to transform orthotropic systems into equivalent isotropic systems [24]. Muzychka et al. [19, 25] implemented a system of stretched coordinates for a flux channel consisting of two transversely isotropic layers with equal in-plane thermal conductivities $k_x = k_y$ that are different than the through-plane conductivity, i.e., $k_x = k_y \neq k_z$, of each layer. The application of the following transformations for each layer (for $i = 1, 2, \ldots, N$):

$$\text{Layer } i: \quad y_i = y/\sqrt{k_{i,y}/k_{i,x}}, \quad \zeta_i = z_i/\sqrt{k_{i,z}/k_{i,x}}, \tag{5.8}$$

leads to the definition of the following effective isotropic properties:

$$\text{Layer } i: \quad k_i = \sqrt{k_{i,x}k_{i,z}}, \quad \bar{t}_i = t_i/\sqrt{k_{i,z}/k_{i,x}}, \quad \bar{d}_i = d/\sqrt{k_{i,y}/k_{i,x}}. \tag{5.9}$$

Under these transformations, the system of governing equations in Eq. (5.1) becomes:

$$\frac{\partial^2\theta_i}{\partial x^2} + \frac{\partial^2\theta_i}{\partial y_i^2} + \frac{\partial^2\theta_i}{\partial \zeta_i^2} = 0, \quad 0 < x < c, \quad 0 < y_i < \bar{d}_i, \quad 0 < \zeta_i < \bar{t}_i. \tag{5.10}$$

Although the direct application of the transformations in Eq. (5.8) is able to transform the governing equations in Eq. (5.1) into an equivalent set of equations given in Eq. (5.10) with isotropic properties, a problem appears when trying to transform the interface boundary conditions given by Eqs. (5.3) and (5.4) using these transformations because we have different stretched coordinates in the y-direction for each layer with different dimensions. In other words, each y_i's coordinates are different. It is important to note that when the in-plane conductivities are equal, i.e., $k_{i,x} = k_{i,y}$, in each layer, the new stretched coordinates in the y-direction are the same for all the layers and equal to the original coordinate, i.e., $y_i = y$; hence, the interface boundary conditions can be transformed directly as in [19, 25]. However, in order to solve the problem in general with different conductivities in the three directions, a second transformation is applied. The y-direction stretched coordinates (y_i) in layers $i = 2, 3, \ldots, N$ can be transformed to the stretched coordinate of the first layer (y_1) by using:

$$y_i = \sqrt{\mu_i}\, y_1, \quad \text{with} \quad \mu_i = \frac{k_{1,x}k_{i,y}}{k_{1,y}k_{i,x}}, \quad i = 2, 3, \ldots, N. \tag{5.11}$$

Hence, the system of equations and boundary conditions given in Eqs. (5.1) – (5.7) can be transformed by using Eqs. (5.8) and (5.11) into the following system:

$$\begin{aligned}
\frac{\partial^2\theta_1}{\partial x^2} + \quad \frac{\partial^2\theta_1}{\partial y_1^2} + \frac{\partial^2\theta_1}{\partial \zeta_1^2} &= 0, \qquad 0 < \zeta_1 < \bar{t}_1 \\
\frac{\partial^2\theta_i}{\partial x^2} + \frac{1}{\mu_i}\frac{\partial^2\theta_i}{\partial y_1^2} + \frac{\partial^2\theta_i}{\partial \zeta_i^2} &= 0, \qquad \begin{matrix} 0 < \zeta_i < \bar{t}_i \\ i = 2, 3, \ldots, N \end{matrix}
\end{aligned} \tag{5.12}$$

with $0 < x < c$ and $0 < y_1 < \bar{d}_1$, and subject to the following boundary conditions:

$$-k_1 \frac{\partial\theta_1}{\partial\zeta_1}\bigg|_{\zeta_1\,=\,0} = \begin{cases} q, & \text{inside transformed source region,} \\ 0, & \text{outside transformed source region} \end{cases} \tag{5.13}$$

at the source plane, while the interfacial boundary conditions are transformed to:

$$k_i \frac{\partial\theta_i}{\partial\zeta_i}\bigg|_{\zeta_i\,=\,\bar{t}_i} = k_{i+1}\frac{\partial\theta_{i+1}}{\partial\zeta_{i+1}}\bigg|_{\zeta_{i+1}\,=\,0}, \tag{5.14}$$

$$-k_i \frac{\partial\theta_i}{\partial\zeta_i}\bigg|_{\zeta_i\,=\,\bar{t}_i} = h_{c_i}\left[\theta_i(x, y_1, \bar{t}_i) - \theta_{i+1}(x, y_1, 0)\right]. \tag{5.15}$$

Along the sink plane, we have:

$$-k_N \frac{\partial\theta_N}{\partial\zeta_N}\bigg|_{\zeta_N\,=\,\bar{t}_N} = h_s\theta_N(x, y_1, \bar{t}_N), \tag{5.16}$$

and for the lateral-edge boundary conditions, we get:

$$\frac{\partial\theta_i}{\partial x}\bigg|_{x\,=\,0,\,c} = 0, \quad \frac{\partial\theta_i}{\partial y_1}\bigg|_{y_1\,=\,0,\,\bar{d}_1} = 0, \quad i = 1, 2, \ldots, N. \tag{5.17}$$

The problem is now in a convenient solvable form. To summarize, the multilayered system of orthotropic layers represented by Eqs. (5.1)-(5.7) has been transformed into an equivalent, simpler system of equations given by Eqs. (5.12)-(5.17) using two transformations. The two transformations associated with Eqs. (5.8) and (5.11), which represent an expansion of the ones introduced by Muzychka et al. in [19, 25], can be

combined by applying only one transformation given by:

$$\text{Layer } i: \quad y_1 = y/\sqrt{k_{1,y}/k_{1,x}}, \quad \zeta_i = z_i/\sqrt{k_{i,z}/k_{i,x}}, \tag{5.18}$$

after which, some simple mathematics can be used to obtain the form given in Eqs. (5.12)-(5.17). It is important to note that although the transformed system is not fully isotropic (because of the existence of the parameters μ_i), the general solution can be obtained using the method of separation of variables in the same manner of solving isotropic system with a slightly different form, as we will see in the following section.

5.2.3 General Solution

The general solution of the first layer temperature excess distribution θ_1 can be found by using the method of separation of variables [26–28], where the solution is assumed to have the form $\theta_1(x, y_1, \zeta_1) = X_1(x) \cdot Y_1(y_1) \cdot Z_1(\zeta_1)$. Applying the method of separation of variables to the first governing equation in Eq. (5.12) and using the boundary conditions along $(x = 0,\ x = c)$ and $(y_1 = 0,\ y_1 = \bar{d}_1)$ yields the following general solution:

$$\begin{aligned}
\theta_1(x, y_1, \zeta_1) = {} & A^1_{00} + B^1_{00}\zeta_1 \\
& + \sum_{m=1}^{\infty} \cos(\lambda^1_m x) \left[A^1_{m0} \cosh(\lambda^1_m \zeta_1) + B^1_{m0} \sinh(\lambda^1_m \zeta_1)\right] \\
& + \sum_{n=1}^{\infty} \cos(\delta^1_n y_1) \left[A^1_{0n} \cosh(\delta^1_n \zeta_1) + B^1_{0n} \sinh(\delta^1_n \zeta_1)\right] \\
& + \sum_{m=1}^{\infty}\sum_{n=1}^{\infty} \cos(\lambda^1_m x)\cos(\delta^1_n y_1) \left[A^1_{mn} \cosh(\beta^1_{mn} \zeta_1) + B^1_{mn} \sinh(\beta^1_{mn} \zeta_1)\right],
\end{aligned} \tag{5.19}$$

where $\lambda_m^1 = m\pi/c$, $\delta_n^1 = n\pi/\bar{d}_1$, and $\beta_{mn}^1 = \sqrt{(\lambda_m^1)^2 + (\delta_n^1)^2}$. The general solution contains four components: a uniform flow solution, and three spreading solutions represented by the series components that vanish when the heat-source area is equal to the sink-plane area (the heat flux is distributed over the entire source-plane surface $\zeta_1 = 0$). The solution for the temperature excess in the other layers (layer $2, 3, \ldots, N$) can be obtained by solving the corresponding governing equations given in Eq. (5.12) also by using the method of separation of variables. It is important to note that in these layers, the governing equations of θ_i are different in the general form than the first one of θ_1. However, the general solution of θ_i may be obtained in the same manner with new eigenvalues that can be related to the eigenvalues of the solution of θ_1. This can be done by assuming the general solution to have the form $\theta_i(x, y_1, \zeta_i) = X_i(x) \cdot Y_i(y_1) \cdot Z_i(\zeta_i)$. Applying the method of separation of variables to the governing equations in Eq. (5.12) and using the boundary conditions along $(x = 0,\ x = c)$ and $(y_1 = 0,\ y_1 = \bar{d}_1)$ yield the following general solution for the ith layer:

$$\begin{aligned}\theta_i(x, y_1, \zeta_i) = {} & A_{00}^i + B_{00}^i \zeta_i \\ & + \sum_{m=1}^{\infty} \cos(\lambda_m^1 x) \left[A_{m0}^i \cosh(\lambda_m^i \zeta_i) + B_{m0}^i \sinh(\lambda_m^i \zeta_i)\right] \\ & + \sum_{n=1}^{\infty} \cos(\delta_n^1 y_1) \left[A_{0n}^i \cosh(\delta_n^i \zeta_i) + B_{0n}^i \sinh(\delta_n^i \zeta_i)\right] \\ & + \sum_{m=1}^{\infty}\sum_{n=1}^{\infty} \cos(\lambda_m^1 x)\cos(\delta_n^1 y_1) \left[A_{mn}^i \cosh(\beta_{mn}^i \zeta_i) + \ B_{mn}^i \sinh(\beta_{mn}^i \zeta_i)\right],\end{aligned} \tag{5.20}$$

where $\lambda_m^i = \lambda_m^1$, $\delta_n^i = \delta_n^1/\sqrt{\mu_i}$, and $\beta_{mn}^i = \sqrt{{\lambda_m^i}^2 + {\delta_n^i}^2} = \sqrt{(\lambda_m^1)^2 + (\delta_n^1)^2/\mu_i}$. Equations (5.19) and (5.20) represent the general solution of the temperature excess in the

first and ith (for $i = 2, 3, \ldots, N$) layers, respectively, after applying the lateral boundary conditions. The interfacial and sink-plane boundary conditions are then used to find a relationship between the Fourier coefficients A^i_{mn} and B^i_{mn} in each layer. We follow the work of Muzychka et al. [19] and Bagnall et al. [23] in which the relationship is represented by a spreading function $\phi_i(\gamma^i)$ defined by:

$$\phi_i(\gamma^i) = -\frac{B^i_{mn}}{A^i_{mn}}, \tag{5.21}$$

where γ^i refers to any of the eigenvalues λ^i_m, δ^i_n, and β^i_{mn}. Firstly, for m, n not both equal to zero, in order to find the relationship between the ith-layer Fourier coefficients (A^i_{mn} and B^i_{mn}), represented by the spreading function $\phi_i(\gamma^i)$, it is important to note that the Fourier coefficients of θ_i depend on the Fourier coefficients of θ_{i+1} (i.e., A^i_{mn} and B^i_{mn} depend on A^{i+1}_{mn} and B^{i+1}_{mn}) when applying the interface boundary conditions; hence, the spreading function $\phi_i(\gamma^i)$ depends on the next layer's spreading function $\phi_{i+1}(\gamma^{i+1})$. Thus, we start with finding the spreading function of the Nth-layer solution, and then a backward recursive formula can be obtained to find $\phi_i(\gamma^i)$. The application of the convection boundary condition at the sink plane ($\zeta_N = \bar{t}_N$) given by Eq. (5.16) leads to:

$$\phi_N(\gamma^N) = -\frac{B^N_{mn}}{A^N_{mn}} = \frac{\gamma^N \tanh(\gamma^N \bar{t}_N) + [h_s/k_N]}{\gamma^N + [h_s/k_N]\tanh(\gamma^N \bar{t}_N)}. \tag{5.22}$$

Now, the application of the continuity of heat flux and the temperature drop boundary conditions, represented by Eqs. (5.14) and (5.15), leads to the following backward recursive relationship:

$$\phi_i(\gamma^i) = \frac{[(k_i\gamma^i)\,/\,(k_{i+1}\gamma^{i+1}) + (k_i\gamma^i/h_{c_i})\,\phi_{i+1}(\gamma^{i+1})]\tanh(\gamma^i\bar{t}_i) + \phi_{i+1}(\gamma^{i+1})}{[(k_i\gamma^i)\,/\,(k_{i+1}\gamma^{i+1}) + (k_i\gamma^i/h_{c_i})\,\phi_{i+1}(\gamma^{i+1})] + \phi_{i+1}(\gamma^{i+1})\tanh(\gamma^i\bar{t}_i)}, \tag{5.23}$$

which is simplified in the case of continuity of temperature excess boundary condition into (as $h_{c_i} \longrightarrow \infty$):

$$\phi_i(\gamma^i) = \frac{[(k_i\gamma^i)\,/\,(k_{i+1}\gamma^{i+1})]\tanh(\gamma^i\bar{t}_i) + \phi_{i+1}(\gamma^{i+1})}{[(k_i\gamma^i)\,/\,(k_{i+1}\gamma^{i+1})] + \phi_{i+1}(\gamma^{i+1})\tanh(\gamma^i\bar{t}_i)}. \tag{5.24}$$

Finally, the boundary condition at the source plane is used to find the Fourier coefficients A^i_{mn} after making use of $B^i_{mn} = -\phi_i(\gamma^i)A^i_{mn}$, starting from finding A^1_{mn} and then a forward recursive formula can be used to obtain the ith-layer Fourier coefficients A^i_{mn} if desired. The Fourier coefficients in the first layer (A^1_{mn}) are obtained by taking Fourier series expansions of the boundary condition at the source plane given by Eq. (5.13) and making use of $B^1_{mn} = -\phi_1(\gamma^1)A^1_{mn}$ to get:

$$A^1_{m0} = \frac{\bar{b}q}{\bar{d}k_1\lambda^1_m\phi_1(\lambda^1_m)} \frac{\displaystyle\int_{X_c-a/2}^{X_c+a/2} \cos(\lambda^1_m x)\,dx}{\displaystyle\int_0^c \cos^2(\lambda^1_m x)\,dx} = \frac{4Q\cos(\lambda^1_m X_c)\sin(\frac{1}{2}\lambda^1_m a)}{acdk_1\,(\lambda^1_m)^2\phi_1(\lambda^1_m)}, \tag{5.25}$$

and

$$A^1_{0n} = \frac{aq}{ck_1\delta^1_n\phi_1(\delta^1_n)} \frac{\displaystyle\int_{\overline{Y}_c-\bar{b}/2}^{\overline{Y}_c+\bar{b}/2} \cos(\delta^1_n y_1)\,dy_1}{\displaystyle\int_0^{\bar{d}} \cos^2(\delta^1_n y_1)\,dy_1} = \frac{4Q\sigma\cos(\delta^1_n\overline{Y}_c)\sin(\frac{1}{2}\delta^1_n\bar{b})}{bcdk_1(\delta^1_n)^2\phi_1(\delta^1_n)}, \tag{5.26}$$

and

$$A^1_{mn} = \frac{q}{k_1\beta^1_{mn}\phi_1(\beta^1_{mn})} \frac{\displaystyle\int_{\overline{Y}_c-\bar{b}/2}^{\overline{Y}_c+\bar{b}/2}\int_{X_c-a/2}^{X_c+a/2} \cos(\lambda^1_m x)\cos(\delta^1_n y_1)\,dxdy_1}{\displaystyle\int_0^{\bar{d}}\int_0^c \cos^2(\lambda^1_m x)\cos^2(\delta^1_n y_1)\,dxdy_1},$$

$$= \frac{16Q\sigma\cos(\lambda^1_m X_c)\sin(\frac{1}{2}\lambda^1_m a)\cos(\delta^1_n\overline{Y}_c)\sin(\frac{1}{2}\delta^1_n\bar{b})}{abcdk_1\beta^1_{mn}\lambda^1_m\delta^1_n\phi_1(\beta^1_{mn})}, \tag{5.27}$$

where $\sigma = \sqrt{k_{1,y}/k_{1,x}}$, $\bar{b} = b/\sigma$, $\bar{Y}_c = Y_c/\sigma$, and $Q = abq$ is the total heat input of the flux channel. Equations (5.25)-(5.27) represent the Fourier coefficients of the first-layer solution for m, n not both equal to zero. To find the Fourier coefficients of the other layers, the following forward recursive formula can be used:

$$A_{mn}^{i+1} = A_{mn}^{i} \left(\frac{\cosh(\gamma^i \bar{t}_i) - \phi_i(\gamma^i) \sinh(\gamma^i \bar{t}_i)}{1 + \frac{k_{i+1}\gamma^{i+1}}{h_{c_i}} \phi_{i+1}(\gamma^{i+1})} \right). \tag{5.28}$$

When $m,\ n$ are both zeros, the zeroth-order Fourier coefficients in the first layer (A_{00}^1 and B_{00}^1) can be found by applying the sink-plane boundary condition and taking the Fourier expansion in the source plane after relating the coefficients between the adjacent layers to get:

$$\begin{aligned} A_{00}^1 &= \frac{Q}{cd} \left[\sum_{l=1}^{N-1} \left(\frac{\bar{t}_l}{k_l} + \frac{1}{h_{c_l}} \right) + \frac{\bar{t}_N}{k_N} + \frac{1}{h_s} \right], \\ B_{00}^1 &= -\frac{Q}{cdk_1}. \end{aligned} \tag{5.29}$$

Moreover, the zeroth-order Fourier coefficients in the other layers (A_{00}^i and B_{00}^i) can be obtained as:

$$\begin{aligned} A_{00}^i &= \frac{Q}{cd} \left[\sum_{l=i}^{N-1} \left(\frac{\bar{t}_l}{k_l} + \frac{1}{h_{c_l}} \right) + \frac{\bar{t}_N}{k_N} + \frac{1}{h_s} \right], \\ B_{00}^i &= -\frac{Q}{cdk_i}. \end{aligned} \tag{5.30}$$

From the previous discussion, the analytical solution for the temperature excess in each layer is illustrated completely along with the proper recursive formulas, which can be used for finding the Fourier coefficients. However, the solution in the first layer $\theta_1(x, y_1, \zeta_1)$ (in particular, the solution in the source plane at $\zeta_1 = 0$) is of most interest for finding the maximum temperature and the total thermal resistance of the

flux channel, which is addressed by:

$$\theta_1(x, y_1, 0) = A^1_{00} + \sum_{m=1}^{\infty} A^1_{m0} \cos(\lambda^1_m x) + \sum_{n=1}^{\infty} A^1_{0n} \cos(\delta^1_n y_1) + \sum_{m=1}^{\infty}\sum_{n=1}^{\infty} A^1_{mn} \cos(\lambda^1_m x) \cos(\delta^1_n y_1), \tag{5.31}$$

and can be transformed back for convenience to the original coordinates, i.e., x and y, by making use of Eq. (5.8) to get:

$$\theta_1(x, y, 0) = A^1_{00} + \sum_{m=1}^{\infty} A^1_{m0} \cos(\lambda^1_m x) + \sum_{n=1}^{\infty} A^1_{0n} \cos(\delta^1_n y/\sigma) + \sum_{m=1}^{\infty}\sum_{n=1}^{\infty} A^1_{mn} \cos(\lambda^1_m x) \cos(\delta^1_n y/\sigma). \tag{5.32}$$

5.2.4 Total Thermal Resistance

For a single heat source spreading to a larger extended sink area, the total thermal resistance can be defined by [16, 19]:

$$R_t = \frac{\overline{T}_c - T_\infty}{Q} = \frac{\bar{\theta}_c}{Q} = R_{1D} + R_{sp}, \tag{5.33}$$

where $\overline{T}_c$ is the heat-source contact mean temperature, $\bar{\theta}_c$ is the mean heat-source contact temperature excess, R_{1D} is the one-dimensional (1D) resistance and R_{sp} is the spreading resistance. The mean source temperature excess is given by:

$$\bar{\theta}_c = \frac{1}{A_c} \iint_{A_c} \theta_1(x, y, 0)\, dA_c, \tag{5.34}$$

where $A_c = ab$ is the heat-source area. The application of Eq. (5.34) to the source-plane solution given by Eq. (5.32) yields:

$$\bar{\theta}_c = A^1_{00} + 2\sum_{m=1}^{\infty} A^1_{m0}\frac{\cos(\lambda^1_m X_c)\sin(\frac{1}{2}\lambda^1_m a)}{a\lambda^1_m} + 2\sum_{n=1}^{\infty} A^1_{0n}\frac{\sigma\cos(\delta^1_n \overline{Y}_c)\sin(\frac{1}{2}\delta^1_n \bar{b})}{b\delta^1_n} + 4\sum_{m=1}^{\infty}\sum_{n=1}^{\infty} A^1_{mn}\frac{\sigma\cos(\lambda^1_m X_c)\sin(\frac{1}{2}\lambda^1_m a)\cos(\delta^1_n \overline{Y}_c)\sin(\frac{1}{2}\delta^1_n \bar{b})}{a\lambda^1_m b\delta^1_n}. \tag{5.35}$$

Thus, the total thermal resistance can be obtained by using Eq. (5.33) as:

$$R_t = R_{1D} + \sum_{m=1}^{\infty} R_{m0} + \sum_{n=1}^{\infty} R_{0n} + \sum_{m=1}^{\infty}\sum_{n=1}^{\infty} R_{mn}, \tag{5.36}$$

where,

$$R_{1D} = \frac{1}{cd}\left[\sum_{l=1}^{N-1}\left(\frac{\bar{t}_l}{k_l} + \frac{1}{h_{c_l}}\right) + \frac{\bar{t}_N}{k_N} + \frac{1}{h_s}\right], \tag{5.37}$$

and

$$R_{m0} = \frac{8\cos^2(\lambda^1_m X_c)\sin^2(\frac{1}{2}\lambda^1_m a)}{a^2 cdk_1\ (\lambda^1_m)^3\phi_1(\lambda^1_m)}, \tag{5.38}$$

and

$$R_{0n} = \frac{8\sigma^2\cos^2(\delta^1_n \overline{Y}_c)\sin^2(\frac{1}{2}\delta^1_n \bar{b})}{b^2 cdk_1(\delta^1_n)^3\phi_1(\delta^1_n)}, \tag{5.39}$$

and

$$R_{mn} = \frac{64\sigma^2\cos^2(\lambda^1_m X_c)\sin^2(\frac{1}{2}\lambda^1_m a)\cos^2(\delta^1_n \overline{Y}_c)\sin^2(\frac{1}{2}\delta^1_n \bar{b})}{a^2 b^2 cdk_1\beta^1_{mn}(\lambda^1_m)^2(\delta^1_n)^2\phi_1(\beta^1_{mn})}. \tag{5.40}$$

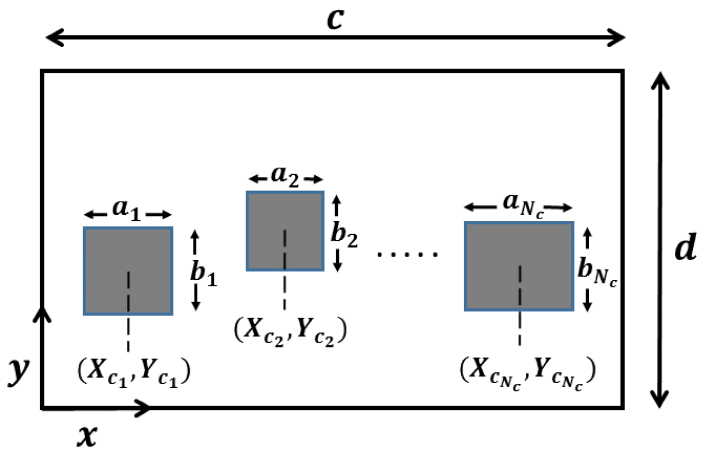

Figure 5.2: Top view a 3D flux channel with multiple heat sources along the source plane.

5.2.5 Extension to Multiple Heat Sources

Consider a system with the same previous discussed configuration except in the heat-source boundary condition. Instead of considering one heat source, we extend the the problem to have a finite number of N_c heat sources distributed nonuniformly along the source plane, as shown in Fig. 5.2. The new source-plane boundary condition is represented by a uniform heat flux q_j specified over the jth heat source (for $j = 1, 2, \ldots, N_c$), while outside the heat-source regions the adiabatic condition is considered. Thus, the heat-source boundary condition is rewritten as:

$$-k_{1,z}\frac{\partial\theta_1}{\partial z_1}\bigg|_{z_1\,=\,0} = \begin{cases} q_j, & \text{inside } j\text{th source region,} \\ 0, & \text{outside source regions.} \end{cases} \tag{5.41}$$

The general solution of the extended problem can be obtained by splitting the problem into N_c problems with a single heat source for each problem and then the general solution can be written as a superposition of these individual solutions. However, it is more convenient and computationally efficient to solve the multiple-heat-source

problem as one problem in which the Fourier coefficients are to be calculated for only one solution instead of finding the Fourier coefficients for N_c problems and then using the superposition. In fact, the same result can be obtained when the individual solutions of the superposition are combined together into one solution. The general solution of the multiple-heat-source problem is the same as the general solution for the single-heat-source problem given in Eqs. (5.19) and (5.20) with the same spreading functions given in Eqs. (5.22) and (5.23). However, the only difference is in the Fourier coefficients; more precisely, the Fourier coefficients of the first-layer solution A^{*1}_{mn}, since all the other Fourier coefficients depend on A^{*1}_{mn} by a recursive formula or a spreading function. For m, n not both equal to zero, the Fourier coefficients of the first-layer solution of the multiple-heat-source problem can be obtained by using the new boundary condition in the source plane Eq. (5.41) to get:

$$A^{*1}_{m0} = \frac{4 \sum_{j=1}^{N_c} b_j q_j \cos(\lambda^1_m X_{c_j}) \sin(\frac{1}{2}\lambda^1_m a_j)}{cdk_1(\lambda^1_m)^2 \phi_1(\lambda^1_m)}, \tag{5.42}$$

and

$$A^{*1}_{0n} = \frac{4\sigma \sum_{j=1}^{N_c} a_j q_j \cos(\delta^1_n \overline{Y}_{c_j}) \sin(\frac{1}{2}\delta^1_n \bar{b}_j)}{cdk_1(\delta^1_n)^2 \phi_1(\delta^1_n)}, \tag{5.43}$$

and

$$A^{*1}_{mn} = \frac{16\sigma \sum_{j=1}^{N_c} q_j \cos(\lambda^1_m X_{c_j}) \sin(\frac{1}{2}\lambda^1_m a_j) \cos(\delta^1_n \overline{Y}_{c_j}) \sin(\frac{1}{2}\delta^1_n \bar{b}_j)}{cdk_1 \beta^1_{mn} \lambda^1_m \delta^1_n \phi_1(\beta^1_{mn})}. \tag{5.44}$$

Regarding the Fourier coefficients of the other layers, the same recursive formula in Eq. (5.28) can be used to find them after replacing A^{i+1}_{mn} and A^{i}_{mn} by A^{*i+1}_{mn} and A^{*i}_{mn}, respectively. Moreover, the zeroth-order Fourier coefficients of the first-layer solution

(A_{00}^{*1} and B_{00}^{*1}) are obtained as:

$$A_{00}^{*1} = \frac{\sum_{j=1}^{N_c} Q_j}{cd}\left[\sum_{l=1}^{N-1}\left(\frac{\bar{t}_l}{k_l}+\frac{1}{h_{c_l}}\right)+\frac{\bar{t}_N}{k_N}+\frac{1}{h_s}\right],$$
$$B_{00}^{*1} = -\frac{\sum_{j=1}^{N_c} Q_j}{cdk_1}. \tag{5.45}$$

While the zeroth-order Fourier coefficients in the other layers (A_{00}^{*i} and B_{00}^{*i}) can be obtained as:

$$A_{00}^{*i} = \frac{\sum_{j=1}^{N_c} Q_j}{cd}\left[\sum_{l=i}^{N-1}\left(\frac{\bar{t}_l}{k_l}+\frac{1}{h_{c_l}}\right)+\frac{\bar{t}_N}{k_N}+\frac{1}{h_s}\right],$$
$$B_{00}^{*i} = -\frac{\sum_{j=1}^{N_c} Q_j}{cdk_i}, \tag{5.46}$$

where $Q_j = a_j b_j q_j$ is the total heat input of the jth heat source. Furthermore, the solution in the source plane can be addressed by:

$$\theta_1^*(x,y,0) = A_{00}^{*1} + \sum_{m=1}^{\infty} A_{m0}^{*1}\cos(\lambda_m^1 x) + \sum_{n=1}^{\infty} A_{0n}^{*1}\cos(\delta_n^1 y/\sigma) + \sum_{m=1}^{\infty}\sum_{n=1}^{\infty} A_{mn}^{*1}\cos(\lambda_m^1 x)\cos(\delta_n^1 y/\sigma). \tag{5.47}$$

Finally, the total thermal resistance for the multiple-heat-source problem can be defined as [22]:

$$R_t^* = \frac{\bar{\theta}_c^*}{\sum_{j=1}^{N_c} Q_j}, \tag{5.48}$$

where $\bar{\theta}_c^*$ is the mean temperature excess of all the heat sources, as defined by:

$$\bar{\theta}_c^* = \frac{1}{\sum_{j=1}^{N_c} A_{c_j}} \sum_{j=1}^{N_c} \iint_{A_{c_j}} \theta_1^*(x, y, 0)\, dA_{c_j}, \tag{5.49}$$

5.3 Results and Discussion

In this section, different validation and parametric studies are used to verify and demonstrate the computational efficiency of the developed analytical solutions. For the purpose of verifying the analytical solutions, numerical analysis has been conducted by solving the problems numerically using the finite element method (FEM) and comparing the numerical results to the analytical results. MATLAB (version 2016b) software is used to carry out the analytical results [29], while the numerical simulations are performed based on the FEM using the ANSYS commercial software package [30].

5.3.1 Single Heat Source

We start our investigation by considering an idealized single gate field-effect transistor model consisting of three layers of Aluminum oxide, Black Phosphorus, and β-Gallium-oxide (Al_2O_3/BP/β-Ga_2O_3). The structure of the model is hypothetically constructed base on two different field-effect transistor models that have been discussed in [5, 7]. We have considered this hypothetical structure in our investigation in order to develop a multilayered structure with enough complexity to demonstrate the accuracy and computational efficiency of the analytical solutions. The model has side dimensions of $c = 28$ μm and $d = 10$ μm, while the heat-source (gate) dimensions are of $a = 2$ μm, and $b = 1$ μm. The center of the heat source is located at the point $(X_c, Y_c) = (10$ μm, 5 μm), as shown in Fig. 5.3. The multilayered structure consists of Al_2O_3 as the first layer of thickness $t_1 = 3$ μm with isotropic thermal conductivities

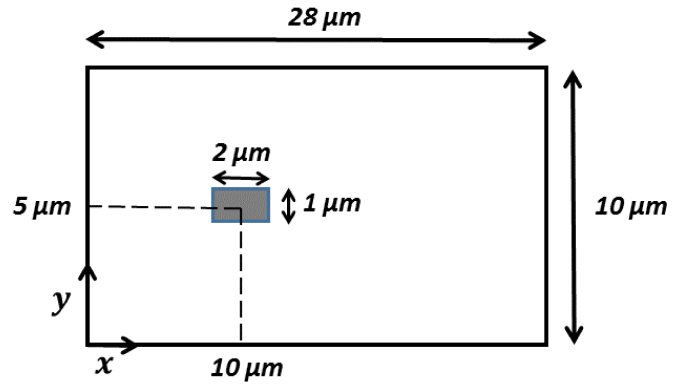

(a)

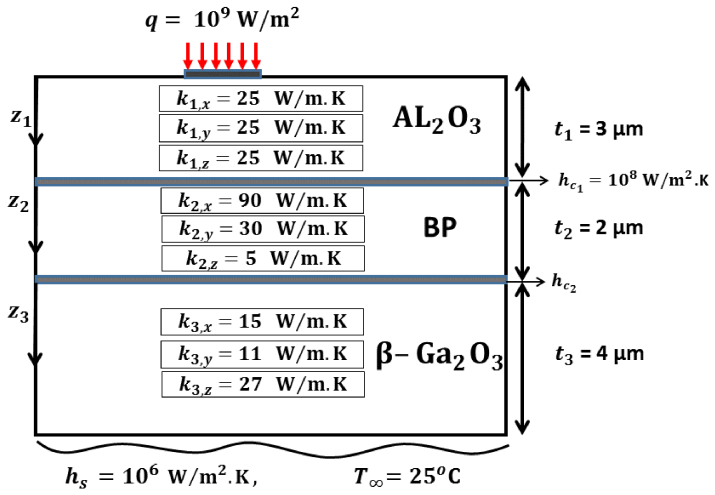

(b)

Figure 5.3: Idealized single-heat-source field-effect transistor layout. (a) Top view. (b) Cross-sectional view.

$k_{1,x} = 25$, $k_{1,y} = 25$, $k_{1,z} = 25$ W/m·K. The second BP layer is of thickness $t_2 = 2$ μm and orthotropic thermal conductivities (fixed at room temperature) $k_{2,x} = 90$, $k_{2,y} = 30$, $k_{2,z} = 5$ W/m·K [4], while the third β-Ga_2O_3 layer is of thickness $t_3 = 4$ μm and orthotropic thermal conductivities $k_{3,x} = 15$, $k_{3,y} = 11$, $k_{3,z} = 27$ W/m·K [8]. Although in practice the thickness of the layers is thinner than the chosen values in this model (varying between few nanometers to hundreds of nanometers), the relatively

thicker layers are chosen in this model to consider the 3D nature of each layer and to guarantee the convergence of the numerical FEM solution for comparison reasons. The heat transfer coefficient along the sink plane is considered as $h_s = 10^6$ W/m^2·K and the ambient temperature is of 25° C. A uniform heat flux of $q = 10^9$ W/m^2 is applied in the source region which corresponds to a uniform power dissipation of 1 W/mm (normalized to the gate length a). The interfacial conductance associated with the Al_2O_3/BP interface h_{c_1} is fixed at the value of $h_{c_1} = 10^8$ W/m^2·K, while the interfacial conductance associated with the BP/β-Ga_2O_3 interface h_{c_2} is varied as $10^6 < h_{c_2} < \infty$ W/m^2·K, where the case of $h_{c_2} \longrightarrow \infty$ indicates that the effect of the interfacial conductance is neglected and the continuity of temperature boundary condition is considered. The analytical solution is used to compute the average ($\overline{T}$) and centroidal ($\hat{T} = T(X_c, Y_c, 0)$) temperatures of the heat source and the total thermal resistance of the system for different values of the interfacial conductance h_{c_2}. The results are compared to numerical results obtained by solving the system numerically using the FEM. In the analytical solution, the number of terms used in the infinite Fourier series summation is chosen of 1000 in each of the summations and the computational time required to find any of the results ($\overline{T}$, $\hat{T}$ or R_t) is found of approximately 0.4 s. The number of terms is chosen based on a sensitivity study to see the effect of increasing the number of terms on the average and centroidal temperatures and it is found that 1000 terms in each of the summations converged with a very small relative error of less than 0.005% compared to using 10^4 terms. Figure 5.4 shows the effect of increasing the number of terms on the average and centroidal temperatures of the heat source for $h_{c_2} = 10^6$ W/m^2·K. Furthermore, the FEM numerical results are obtained with a tetrahedral mesh and the convergence is checked by refining the mesh. In particular, most of the refinement is required around the heat source and interfacial contact regions due to the rapid change in temperature around these regions.

The system with a tetrahedral mesh consisting of approximately 3.8×10^5 elements is found to be sufficient to solve the problem with a very small loss in accuracy (relative error of less than 0.1% compared to using approximately 6.5×10^5 elements) with computational time of approximately 3 min. The analytical and numerical results of the average and centroidal temperatures of the heat source and the thermal resistance of the system for different values of the interfacial conductance h_{c_2} are shown in Table 5.1 and Table 5.2, respectively. The agreement between the analytical and FEM results is considerably very good with a relative error of less than 0.3% for all the results. In addition, the effect of increasing the value of the interfacial conductance h_{c_2} is obvious, where both the temperature rise in the heat-source region and the thermal resistance of the system decrease by increasing the value of interfacial conductance. The minimum values are recorded when $h_{c_2} \longrightarrow \infty$.

Finally, one more study is conducted by changing the thermal conductivities of the first layer to $k_{1,x} = 50$, $k_{1,y} = 25$, $k_{1,z} = 15$ W/m·K. Although the thermal conductivity of the first Al_2O_3 layer is isotropic, this study is conducted as a validation study of the analytical solution with orthotropic properties in all the layers. The analytical and numerical results of the average and centroidal temperatures of the heat source for different values of the interfacial conductance h_{c_2} are shown in Table 5.3 with very good agreement. Moreover, the effect of changing the thermal conductivities on the centroidal and average temperatures is obvious compared to considering the isotropic values with differences of approximately three degrees.

5.3.2 Multiple Heat Sources

To demonstrate the computational efficiency of the developed analytical solution for multiple-heat-source problems, the same previous model for the single-heat-source problem with the same channel configuration and thermal properties shown in Fig. 5.3

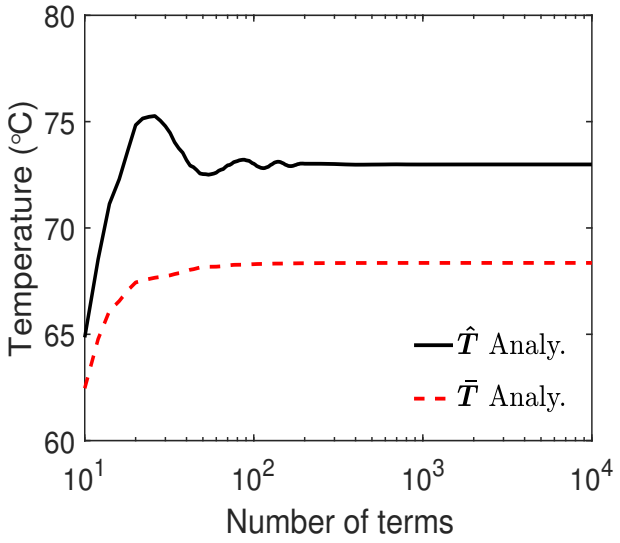

Figure 5.4: Analytical centroidal and average temperatures of the single-heat-source problem computed as a function of the number of terms in the summations for $h_{c_2} = 10^6$ W/m^2·K.

	Analytical		**FEM**	
h_{c_2} (W/m^2·K)	$\hat{T}$ (°C)	$\bar{T}$ (°C)	$\hat{T}$ (°C)	$\bar{T}$ (°C)
10^6	72.985	68.356	73.031	68.227
5×10^6	67.224	62.596	67.271	62.467
10^7	66.500	61.871	66.547	61.743
5×10^7	65.919	61.291	65.966	61.162
10^8	65.846	61.218	65.893	61.089
∞	65.773	61.145	65.827	61.083

Table 5.1: Centroidal and average temperatures of the single-heat-source validation study for $h_{c_1} = 10^8$ W/m^2·K and different values of the interfacial conductance h_{c_2}.

	Analytical			**FEM**
h_{c_2} (W/m^2·K)	R_{1D} (K/W)	R_{sp} (K/W)	R_t (K/W)	R_t (K/W)
10^6	9564.8	12113	21678	21614
5×10^6	6707.7	12090	18798	18733
10^7	6350.5	12085	18436	18371
5×10^7	6064.8	12080	18145	18081
10^8	6029.1	12080	18109	18045
∞	5993.4	12079	18072	18042

Table 5.2: Thermal resistance of the single-heat-source validation study for $h_{c_1} = 10^8$ W/m^2·K and different values of the interfacial conductance h_{c_2}.

	Analytical		FEM	
h_{c_2} (W/m^2·K)	$\hat{T}$ (°C)	$\overline{T}$ (°C)	$\hat{T}$ (°C)	$\overline{T}$ (°C)
10^6	76.301	71.005	76.294	70.799
5×10^6	70.566	65.269	70.558	65.063
10^7	69.847	64.550	69.839	64.344
5×10^7	69.271	63.974	69.263	63.768
10^8	69.199	63.902	69.191	63.696
∞	69.126	63.830	69.173	63.645

Table 5.3: Centroidal and average temperatures of the single-heat-source validation study with $k_{1,x} = 50$, $k_{1,y} = 25$, $k_{1,z} = 15$ W/m·K for $h_{c_1} = 10^8$ W/m^2·K and different values of the interfacial conductance h_{c_2}.

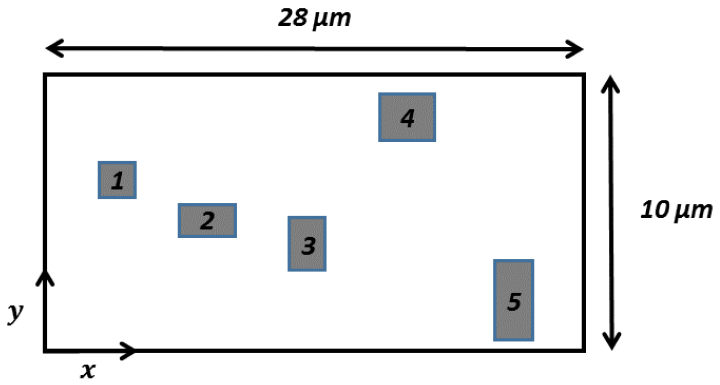

Figure 5.5: Source-plane layout of the multiple-heat-source problem.

is considered but by considering multiple heat sources distributed nonuniformly in the source plane instead of one heat source. In the new source plane, five eccentric heat sources are considered with different dimensions and positions distributed along the source plane. Configuration and properties of the five heat sources are shown in Fig. 5.5 and Table 5.4.

The multiple-heat-source analytical solution is used to solve the problem with 1000 terms for each of the summations in the infinite Fourier series summation and the computational time required to find any of the results is of approximately 0.7 s. The number of terms is chosen according to the fact that the multiple-heat-source solution

Source j	a_j (μm)	b_j (μm)	X_{c_j} (μm)	Y_{c_j} (μm)	q_j (W/m^2)
1	1	1	5	6	8×10^8
2	2	1	10	5	1×10^9
3	1	2	15	4	9×10^8
4	2	2	20	8	8.5×10^8
5	1	3	25	2	7×10^8

Table 5.4: Heat-source dimensions and properties of the multiple-heat-source problem.

	Analytical	**FEM**	**Relative Error**
h_{c_2} (W/m^2·K)	R_t^* (K/W)	R_t^* (K/W)	(%)
10^6	11728	11720	0.07%
5×10^6	8860.8	8853.9	0.08%
10^7	8501.5	8494.8	0.08%
5×10^7	8213.9	8207.1	0.09%
10^8	8177.9	8171.2	0.09%
∞	8141.9	8136.2	0.07%

Table 5.5: Thermal resistance of the multiple-heat-source validation study for $h_{c_1} = 10^8$ W/m^2·K and different values of the interfacial conductance h_{c_2}.

can be considered as a superposition of five single-heat-source solutions; hence, the number of terms for the multiple-heat-source is chosen as the same number of terms used for the single-source problem and is found to be sufficient to obtain the results. This can be seen from Fig. 5.6 which shows a sensitivity study of increasing the number of terms on the centroidal temperature of each heat source for $h_{c_2} = 10^6$ W/m^2·K. In addition, the problem is solved numerically using the FEM with a tetrahedral mesh consisting of approximately 6×10^5 elements with computational time of approximately 7 min. The total thermal resistance R_t^* of the analytical and numerical results for different values of the interfacial conductance h_{c_2} are shown in Table 5.5. The results show very good agreement between the analytical and numerical solution results with a relative error of less than 0.2%. Moreover, the centroidal and average temperatures of each heat source for one value of the interfacial conductance $h_{c_2} = 10^6$ W/m^2·K are shown in Table 5.6.

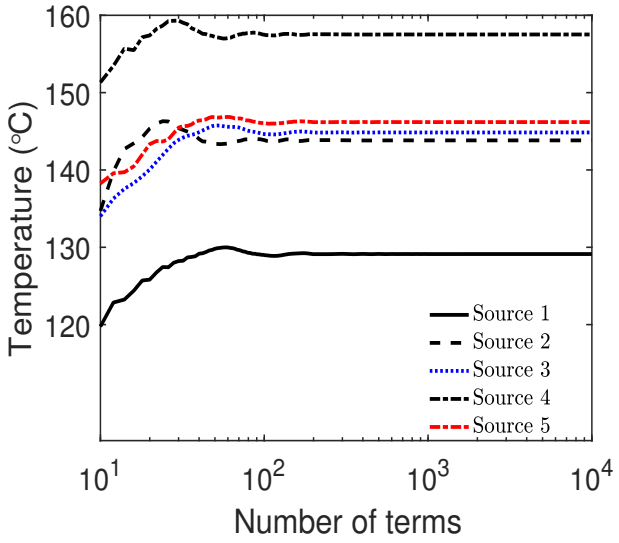

Figure 5.6: Analytical centroidal temperature of each heat source in the multiple-heat-source validation study computed as a function of the number of terms in the summations for $h_{c_2} = 10^6$ W/m^2·K.

	Analytical		**FEM**	
Source j	$\hat{T}$ (°C)	$\bar{T}$ (°C)	$\hat{T}$ (°C)	$\bar{T}$ (°C)
1	129.12	126.33	129.20	126.25
2	143.82	139.25	143.93	139.40
3	144.85	140.71	144.83	140.59
4	157.52	151.64	157.79	151.56
5	146.19	142.86	146.37	142.83

Table 5.6: Centroidal and average temperatures of each heat source in the multiple-heat-source validation study for $h_{c_1} = 10^8$ W/m^2·K and $h_{c_2} = 10^6$ W/m^2·K.

From the previous discussion, the computational efficiency of the developed analytical solution is obvious compared to solving the problem numerically. In particular, when the problem contains multiple heat sources in the source plane, a large number of elements is required around each heat source and along the flux channel to solve the problem numerically using the FEM which will increase the computational time and the complexity of the problem. However, in the analytical solution, the same number of terms in the summations as used to solve the single-heat-source problem

is found sufficient to solve the multiple-heat-source problem without loss of any accuracy. Further, the complexity of the problem for solving the multiple-heat-source problem is found to be about twice that for solving the single-heat-source problem.

5.4 Conclusion

In this chapter, general analytical solutions for the temperature distribution and thermal resistance of a 3D multilayered orthotropic flux channel consisting of N-layers with interfacial conductance between the layers were developed. The solutions account for using anisotropic materials with different thermal conductivities in the three spatial directions of each layer. The developed solutions were extended to account for problems with multiple heat sources in the source plane. The solutions were validated by comparing the developed analytical solution results with the results obtained by solving the problem numerically based on the FEM using the ANSYS commercial software package [30] where very good agreement was found. In addition, the computational efficiency of the developed solutions was also discussed in comparison with using numerical solutions.

References

[1] B. Al-Khamaiseh, Y. S. Muzychka, and S. Kocabiyik, "Spreading resistance in multilayered orthotropic flux channels with different conductivities in the three spatial directions," *ASME-Journal of Heat Transfer*, vol. 140, no. 7, pp. 1–10, 2018, doi:http://doi.org/10.1115/1.4038712.

[2] M. Higashiwaki, K. Sasaki, A. Kuramata, T. Masui, and S. Yamakoshi, "Development of gallium oxide power devices," *Phys. Status Solidi A*, vol. 211, no. 1, pp. 21–26, 2014.

[3] A. Jain and A. J. H. McGaughey, "Strongly anisotropic in-plane thermal transport in single-layer black phosphorene," *Sci. Rep.*, vol. 5, pp. 8501–1–8501–5, 2015.

[4] J. Zhu, J. Y. Chen, H. Park, X. Gu, H. Zhang, S. Karthikeyan, N. Wendel, S. A. Campbell, M. Dawber, X. Du, M. Li, J. P. Wang, R. Yang, and X. Wang, "Revealing the origins of 3D anisotropic thermal conductivities of black phosphorus," *Adv. Electron. Mater.*, vol. 2, no. 5, pp. 1 600 040–1–1 600 040–9, 2016.

[5] J. S. Kim, P. J. Jeon, J. Lee, K. Choi, H. S. Lee, Y. Cho, Y. T. Lee, D. K. Hwang, and S. Im, "Dual gate black phosphorus field effect transistors on glass for nor logic and organic light emitting diode switching," *Nano Lett.*, vol. 15, no. 9, pp. 5778–5783, 2015.

[6] G. Liu, H. Y. Sun, J. Zhou, Q. F. Li, and X. G. Wan, "First-principles study of lattice thermal conductivity of Td-WTe_2," *New J. Phys.*, vol. 18, pp. 033 017–1–033 017–8, 2016.

[7] M. H. Wong, Y. Morikawa, K. Sasaki, A. Kuramata, S. Yamakoshi, and M. Higashiwaki, "Characterization of channel temperature in Ga_2O_3 metal-oxide-semiconductor field-effect transistors by electrical measurements and thermal modeling," *Appl. Phys. Lett.*, vol. 109, no. 19, pp. 193 503–1–193 503–5, 2016.

[8] Z. Guo, A. Verma, X. Wu, F. Sun, A. Hickman, T. Masui, A. Kuramata, M. Higashiwaki, D. Jena, and T. Luo, "Anisotropic thermal conductivity in single crystal β-gallium oxide," *Appl. Phys. Lett.*, vol. 106, pp. 111 909–1–111 909–5, 2015.

[9] A. M. Darwish, A. J. Bayba, and H. A. Hung, "Thermal resistance calculation of AlGaN-GaN devices," *IEEE Trans. Microwave Theory Tech.*, vol. 52, no. 11, pp. 2611–2620, Nov. 2004.

[10] D. P. Kennedy, "Spreading resistance in cylindrical semiconductor devices," *J. Appl. Phys.*, vol. 31, no. 8, pp. 1490–1497, 1960.

[11] A. G. Kokkas, "Thermal analysis of multiple-layer structures," *IEEE Trans. Electron Devices*, vol. Ed-21, no. 11, pp. 674–681, Nov. 1974.

[12] M. M. Yovanovich, "General expression for constriction resistances due to arbitrary flux distribution at non-symmetric, coaxial contacts," in *AIAA 13th Aerosp. Sci. Meeting*, Pasadena, CA, USA, 1975, pp. 381–396.

[13] M. M. Yovanovich, Y. S. Muzychka, and J. R. Culham, "Spreading resistance in isoflux rectangles and strips on compound flux channels," *J. Thermophys. Heat Transf.*, vol. 13, no. 4, pp. 495–500, 1999.

[14] M. M. Yovanovich, "Thermal resistances of circular source on finite circular cylinder with side and end cooling," *J. Electron. Packag.*, vol. 125, no. 2, pp. 169–177, Jun. 2003.

[15] ——, "Four decades of research on thermal contact, gap and joint resistance in microelectronics," *IEEE Trans. Compon. Packag. Technol.*, vol. 28, no. 2, pp. 182–206, Jun. 2005.

[16] Y. S. Muzychka, J. R. Culham, and M. M. Yovanovich, "Thermal spreading resistance of eccentric heat sources on rectangular flux channels," *J. Electron. Packag.*, vol. 125, no. 2, pp. 178–185, Jun. 2003.

[17] Y. S. Muzychka, M. M. Yovanovich, and J. R. Culham, "Influence of geometry and edge cooling on thermal spreading resistance," *J. Thermophys. Heat Transf.*, vol. 20, no. 2, pp. 247–255, 2006.

[18] Y. S. Muzychka, "Influence coefficient method for calculating discrete heat source temperature on finite convectively cooled substrates," *IEEE Trans. Compon. Packag. Technol.*, vol. 29, no. 3, pp. 636–643, Sep. 2006.

[19] Y. S. Muzychka, K. R. Bagnall, and E. N. Wang, "Thermal spreading resistance and heat source temperature in compound orthotropic systems with interfacial resistance," *IEEE Trans. Compon., Packag., Manuf. Technol.*, vol. 3, no. 11, pp. 1826–1841, Nov. 2013.

[20] Y. S. Muzychka, "Spreading resistance in compound orthotropic flux tubes and channels with interfacial resistance," *J. Thermophys. Heat Transf.*, vol. 28, no. 2, pp. 313–319, Mar. 2014.

[21] ——, "Thermal spreading resistance in a multilayered orthotropic circular disk with interfacial resistance and variable heat flux," in *ASME 2015 Int. Tech. Conf.*

and Exhibition on Packag. and Integ. of Electron. and Photon. Microsys. San Francisco, California: Paper No. IPACK2015-48243, Jul. 6-9 2015.

[22] A. Gholami and M. Bahrami, "Thermal spreading resistance inside anisotropic plates with arbitrarily located hotspots," *J. Thermophys. Heat Transf.*, vol. 28, no. 4, pp. 679–686, Oct.-Dec. 2014.

[23] K. R. Bagnall, Y. S. Muzychka, and E. N. Wang, "Analytical solution for temperature rise in complex, multilayer structures with discrete heat sources," *IEEE Trans. Compon., Packag., Manuf. Technol.*, vol. 4, no. 5, pp. 817–830, May 2014.

[24] D. W. Hahn and M. N. Özisik, *Heat Conduction.* Hoboken, NJ, USA: Wiley, 2012.

[25] Y. S. Muzychka, M. M. Yovanovich, and J. R. Culham, "Thermal spreading resistance in compound and orthotropic systems," *J. Thermophys. Heat Transf.*, vol. 18, no. 1, pp. 45–51, Jan.-Mar. 2004.

[26] V. S. Arpaci, *Conduction Heat Transfer.* New York, NY, USA: Addison-Wesley, 1966.

[27] M. N. Özisik, *Boundary Value Problems of Heat Conduction.* Scranton, PA, USA: International Textbook, 1968.

[28] S. Kakac and Y. Yener, *Heat Conduction, 3rd ed.* Malabar, FL, USA: Taylor & Francis, 1993.

[29] MATLAB Release 2016b, The MathWorks, Inc., Natick, MA, USA, 2016.

[30] ANSYS® Release 16.2, ANSYS, Inc., Canonsburg, PA, USA, 2015.

Statement of co-authorship

This statement describes the authors' research contributions in the following journal manuscript.

Title: **Spreading Resistance in Multilayered Orthotropic Flux Channel with Temperature-Dependent Thermal Conductivities**
Located in Chapter 6.

The following people contributed to the conception of this paper:
Author 1: Belal Al-Khamaiseh
Author 2: Dr. Yuri S. Muzychka
Author 3: Dr. Serpil Kocabiyik

Belal Al-Khamaiseh was the primary author of this research. He played a major role in constructing the model of the problem, developing the analytical solutions, conducting the computational part, analyzing the results, and comparing the analytical results with numerical results for verification purposes. Dr. Yuri S. Muzychka and Dr. Serpil Kocabiyik contributed to the conception and design of this research. They also guided it's analytical and computational components.

Chapter 6

Spreading Resistance in Multilayered Orthotropic Flux Channel with Temperature-Dependent Thermal Conductivities

6.1 Introduction

In the modern microelectronics industry, as the size of microelectronic devices continues to decrease with a remarkable growth in power densities, thermal management of microelectronic systems becomes more important for maintaining device functionality

Published in the AIAA-Journal of Thermophysics and Heat Transfer [1].

and reliability. Accurate thermal analysis is considered as a significant factor in the development of microelectronic systems for retaining device performance and to produce a durable device. Most microelectronic systems are modeled as rectangular flux channels, where heat enters the channel through small heat source(s) and flows by conduction through the system to spread the heat into a larger convective heat-sink area, and this process gives rise to thermal spreading resistance. The multilayered structure is a widely used structure in the microelectronic industry where devices are designed as a compound system of attached layers of different materials. Recently, some anisotropic materials have received exceptional attention in the development of the microelectronics in which the thermal conductivity varies with direction [2]. Orthotropic materials are of particular interest, where the thermal conductivity in these materials is different in the three principal spatial directions. Such anisotropic materials include β-Gallium-oxide (β-Ga_2O_3) [3, 4], and Black Phosphorus (BP) [5]. The orthotropic different thermal conductivities in many materials are varying with temperature and usually are approximated by constant thermal conductivities. However, the assumption of constant thermal conductivities within the whole temperature variation intervals may lead to unreliable results in thermal analysis [6, 7].

When considering temperature-dependent thermal conductivities in multilayered orthotropic structures, the governing heat conduction equations of the system become nonlinear. In general, analytical solutions of nonlinear systems are challenging, and usually numerical methods are used to solve the nonlinear systems. However, when the problem under consideration is complex, the numerical methods are computationally expensive and less flexible for optimization studies. Moreover, the complexity of solving nonlinear systems numerically is larger than solving linear systems. Hence, analytical solutions (if possible) are advantageous for presenting accurate results and for saving computational work.

The Kirchhoff transform method is considered as an attractive technique for solving nonlinear conduction systems with temperature-dependent thermal conductivities, because it can be used to transform the nonlinear governing system of equations into a linear system of equations that can be solved using existing analytical solutions of linear systems, and then the solution of the linearized system can be transformed back to get the solution of the original nonlinear system using the inverse Kirchhoff transform [8–11].

In the past few decades, analytical solutions of the temperature distribution and thermal spreading resistance in flux channels have been studied comprehensively, and many related studies can be found in the literature. However, in most of the existing work, attention has been focused on problems with constant thermal conductivities. Yovanovich studied different problems on spreading resistance in flux channels and flux tubes, and he summarized the most important models of thermal spreading resistance for more than 40 years in a review paper [12]. Muzychka et al. [13–18] have conducted comprehensive research on different spreading resistance problems including different geometries, boundaries, and properties for single and multilayered structures. Bagnall et al. [19] studied temperature rise and thermal spreading resistance in multilayered flux channels with constant isotropic and transversely isotropic thermal conductivities. Bonani and Ghione [6] used the Kirchhoff transform to study a composite medium consisting of two layers with temperature-dependent and piecewise inhomogeneous thermal conductivity. Ditri [20] studied a single-layer flux channel with orthotropic temperature-dependent thermal conductivities and a fixed-temperature boundary condition along the sink plane. Bagnall et al. [21] studied the temperature rise in problems with temperature-dependent thermal conductivities and convection boundary conditions along the sink plane using the Kirchhoff transform.

In this chapter, the Kirchhoff transform is used to obtain general analytical solutions of the temperature rise and thermal resistance in a multilayered orthotropic flux channel consisting of N composite layers with different temperature-dependent thermal conductivities in the three spatial directions of each layer. The Kirchhoff transform is used to transform the nonlinear system into a linear system, and then stretched coordinate transformations and the method of separation of variables are used to solve the linear system, where the solution the linear system is used to find the solution of the original nonlinear system by means of the inverse Kirchhoff transform. Moreover, an efficient approximation of the total thermal resistance of the nonlinear system is presented. The solutions have been extended to account for multiple eccentric heat sources in the source plane.

6.2 Mathematical Theory

In this section, we present the mathematical formulation of the problem including the nonlinear governing equations of the temperature distribution for the multilayered structure along with the appropriate boundary conditions. Then the analytical solution of the problem is illustrated after making use of the Kirchhoff and the stretched coordinate transformations. The analytical solution is then used to present the total thermal resistance of the system. Finally, an extension of the solution to account for multiple heat sources in the source plane is introduced.

6.2.1 Problem Statement

The system under consideration is a composite three-dimensional (3D) rectangular flux channel consisting of N bonded layers, which represents the general geometry of many modern microelectronic devices. The heat enters the system from a small

heated spot represented by an eccentric heat source of a rectangular shape and flows by conduction through the layers to reach a convective heat sink with a uniform heat transfer coefficient. Furthermore, all the lateral edges are assumed to be adiabatic, and the adjacent layers are assumed to be in perfect contact with no interfacial resistance. The layers are assumed to be of different thermal properties. In particular, the material of each layer is assumed to be orthotropic, with different temperature-dependent thermal conductivities in the three spatial directions (x, y, z_i), as shown in Fig. 6.1. For convenience, the system is modeled using a local system of coordinates in each layer with different through-plane (vertical) coordinates $0 < z_i < t_i$ and the same in-plane (horizontal) coordinates with $0 < x < c$ and $0 < y < d$ for all the layers.

The steady-state heat conduction in each layer is governed by a nonlinear heat equation because of the dependency of the thermal conductivities on temperature. The general system of nonlinear equations that represents the governing equations of heat conduction in the N-multilayered structure with orthotropic temperature-dependent thermal conductivities can be addressed by:

$$\frac{\partial}{\partial x}\left(k_{i,x}(T_i)\frac{\partial T_i}{\partial x}\right)+\frac{\partial}{\partial y}\left(k_{i,y}(T_i)\frac{\partial T_i}{\partial y}\right)+\frac{\partial}{\partial z_i}\left(k_{i,z}(T_i)\frac{\partial T_i}{\partial z_i}\right)=0, \quad 0<z_i<t_i, \quad (6.1)$$

for $i = 1, 2, \ldots, N$. The boundary conditions of the system are addressed based on the general nature of heat flow in the flux channel, where heat enters the system from the source region and is removed from the system by convection through the sink plane. In the source plane, a uniform heat flux is specified inside the rectangular heat-source region, whereas the remainder of the source plane is considered as adiabatic. Hence,

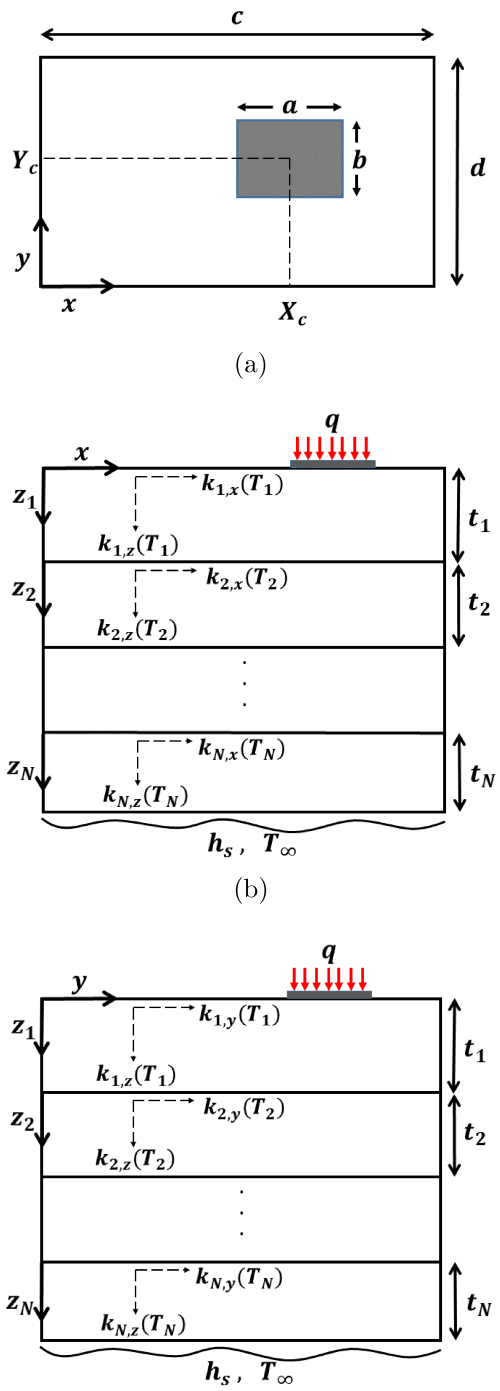

Figure 6.1: Schematic view of a 3D flux channel layout. (a) Top view. (b) Cross-sectional view in the xz-plane. (c) Cross-sectional view in the yz-plane.

the source-plane boundary condition is given by:

$$-k_{1,z}(T_1)\frac{\partial T_1}{\partial z_1}\bigg|_{z_1\,=\,0} = \begin{cases} q, & \text{inside source region,} \\ 0, & \text{outside source region.} \end{cases} \tag{6.2}$$

The interface boundary conditions between the adjacent layers (for $i = 1, 2, \ldots, N-1$) are the continuity of heat flux and the continuity of temperature, respectively:

$$k_{i,z}(T_i)\frac{\partial T_i}{\partial z_i}\bigg|_{z_i\,=\,t_i} = k_{i+1,z}(T_{i+1})\frac{\partial T_{i+1}}{\partial z_{i+1}}\bigg|_{z_{i+1}\,=\,0}, \tag{6.3}$$

$$T_i(x, y, t_i) = T_{i+1}(x, y, 0). \tag{6.4}$$

Along the sink plane, a convection boundary condition with a uniform heat transfer coefficient h_s exists, and the boundary condition is given by:

$$-k_{N,z}(T_N)\frac{\partial T_N}{\partial z_N}\bigg|_{z_N\,=\,t_N} = h_s\left(T_N(x, y, t_N) - T_\infty\right). \tag{6.5}$$

The lateral edges of the system are considered as adiabatic; hence, the lateral-edge boundary conditions are:

$$\frac{\partial T_i}{\partial x}\bigg|_{x\,=\,0,\,c} = 0, \quad \frac{\partial T_i}{\partial y}\bigg|_{y\,=\,0,\,d} = 0, \quad i = 1, 2, \ldots, N. \tag{6.6}$$

The governing equations along with the boundary conditions of the temperature distribution in the multilayered system are completely illustrated in Eqs. (6.1)-(6.6). Although the general form of the governing equations in Eq. (6.1) governs the problem for different thermal conductivity functions in the three spatial directions of each layer ($k_{i,x}(T_i) \neq k_{i,y}(T_i) \neq k_{i,z_i}(T_i)$), the analytical solution of the proposed problem requires that all the thermal conductivity functions in the system must depend on

temperature in the same manner [6, 20]. In other words, the temperature-dependent thermal conductivities can be written as:

$$k_{i,u}(T) = k^0_{i,u}\hat{k}(T), \tag{6.7}$$

where u refers to any of the coordinates x, y or z_i; $k^0_{i,u}$ is a constant thermal conductivity; and $\hat{k}(T)$ is a functional relationship of temperature, for example, $\hat{k}(T) = 1 + T$. Under this assumption, the governing equations in Eq. (6.1) can be rewritten as:

$$k^0_{i,x}\frac{\partial}{\partial x}\left(\hat{k}(T_i)\frac{\partial T_i}{\partial x}\right) + k^0_{i,y}\frac{\partial}{\partial y}\left(\hat{k}(T_i)\frac{\partial T_i}{\partial y}\right) + k^0_{i,z}\frac{\partial}{\partial z_i}\left(\hat{k}(T_i)\frac{\partial T_i}{\partial z_i}\right) = 0, \quad 0 < z_i < t_i. \tag{6.8}$$

We then proceed to obtain the analytical solution of the problem using some mathematical transformations.

6.2.2 Kirchhoff Transform

The Kirchhoff transform is considered to be a powerful method for linearizing nonlinear heat conduction problems with temperature-dependent thermal conductivity. The idea behind the Kirchhoff transform is to present a new variable θ (usually referred to as the apparent temperature) as an integral function of the temperature-dependent thermal conductivity, where the nonlinear system can be transformed under the Kirchhoff transform into a linear system in terms of the new variable θ. Furthermore, the linearized system can be solved using existing analytical methods for solving linear problems, and then the solution of the linear system can be transformed back to the solution of the nonlinear system through the inverse Kirchhoff transform. The Kirchhoff transform can be found in the literature in many forms depending on the problem under investigation [9, 21–23]; however, all forms share the same general

idea. For the multilayered system, the following general form of the Kirchhoff transform is considered in each layer because it facilitates the multilayered structure and the transformation of the convective boundary condition along the sink plane:

$$\theta_i = K\{T_i\} = T_0 + \int_{T_0}^{T_i} \hat{k}(\tau)d\tau. \tag{6.9}$$

where T_0 is a convenient reference temperature. Applying the Kirchhoff transform given by Eq. (6.9) to the nonlinear system, Eq. (6.8), the nonlinear system is transformed into a linear orthotropic system of equations with constant thermal conductivities given by:

$$k^0_{i,x}\frac{\partial^2\theta_i}{\partial x^2} + k^0_{i,y}\frac{\partial^2\theta_i}{\partial y^2} + k^0_{i,z}\frac{\partial^2\theta_i}{\partial z_i^2} = 0, \quad \text{for } \; i = 1, 2, \ldots, N. \tag{6.10}$$

Moreover, the boundary conditions of the nonlinear system are transformed through the Kirchhoff transform into the following boundary conditions. The source-plane boundary condition in Eq. (6.2) is transformed to:

$$-k^0_{1,z}\left.\frac{\partial\theta_1}{\partial z_1}\right|_{z_1\,=\,0} = \begin{cases} q, & \text{inside source region,} \\ 0, & \text{outside source region.} \end{cases} \tag{6.11}$$

The interface boundary conditions in Eqs. (6.3) and (6.4) are transformed to [6]:

$$k^0_{i,z}\left.\frac{\partial\theta_i}{\partial z_i}\right|_{z_i\,=\,t_i} = k^0_{i+1,z}\left.\frac{\partial\theta_{i+1}}{\partial z_{i+1}}\right|_{z_{i+1}\,=\,0}, \tag{6.12}$$

$$\theta_i(x, y, t_i) = \theta_{i+1}(x, y, 0). \tag{6.13}$$

The lateral-edge boundary conditions in Eq. (6.6) are transformed to:

$$\left.\frac{\partial \theta_i}{\partial x}\right|_{x\,=\,0,\,c} = 0, \quad \left.\frac{\partial \theta_i}{\partial y}\right|_{y\,=\,0,\,d} = 0, \quad i = 1, 2, \ldots, N. \tag{6.14}$$

Although the source plane, interfacial, and lateral-edge boundary conditions are transformed easily into linear boundary conditions through the Kirchhoff transform, this is not the case, in general, when considering the convective sink-plane boundary condition. In fact, when convective boundary conditions (third kind or Robin) are present, the transformed boundary conditions are, in general, nonlinear boundary conditions [9, 10]. This can be seen by considering the sink-plane boundary condition:

$$-k_{N,z}(T_N)\left.\frac{\partial T_N}{\partial z_N}\right|_{z_N\,=\,t_N} = h_s\left(T_N(x, y, t_N) - T_\infty\right). \tag{6.15}$$

When the Kirchhoff transform is considered, the boundary condition is transformed to:

$$-k^0_{N,z}\left.\frac{\partial \theta_N}{\partial z_N}\right|_{z_N\,=\,t_N} = h_s\left(K^{-1}\{\theta_N(x, y, t_N)\} - T_\infty\right), \tag{6.16}$$

which is a nonlinear boundary condition because $K^{-1}\{\theta_N\}$ is, in general, a nonlinear function of θ_N, and this makes it difficult when trying to solve the transformed linear problem. However, when the temperature distribution along the sink plane can be approximated before using the Kirchhoff transform and used as a reference temperature T_0 in the definition of the transform, Eq. (6.9), the transform can be applied for the convective boundary condition in Eq. (6.15) to get a linear transformed boundary condition [21]. By considering the problem under study, heat enters the system through the small heat-source region and flows by conduction to spread the heat out from the heat-source area into the larger heat-sink area. Hence, the temperature along the sink plane can be approximated by the mean sink-plane temperature using the conservation of energy, and then the approximated temperature can be used as the

reference temperature in the Kirchhoff transform, i.e.,

$$T_0 = \bar{T}_N|_{z=t} = \frac{1}{h_s}\frac{Q}{cd} + T_\infty. \tag{6.17}$$

Thus, when the approximated sink-plane temperature in Eq. (6.17) is used as the reference temperature in the Kirchhoff transform Eq. (6.9), the convective boundary condition in Eq. (6.15) can be transformed into the following approximate linear boundary condition [21]:

$$-k^0_{N,z}\frac{\partial \theta_N}{\partial z_N}\bigg|_{z_N\,=\,t_N} = h_s\left(\theta_N(x,y,t_N) - T_\infty\right). \tag{6.18}$$

To summarize, by considering the average sink temperature defined in Eq. (6.17) as a reference temperature in the Kirchhoff transform, the nonlinear system Eqs. (6.1)-(6.6) is transformed to the linear system represented by Eqs. (6.10)-(6.14) and Eq. (6.18). Once the solution of the linearized system is obtained, the solution can be transformed to the approximate actual temperature of the nonlinear problem by employing the inverse Kirchhoff transform. It is worth mentioning that the explicit functional relationship between the actual temperature T_i and the apparent temperature θ_i depends on the specific nature of the temperature-dependent function $\hat{k}(T)$. Different dependency functions of the thermal conductivity on temperature can be found in the literature [21, 23, 24]. In this study, we will consider three general forms of the thermal conductivity functions given by:

$$\hat{k}_1(T) = 1 + \omega_1(T - T_0), \tag{6.19}$$

$$\hat{k}_2(T) = \exp[\omega_2(T - T_0)], \tag{6.20}$$

$$\hat{k}_3(T) = \left(\frac{T_0}{T}\right)^s, \tag{6.21}$$

where ω_1, ω_2 are dependency parameters called the temperature coefficients of thermal conductivity [11], and s is a real-number exponent. The functional relationship between the apparent temperature θ_i and the actual temperature T_i can be obtained for the three general conductivity functions using Eq. (6.9), and then the actual temperature T_i can be obtained in terms of the apparent temperature θ_i that represents the inverse Kirchhoff transform by solving the relationships for T_i to get the following results for the three general functions, respectively:

$$T_i = K_1^{-1}\{\theta_i\} = T_0 + \frac{1}{\omega_1}\left[\sqrt{2\omega_1(\theta_i - T_0) + 1} - 1\right], \tag{6.22}$$

$$T_i = K_2^{-1}\{\theta_i\} = T_0 + \frac{1}{\omega_2}\ln(1 + \omega_2(\theta_i - T_0)), \tag{6.23}$$

$$T_i = K_3^{-1}\{\theta_i\} = \begin{cases} T_0 \exp(\theta_i/T_0 - 1), & s = 1 \\ T_0\left[\dfrac{(1-s)\theta_i}{T_0} + s\right]^{1/(1-s)}, & s \neq 1 \end{cases} \tag{6.24}$$

6.2.3 Linear System Solution

The solution of the nonlinear system requires finding the solution of the linearized system for the apparent temperature first, and then, by using any of the functional relationships in Eqs. (6.22)-(6.24) that corresponds to the used conductivity function, these solutions can be transformed to the solution of the nonlinear system. The general solution of the linearized system can be obtained by using stretched coordinate transformations combined with the method of separation of variables. The application of the following stretched coordinates transformations for each layer (for $i = 1, 2, \ldots, N$),

$$\text{Layer } i: \quad y_1 = y/\sqrt{k_{1,y}^0/k_{1,x}^0}, \quad \zeta_i = z_i/\sqrt{k_{i,z}^0/k_{i,x}^0}, \tag{6.25}$$

leads to the definition of the following effective properties:

$$\text{Layer } i: \quad k_i = \sqrt{k_{i,x}^0 k_{i,z}^0}, \quad \mu_i = \frac{k_{1,x}^0 k_{i,y}^0}{k_{1,y}^0 k_{i,x}^0}, \quad \bar{t}_i = t_i / \sqrt{k_{i,z}^0 / k_{i,x}^0}, \quad \bar{d} = d / \sqrt{k_{1,y}^0 / k_{1,x}^0}. \tag{6.26}$$

Hence, the linear system of equations and boundary conditions of θ_i can be transformed under Eq. (6.25) into the following system:

$$\begin{aligned} &\frac{\partial^2 \theta_1}{\partial x^2} + \quad \frac{\partial^2 \theta_1}{\partial y_1^2} + \frac{\partial^2 \theta_1}{\partial \zeta_1^2} = 0, && 0 < \zeta_1 < \bar{t}_1 \\ &\frac{\partial^2 \theta_i}{\partial x^2} + \frac{1}{\mu_i}\frac{\partial^2 \theta_i}{\partial y_1^2} + \frac{\partial^2 \theta_i}{\partial \zeta_i^2} = 0, && 0 < \zeta_i < \bar{t}_i \\ & && i = 2, 3, \ldots, N \end{aligned} \tag{6.27}$$

with $0 < x < c$ and $0 < y_1 < \bar{d}$, and subject to the following boundary conditions:

$$-k_1 \left.\frac{\partial \theta_1}{\partial \zeta_1}\right|_{\zeta_1 = 0} = \begin{cases} q, & \text{inside stretched source region,} \\ 0, & \text{outside stretched source region,} \end{cases} \tag{6.28}$$

in the source plane, whereas the interfacial boundary conditions are transformed to:

$$k_i \left.\frac{\partial \theta_i}{\partial \zeta_i}\right|_{\zeta_i = \bar{t}_i} = k_{i+1} \left.\frac{\partial \theta_{i+1}}{\partial \zeta_{i+1}}\right|_{\zeta_{i+1} = 0}, \tag{6.29}$$

$$\theta_i(x, y_1, \bar{t}_i) = \theta_{i+1}(x, y_1, 0). \tag{6.30}$$

Along the sink plane, we have:

$$-k_N \left.\frac{\partial \theta_N}{\partial \zeta_N}\right|_{\zeta_N = \bar{t}_N} = h_s(\theta_N(x, y_1, \bar{t}_N) - T_\infty), \tag{6.31}$$

and for the lateral-edge boundary conditions, we get:

$$\left.\frac{\partial\theta_i}{\partial x}\right|_{x\,=\,0,\,c} = 0, \quad \left.\frac{\partial\theta_i}{\partial y_1}\right|_{y_1\,=\,0,\,\bar{d}} = 0, \quad i = 1, 2, \ldots, N. \tag{6.32}$$

By introducing $\theta_i' = \theta_i - T_\infty$, the linear system of θ_i' is the same as the linear system of θ_i but with a homogenous boundary condition along the sink plane. The application of the method of separation of variables by assuming the general solution in each layer to have the form $\theta_i'(x, y_1, \zeta_i) = X_i(x) \cdot Y_i(y_1) \cdot Z_i(\zeta_i)$ and using the boundary conditions along $(x = 0,\ x = c)$ and $(y_1 = 0,\ y_1 = \bar{d})$ yield the following general solutions for $i = 1, 2, \ldots, N$:

$$\begin{aligned}
\theta_i'(x, y_1, \zeta_i) = {} & A_{00}^i + B_{00}^i \zeta_i \\
& + \sum_{m=1}^{\infty} \cos(\lambda_m^1 x) \left[A_{m0}^i \cosh(\lambda_m^i \zeta_i) + B_{m0}^i \sinh(\lambda_m^i \zeta_i) \right] \\
& + \sum_{n=1}^{\infty} \cos(\delta_n^1 y_1) \left[A_{0n}^i \cosh(\delta_n^i \zeta_i) + B_{0n}^i \sinh(\delta_n^i \zeta_i) \right] \\
& + \sum_{m=1}^{\infty} \sum_{n=1}^{\infty} \cos(\lambda_m^1 x) \cos(\delta_n^1 y_1) \left[A_{mn}^i \cosh(\beta_{mn}^i \zeta_i) + \ B_{mn}^i \sinh(\beta_{mn}^i \zeta_i) \right],
\end{aligned} \tag{6.33}$$

where λ_m^i, δ_n^i, and β_{mn}^i are the corresponding eigenvalues in each layer. The eigenvalues in the first layer are defined by:

$$\lambda_m^1 = m\pi/c, \quad \delta_n^1 = n\pi/\bar{d}, \quad \beta_{mn}^1 = \sqrt{(\lambda_m^1)^2 + (\delta_n^1)^2}, \tag{6.34}$$

whereas the eigenvalues in the other layers can be related to the eigenvalues of the first layer as:

$$\lambda_m^i = \lambda_m^1, \quad \delta_n^i = \frac{1}{\sqrt{\mu_i}} \delta_n^1, \quad \beta_{mn}^i = \sqrt{{\lambda_m^i}^2 + {\delta_n^i}^2} = \sqrt{(\lambda_m^1)^2 + \frac{1}{\mu_i}(\delta_n^1)^2}. \tag{6.35}$$

The interfacial and sink-plane boundary conditions are then used to find a relationship between the Fourier coefficients A^i_{mn} and B^i_{mn} in each layer. We follow the work of Muzychka et al. [17] and Bagnall et al. [19] in which the relationship is represented by a spreading function $\phi_i(\gamma^i)$ defined by:

$$\phi_i(\gamma^i) = -\frac{B^i_{mn}}{A^i_{mn}}, \tag{6.36}$$

where γ^i refers to any of the eigenvalues λ^i_m, δ^i_n, or β^i_{mn}. For m, n not both equal to zero, we start with finding the spreading function of the Nth-layer solution by applying the convection boundary condition at the sink plane Eq. (6.31) to get:

$$\phi_N(\gamma^N) = -\frac{B^N_{mn}}{A^N_{mn}} = \frac{\gamma^N \tanh(\gamma^N \bar{t}_N) + [h_s/k_N]}{\gamma^N + [h_s/k_N]\tanh(\gamma^N \bar{t}_N)}. \tag{6.37}$$

The application of the interfacial boundary conditions Eqs. (6.29) and (6.30) leads to the following backward recursive formula for finding $\phi_i(\gamma^i)$:

$$\phi_i(\gamma^i) = \frac{[(k_i\gamma^i)\,/\,(k_{i+1}\gamma^{i+1})]\tanh(\gamma^i \bar{t}_i) + \phi_{i+1}(\gamma^{i+1})}{[(k_i\gamma^i)\,/\,(k_{i+1}\gamma^{i+1})] + \phi_{i+1}(\gamma^{i+1})\tanh(\gamma^i \bar{t}_i)}. \tag{6.38}$$

Finding the total thermal resistance and the maximum temperature of the channel requires obtaining the solution in the first layer θ_1 (in particular, the solution at $\zeta_1 = 0$). Hence, the Fourier coefficients A^1_{mn} and B^1_{mn} are of most interest. The Fourier coefficients of the first-layer solution (A^1_{mn}) are obtained by taking Fourier series expansions of the boundary condition at the source plane Eq. (6.28) and making use of $B^1_{mn} = -\phi_1(\gamma^1)A^1_{mn}$ to get:

$$A^1_{m0} = \frac{\bar{b}q}{\bar{d}k_1\lambda^1_m\phi_1(\lambda^1_m)} \frac{\displaystyle\int_{X_c-a/2}^{X_c+a/2} \cos(\lambda^1_m x)\,dx}{\displaystyle\int_0^c \cos^2(\lambda^1_m x)\,dx} = \frac{4Q\cos(\lambda^1_m X_c)\sin(\frac{1}{2}\lambda^1_m a)}{acdk_1\,(\lambda^1_m)^2\phi_1(\lambda^1_m)}, \tag{6.39}$$

and

$$A^1_{0n} = \frac{aq}{ck_1\delta^1_n\phi_1(\delta^1_n)} \frac{\int_{\overline{Y}_c-\bar{b}/2}^{\overline{Y}_c+\bar{b}/2} \cos(\delta^1_n y_1)\, dy_1}{\int_0^{\bar{d}} \cos^2(\delta^1_n y_1)\, dy_1} = \frac{4Q\sigma \cos(\delta^1_n \overline{Y}_c)\sin(\frac{1}{2}\delta^1_n \bar{b})}{bcdk_1(\delta^1_n)^2\phi_1(\delta^1_n)}, \tag{6.40}$$

and

$$A^1_{mn} = \frac{q}{k_1\beta^1_{mn}\phi_1(\beta^1_{mn})} \frac{\int_{\overline{Y}_c-\bar{b}/2}^{\overline{Y}_c+\bar{b}/2} \int_{X_c-a/2}^{X_c+a/2} \cos(\lambda^1_m x)\cos(\delta^1_n y_1)\, dxdy_1}{\int_0^{\bar{d}}\int_0^{c} \cos^2(\lambda^1_m x)\cos^2(\delta^1_n y_1)\, dxdy_1},$$

$$= \frac{16Q\sigma \cos(\lambda^1_m X_c)\sin(\frac{1}{2}\lambda^1_m a)\cos(\delta^1_n \overline{Y}_c)\sin(\frac{1}{2}\delta^1_n \bar{b})}{abcdk_1\beta^1_{mn}\lambda^1_m\delta^1_n\phi_1(\beta^1_{mn})}, \tag{6.41}$$

where $\sigma = \sqrt{k_{1,y}/k_{1,x}}$, $\bar{b} = b/\sigma$, $\overline{Y}_c = Y_c/\sigma$, and $Q = abq$ is the total heat input of the flux channel. When m, n are both zeros, the zeroth-order Fourier coefficients in the first-layer solution (A^1_{00} and B^1_{00}) can be found by applying the sink-plane boundary condition and taking the Fourier expansion in the source plane after relating the coefficients between the adjacent layers to get:

$$\begin{aligned} A^1_{00} &= \frac{Q}{cd}\left[\sum_{l=1}^{N}\left(\frac{\bar{t}_l}{k_l}\right) + \frac{1}{h_s}\right], \\ B^1_{00} &= -\frac{Q}{cdk_1}. \end{aligned} \tag{6.42}$$

The solution in the source plane at $\zeta_1 = 0$ is of most interest, which can be addressed in terms of the original coordinates, i.e., x and y, by:

$$\begin{aligned} \theta_1(x,y,0) = T_\infty + A^1_{00} + \sum_{m=1}^{\infty} A^1_{m0}\cos(\lambda^1_m x) + \sum_{n=1}^{\infty} A^1_{0n}\cos(\delta^1_n y/\sigma) \\ + \sum_{m=1}^{\infty}\sum_{n=1}^{\infty} A^1_{mn}\cos(\lambda^1_m x)\cos(\delta^1_n y/\sigma). \end{aligned} \tag{6.43}$$

Thus, the solution of the nonlinear problem in the source plane $T_1(x, y, 0)$ can be obtained by substituting the solution of the linear system given in Eq. (6.43) into the corresponding functional relationships in Eqs. (6.22)-(6.24).

6.2.4 Total Thermal Resistance

For a single heat source spreading heat to a larger sink area, the total thermal resistance can be defined by [13, 17, 25]:

$$R_t = \frac{\overline{T}_c - T_\infty}{Q}, \tag{6.44}$$

where $\overline{T}_c$ is the mean temperature over the heat-source area defined by:

$$\overline{T}_c = \frac{1}{A_c} \iint_{A_c} T_1(x, y, 0)\, dA_c, \tag{6.45}$$

with $A_c = ab$ is the area of the heat source. It can be seen that the solution $T_1(x, y, 0)$ is complicated to be integrated explicitly over the heat-source area because of the complexity of the inverse Kirchhoff transform functions. Thus, numerical integration can be used to evaluate the integrals in Eq. (6.45). However, a good approximation of the temperature field $T_1(x, y, 0)$ is the first-order Taylor series approximation of the functional relationships between the actual temperature T_1 and the apparent temperature θ_1 denoted by the inverse Kirchhoff transform K^{-1} around the centroidal temperature of the linear solution $\hat{\theta}_1 = \theta_1(X_c, Y_c, 0)$. Thus, the solution in the heat-source region can be approximated by:

$$T_1(x, y, 0) = K^{-1}\{\hat{\theta}_1\} + K^{'-1}\{\hat{\theta}_1\}(\theta_1(x, y, 0) - \hat{\theta}_1), \tag{6.46}$$

where K^{-1} stands for any the functional relationships in Eqs. (6.22)-(6.24) and $K^{'-1}$

is the derivative of the functional relationships with respect to the dependent variable θ. Hence, the mean source temperature $\overline{T}_c$ can be approximated explicitly by:

$$\overline{T}_c(\text{approx.}) = K^{-1}\{\hat{\theta}_1\} + K^{'-1}\{\hat{\theta}_1\}(\bar{\theta}_c - \hat{\theta}_1), \tag{6.47}$$

where $\bar{\theta}_c$ is the mean temperature of the linear solution over the heat-source area that can be calculated by:

$$\begin{aligned}\bar{\theta}_c = T_\infty + A^1_{00} + 2\sum_{m=1}^{\infty} A^1_{m0}\frac{\cos(\lambda^1_m X_c)\sin(\frac{1}{2}\lambda^1_m a)}{a\lambda^1_m} + 2\sum_{n=1}^{\infty} A^1_{0n}\frac{\sigma\cos(\delta^1_n \overline{Y}_c)\sin(\frac{1}{2}\delta^1_n \bar{b})}{b\delta^1_n} \\ + 4\sum_{m=1}^{\infty}\sum_{n=1}^{\infty} A^1_{mn}\frac{\sigma\cos(\lambda^1_m X_c)\sin(\frac{1}{2}\lambda^1_m a)\cos(\delta^1_n \overline{Y}_c)\sin(\frac{1}{2}\delta^1_n \bar{b})}{a\lambda^1_m b\delta^1_n}.\end{aligned} \tag{6.48}$$

6.2.5 Extension to Multiple Heat Sources

In many applications, heat enters the system through multiple heat sources distributed along the source plane instead of a single heat source. We extend the problem to contain a finite number of N_c rectangular heat sources distributed nonuniformly along the source plane, as shown in Fig. 6.2. With this extension, the only change that happens to the problem statement is in the source-plane boundary condition. The new source-plane boundary condition is expressed by considering a uniform heat flux q_j distributed over the jth heat source (for $j = 1, 2, \ldots, N_c$), and outside the heat-source regions, the surface is considered as adiabatic. Thus, the source-plane boundary condition Eq. (6.2) is rewritten as:

$$-k_{1,z}(T_1)\frac{\partial T_1}{\partial z_1}\bigg|_{z_1\,=\,0} = \begin{cases} q_j, & \text{inside } j\text{th source region,} \\ 0, & \text{outside source regions.}\end{cases} \tag{6.49}$$

Applying the Kirchhoff transform Eq. (6.9) to the new extended problem with a

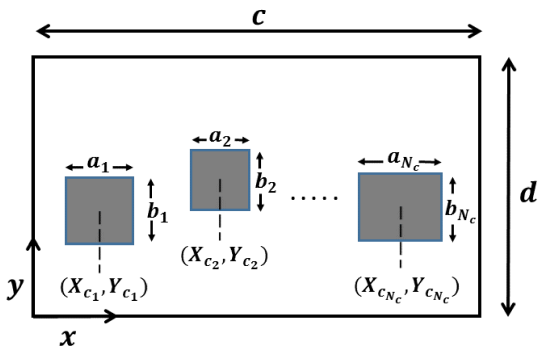

Figure 6.2: Top view a 3D flux channel with multiple heat sources along the source plane.

reference temperature defined by:

$$T_0 = \overline{T}_N|_{z=t} = \frac{1}{h_s}\frac{\sum_{j=1}^{N_c} Q_j}{cd} + T_\infty, \tag{6.50}$$

where $Q_j = a_j b_j q_j$ is the total heat input of the jth heat source, the nonlinear system is transformed into the same linear system represented in Eqs. (6.10)-(6.14) and (6.18) but with a different source-plane boundary condition given by:

$$-k_{1,z}^0 \frac{\partial \theta_1}{\partial z_1}\bigg|_{z_1=0} = \begin{cases} q_j, & \text{inside } j\text{th source region,} \\ 0, & \text{outside source regions.} \end{cases} \tag{6.51}$$

The general solution of the new linear system for the extended problem can be obtained in the same previously discussed manner for the single-heat-source problem with the same spreading functions given in Eqs. (6.37) and (6.38). The solution in the source plane can be written as:

$$\begin{aligned} \theta_1^*(x,y,0) = T_\infty + A_{00}^{*1} + \sum_{m=1}^{\infty} A_{m0}^{*1}\cos(\lambda_m^1 x) + \sum_{n=1}^{\infty} A_{0n}^{*1}\cos(\delta_n^1 y/\sigma) \\ + \sum_{m=1}^{\infty}\sum_{n=1}^{\infty} A_{mn}^{*1}\cos(\lambda_m^1 x)\cos(\delta_n^1 y/\sigma), \end{aligned} \tag{6.52}$$

where the Fourier coefficients of the multiple-source problem are given by,

$$A_{m0}^{*1} = \frac{4\sum_{j=1}^{N_c} b_j q_j \cos(\lambda_m^1 X_{c_j}) \sin(\frac{1}{2}\lambda_m^1 a_j)}{cdk_1(\lambda_m^1)^2 \phi_1(\lambda_m^1)}, \tag{6.53}$$

and

$$A_{0n}^{*1} = \frac{4\sigma\sum_{j=1}^{N_c} a_j q_j \cos(\delta_n^1 \overline{Y}_{c_j}) \sin(\frac{1}{2}\delta_n^1 \bar{b}_j)}{cdk_1(\delta_n^1)^2 \phi_1(\delta_n^1)}, \tag{6.54}$$

and

$$A_{mn}^{*1} = \frac{16\sigma\sum_{j=1}^{N_c} q_j \cos(\lambda_m^1 X_{c_j}) \sin(\frac{1}{2}\lambda_m^1 a_j) \cos(\delta_n^1 \overline{Y}_{c_j}) \sin(\frac{1}{2}\delta_n^1 \bar{b}_j)}{cdk_1 \beta_{mn}^1 \lambda_m^1 \delta_n^1 \phi_1(\beta_{mn}^1)}. \tag{6.55}$$

Moreover, the zeroth-order Fourier coefficients of the first-layer solution (A_{00}^{*1} and B_{00}^{*1}) are obtained as:

$$\begin{aligned} A_{00}^{*1} &= \frac{\sum_{j=1}^{N_c} Q_j}{cd}\left[\sum_{l=1}^{N}\left(\frac{\bar{t}_l}{k_l}\right) + \frac{1}{h_s}\right], \\ B_{00}^{*1} &= -\frac{\sum_{j=1}^{N_c} Q_j}{cdk_1}. \end{aligned} \tag{6.56}$$

Furthermore, the same functions that represent the inverse Kirchhoff transform can be used to find the source-plane solution for the actual temperature $T_1^*(x, y, 0)$. Finally, the total thermal resistance for the multiple-heat-source problem can be defined as [2]:

$$R_t^* = \frac{\overline{T}_c^* - T_\infty}{\sum_{j=1}^{N_c} Q_j}, \tag{6.57}$$

where $\overline{T}_c^*$ is the mean temperature of all the heat sources, defined by:

$$\overline{T}_c^* = \frac{1}{\sum_{j=1}^{N_c} A_{c_j}} \sum_{j=1}^{N_c} \iint_{A_{c_j}} T_1^*(x, y, 0)\, dA_{c_j}. \tag{6.58}$$

6.3 Results and discussion

In this section, different parametric studies are considered to validate the developed analytical solutions and to demonstrate their computational efficiency. Further, the influence of the different temperature-dependent thermal conductivity functions on the temperature rise and the total thermal resistance is also discussed. The analytical solution results are compared with numerical solution results that have been conducted by solving the problem numerically based on the finite element method (FEM). For the analytical results, MATLAB (version 2016b) software is used to carry out the results [26], while the numerical results are obtained based on the FEM using the ANSYS commercial software package [27].

6.3.1 Single Heat Source

We start our investigation by considering a multilayered 3D rectangular flux channel consisting of three layers with orthotropic temperature-dependent thermal conductivities in which heat enters the system from a rectangular single heat source and flows by conduction through the channel to reach a convective heat sink. The heat source is of dimensions $a = 1$ mm, and $b = 2$ mm with its center located at the point $(X_c, Y_c) = (15 \text{ mm}, 4 \text{ mm})$, while the side dimensions of the channel are $c = 30$ mm and $d = 10$ mm, as shown in Fig. 6.3. In each layer, the orthotropic thermal conductivities are presented as a product of different constant thermal conductivities in the three spatial direction times any of the temperature-dependent conductivity functions given in Eqs. (6.19)-(6.21). The first layer is considered of thickness $t_1 = 1$ mm and

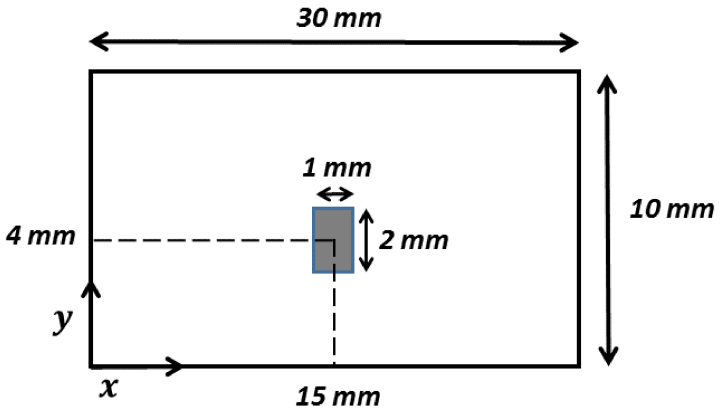

(a)

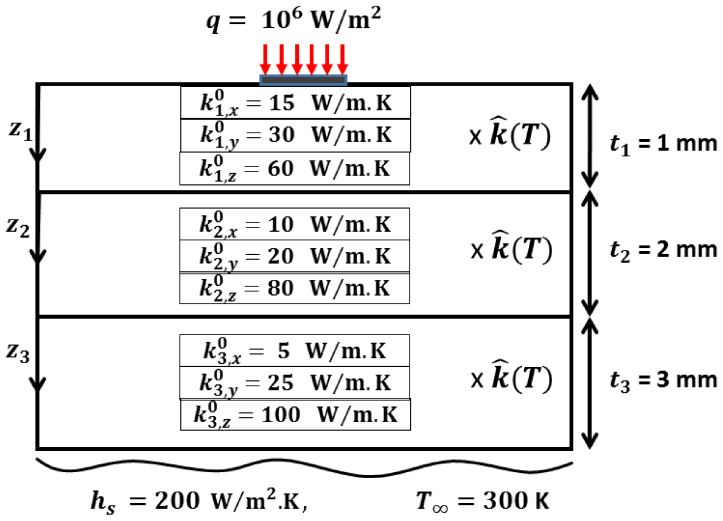

(b)

Figure 6.3: Single-heat-source validation study layout. (a) Top view. (b) Cross section with corresponding thermal conductivities.

corresponding constant thermal conductivities $k^0_{1,x} = 15$, $k^0_{1,y} = 30$, $k^0_{1,z} = 60$ W/m·K; the thickness of the second layer is $t_2 = 2$ mm with corresponding thermal conductivities $k^0_{2,x} = 10$, $k^0_{2,y} = 20$, $k^0_{2,z} = 80$ W/m·K; and the third layer is of thickness $t_3 = 3$ mm and corresponding thermal conductivities $k^0_{3,x} = 5$, $k^0_{3,y} = 25$, $k^0_{2,z} = 100$ W/m·K. Inside the source region, a uniform heat flux of $q = 10^6$ W/m^2 is applied, whereas

along the sink plane, a heat transfer coefficient of $h_s = 200$ W/m^2·K exists. The ambient temperature is of 300 K. The developed analytical solution is used to compute the centroidal ($\hat{T} = T(X_c, Y_c, 0)$) and the average ($\overline{T}$) temperatures of the heat source for the three general forms of the thermal conductivity functions Eqs. (6.19)-(6.21) with different parameters. The average sink plane reference temperature is obtained using Eq. (6.17) as $T_0 = 333.3$ K, which has been used as the reference temperature in the definition of the Kirchhoff transform. The analytical solution is addressed by obtaining the linear system solution first, and then the inverse Kirchhoff transform is used to obtain the solution of the actual temperature. The number of terms used to truncate the infinite Fourier series summations of the linear system solution is 1000 in each of the summations, and the computational time required to find the temperature of any point in the source plane is found of approximately 0.4 s. Moreover, a convergence study on the number of terms in the series is performed by increasing the number of terms, and it is found that the change in the results is negligible. The average source temperature that can be used to find the total thermal resistance of the channel is computed using the two previously addressed methods, first by performing numerical integration over the source contact area to get $\overline{T}_c$, and second by considering the result in Eq. (6.47) where the average source temperature is approximated using the first order Taylor approximation to get $\overline{T}_c$(approx.). It is found that the approximate average has good agreement with the numerically integrated average with shorter computational time compared to using the numerical integration of the analytical solution. Furthermore, the analytical results were validated by numerical results obtained by solving the system numerically using the FEM. In the numerical solution, the results were obtained with a tetrahedral mesh with high element density around the source region, and the convergence was checked by refining the mesh, where a mesh consisting of approximately 2.5×10^5 elements is found to be sufficient

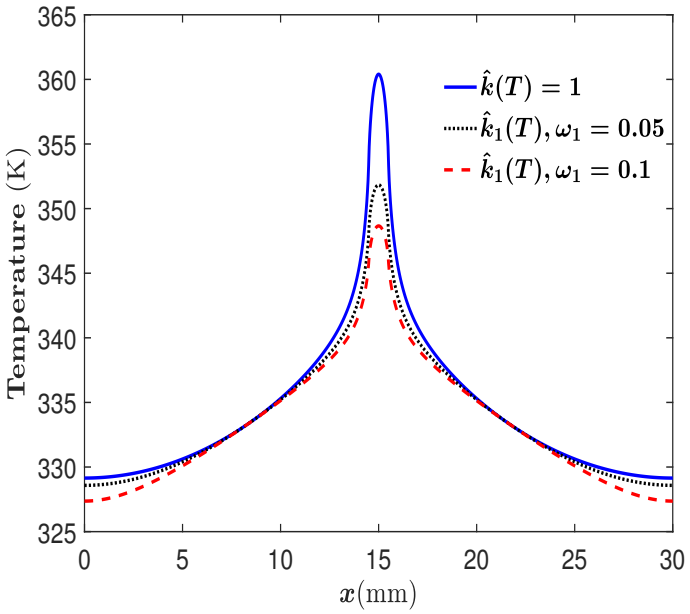

Figure 6.4: Temperature profile along x-axis in the source plane (at $y = Y_c$) by considering the thermal conductivity function $k_1(T)$ for the single-source study.

to simulate the problem. The analytical and the numerical results of the average and the centroidal temperatures of the heat source for the three general forms of thermal conductivity functions with different parameters are shown in Table 6.1, where a very good agreement between the analytical and the numerical results can be observed.

Figures 6.4-6.6 show the temperature profiles along the source plane in the x-axis direction that passes through the heat-source center, i.e., when $y = Y_c$, for the three different conductivity functions with different parameters. In these figures, the effect of changing the temperature-dependent thermal conductivity function on the temperature rise is clear compared to using constant thermal conductivities, i.e., $\hat{k}(T) = 1$. Moreover, when considering $k_1(T)$ or $k_2(T)$ as the temperature-dependent thermal conductivity function, it can be seen from the definition of these functions that the thermal conductivity is an increasing function with respect to temperature; hence, the temperature rise along the source region is less in magnitude than the temperature rise when considering constant thermal conductivities, as shown in Figs. 6.4 and 6.5.

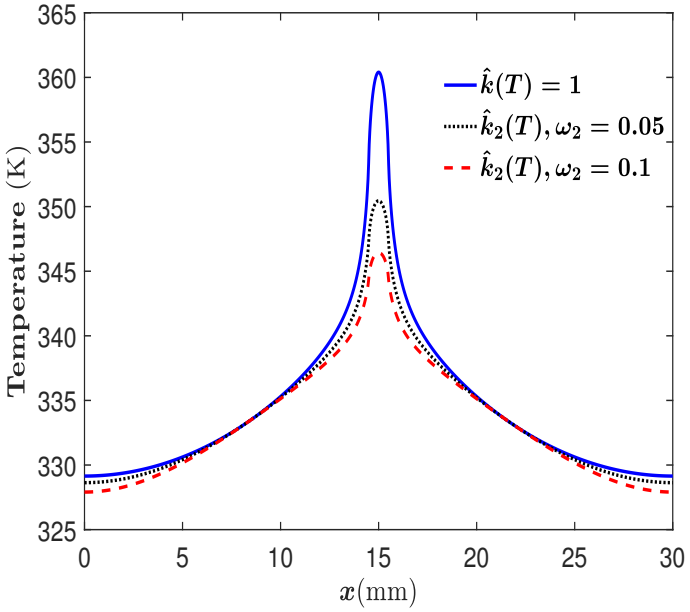

Figure 6.5: Temperature profile along x-axis in the source plane (at $y = Y_c$) by considering the thermal conductivity function $k_2(T)$ for the single-source study.

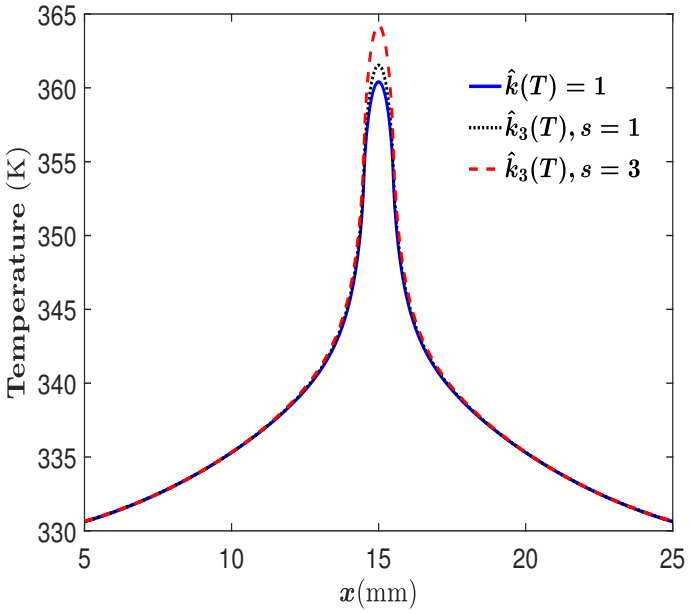

Figure 6.6: Temperature profile along x-axis in the source plane (at $y = Y_c$) by considering the thermal conductivity function $k_3(T)$ for the single-source study.

However, for the case of considering $k_3(T)$, the thermal conductivity is a decreasing function with respect to temperature, and one can see from Fig. 6.6 that the magnitude

	Analytical			FEM	
$\hat{k}(T)$	$\hat{T}$ (K)	$\overline{T}_c$ (K)	$\overline{T}_c$(approx.) (K)	$\hat{T}$ (K)	$\overline{T}_c$ (K)
$\hat{k}(T) = 1$	360.403	356.902	356.902	359.94	356.346
$\hat{k}_1(T), \omega_1 = 0.05$	351.840	349.9536	350.022	351.80	349.857
$\hat{k}_1(T), \omega_1 = 0.1$	348.659	347.216	347.277	348.77	347.285
$\hat{k}_2(T), \omega_2 = 0.05$	350.451	348.875	348.964	350.42	348.791
$\hat{k}_2(T), \omega_2 = 0.1$	346.435	345.418	345.491	346.50	345.462
$\hat{k}_3(T), s = 1$	361.532	357.764	357.735	361.00	357.137
$\hat{k}_3(T), s = 3$	364.220	359.774	359.654	363.46	358.946

Table 6.1: Source centroidal and average temperatures of the single-source study for the different thermal conductivity functions.

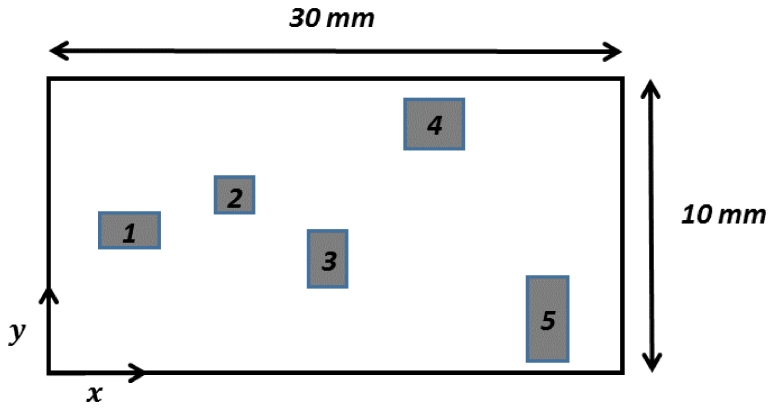

Figure 6.7: Source-plane layout of the multiple-heat-source problem.

of temperature rise is larger than the case of constant conductivities.

6.3.2 Multiple Heat Sources

In the multiple-source problem, the same previous three-layer system is considered with the same properties but with multiple heat sources along the source plane instead of considering a single heat source. Four new heat sources are added to the existing heat source to get a new source plane of five eccentric heat sources. A schematic view of the new source plane is shown in Fig. 6.7, and the heat-source dimensions and specifications are shown in Table 6.2.

Source j	a_j (mm)	b_j (mm)	X_{c_j} (mm)	Y_{c_j} (mm)	q_j (W/m^2)
1	2	1	5	5	9×10^5
2	1	1	10	6	8×10^5
3	1	2	15	4	1×10^6
4	2	2	20	8	2×10^2
5	1	3	25	2	7×10^5

Table 6.2: Heat-source dimensions and properties of the multiple-heat-source problem.

$\hat{k}(T)$	$\overline{T}_c^*$ (K) (Analytical)	$\overline{T}_c^*$ (K) (FEM)	**Relative Error**
$\hat{k}(T) = 1$	437.900	437.479	0.1%
$\hat{k}_1(T), \omega_1 = 0.05$	435.0269	434.895	0.03%
$\hat{k}_1(T), \omega_1 = 0.1$	433.674	433.739	0.02%
$\hat{k}_2(T), \omega_2 = 0.05$	434.651	434.531	0.03%
$\hat{k}_2(T), \omega_2 = 0.1$	432.967	432.976	0.01%
$\hat{k}_3(T), s = 1$	438.137	437.679	0.1%
$\hat{k}_3(T), s = 3$	438.6549	438.121	0.1%

Table 6.3: Average temperature of all the heat sources of the multiple-source study for the different thermal conductivity functions.

Both analytical and numerical solutions of the multiple-source problem have been conducted, where, in the analytical results, the number of terms in each of the truncations of the infinite Fourier series summation is taken the same number of terms used for the single-source problem of 1000 terms, and the computational time required to find the temperature at any point in the source plane is found of approximately 0.7 s. The number of terms is chosen according to the fact that the multiple-heat-source solution of the linear system can be considered as a superposition of five single-heat-source solutions; hence, the number of terms for the multiple heat sources is chosen as the same number of terms used for the single-source problem and is found to be sufficient to obtain the results. In the numerical results, a tetrahedral mesh consisting of approximately 4.6×10^5 elements is found to be sufficient to simulate the problem. According to the new source-plane configuration, the average sink-plane

reference temperature that has been used as the reference temperature in the Kirchhoff transform is found of $T_0 = 425$ K using Eq. (6.50). Table 6.3 show the average temperature of all the heat sources for the analytical and numerical solution, where very good agreement can be observed.

Finally, it is worth mentioning that, in all of the previous analyses for the single- and the multiple-source problems, although the numerical solutions of the problem are flexible and has good agreement with the analytical solutions, the computational time required to obtain the numerical results is much larger than the computational time for the analytical solution. Moreover, simulating the nonlinear problems with temperature-dependent thermal conductivities numerically requires more time than simulating the linear problems with constant thermal conductivities.

6.4 Conclusion

In this chapter, general analytical solutions for the temperature distribution and the total thermal resistance of a 3D multilayered flux channel with orthotropic temperature-dependent thermal conductivities using the Kirchhoff transform were developed. Different thermal conductivity functions were considered to study the effect of changing the temperature-dependent conductivity function on the temperature rise and the total thermal resistance. An extension of the solutions for problems with multiple heat sources in the source plane was illustrated. All the analytical results have been validated with numerical results obtained by solving the problem numerically with the FEM, where very good agreement has been shown. Further, the computational efficiency of the developed analytical solution is also addressed.

References

[1] B. Al-Khamaiseh, Y. S. Muzychka, and S. Kocabiyik, "Spreading resistance in multilayered orthotropic flux channel with temperature-dependent thermal conductivities," *AIAA-Journal of Thermophysics and Heat Transfer*, vol. 32, no. 2, pp. 392–400, 2018, doi:http://doi.org/10.2514/1.T5337.

[2] A. Gholami and M. Bahrami, "Thermal spreading resistance inside anisotropic plates with arbitrarily located hotspots," *J. Thermophys. Heat Transf.*, vol. 28, no. 4, pp. 679–686, Oct.-Dec. 2014.

[3] M. Higashiwaki, K. Sasaki, A. Kuramata, T. Masui, and S. Yamakoshi, "Development of gallium oxide power devices," *Phys. Status Solidi A*, vol. 211, no. 1, pp. 21–26, 2014.

[4] Z. Guo, A. Verma, X. Wu, F. Sun, A. Hickman, T. Masui, A. Kuramata, M. Higashiwaki, D. Jena, and T. Luo, "Anisotropic thermal conductivity in single crystal β-gallium oxide," *Appl. Phys. Lett.*, vol. 106, pp. 111 909–1–111 909–5, 2015.

[5] J. Zhu, J. Y. Chen, H. Park, X. Gu, H. Zhang, S. Karthikeyan, N. Wendel, S. A. Campbell, M. Dawber, X. Du, M. Li, J. P. Wang, R. Yang, and X. Wang, "Revealing the origins of 3D anisotropic thermal conductivities of black phosphorus," *Adv. Electron. Mater.*, vol. 2, no. 5, pp. 1 600 040–1–1 600 040–9, 2016.

[6] F. Bonani and G. Ghione, "On the application of the Kirchhoff transformation to the steady-state thermal analysis of semiconductor devices with temperature-dependent and piecewise inhomogenous thermal conductivity," *Solid-State Electron.*, vol. 38, no. 7, pp. 1409–1412, 1995.

[7] A. Karageorghis and D. Lesnic, "Steady-state nonlinear heat conduction in composite materials using the method of fundamental solutions," *Comput. Methods in Appl. Mech. Eng.*, vol. 197, pp. 3122 –3137, Jun. 2008.

[8] J. H. Knight and J. R. Philip, "Exact solutions in nonlinear diffusion," *J. Eng. Math.*, vol. 8, no. 3, pp. 219–227, Jul. 1974.

[9] M. N. Özisik, *Boundary Value Problems of Heat Conduction.* Scranton, PA, USA: International Textbook, 1968.

[10] H. S. Carslaw and J. C. Jaeger, *Conduction of Heat in Solids.* UK: Oxford Univ. Press, 1959.

[11] S. Kakac and Y. Yener, *Heat Conduction, 3rd ed.* Malabar, FL, USA: Taylor & Francis, 1993.

[12] M. M. Yovanovich, "Four decades of research on thermal contact, gap and joint resistance in microelectronics," *IEEE Trans. Compon. Packag. Technol.*, vol. 28, no. 2, pp. 182–206, Jun. 2005.

[13] Y. S. Muzychka, J. R. Culham, and M. M. Yovanovich, "Thermal spreading resistance of eccentric heat sources on rectangular flux channels," *J. Electron. Packag.*, vol. 125, no. 2, pp. 178–185, Jun. 2003.

[14] Y. S. Muzychka, M. M. Yovanovich, and J. R. Culham, "Thermal spreading

resistance in compound and orthotropic systems," *J. Thermophys. Heat Transf.*, vol. 18, no. 1, pp. 45–51, Jan.-Mar. 2004.

[15] ——, "Influence of geometry and edge cooling on thermal spreading resistance," *J. Thermophys. Heat Transf.*, vol. 20, no. 2, pp. 247–255, 2006.

[16] Y. S. Muzychka, "Influence coefficient method for calculating discrete heat source temperature on finite convectively cooled substrates," *IEEE Trans. Compon. Packag. Technol.*, vol. 29, no. 3, pp. 636–643, Sep. 2006.

[17] Y. S. Muzychka, K. R. Bagnall, and E. N. Wang, "Thermal spreading resistance and heat source temperature in compound orthotropic systems with interfacial resistance," *IEEE Trans. Compon., Packag., Manuf. Technol.*, vol. 3, no. 11, pp. 1826–1841, Nov. 2013.

[18] Y. S. Muzychka, "Spreading resistance in compound orthotropic flux tubes and channels with interfacial resistance," *J. Thermophys. Heat Transf.*, vol. 28, no. 2, pp. 313–319, Mar. 2014.

[19] K. R. Bagnall, Y. S. Muzychka, and E. N. Wang, "Analytical solution for temperature rise in complex, multilayer structures with discrete heat sources," *IEEE Trans. Compon., Packag., Manuf. Technol.*, vol. 4, no. 5, pp. 817–830, May 2014.

[20] J. Ditri, "Heat conduction in microwave devices with orthotropic and temperature-dependent thermal conductivity," *IEEE Trans. Microwave Theory Tech.*, vol. 55, no. 3, pp. 555–560, Mar. 2007.

[21] K. R. Bagnall, Y. S. Muzychka, and E. N. Wang, "Application of the Kirchhoff transform to thermal spreading problems with convection boundary conditions," *IEEE Trans. Compon., Packag., Manuf. Technol.*, vol. 4, no. 3, pp. 408–420, Mar. 2014.

[22] V. S. Arpaci, *Conduction Heat Transfer*. New York, NY, USA: Addison-Wesley, 1966.

[23] P. Vadasz, "Analytical solution to nonlinear thermal diffusion: Kirchhoff versus Cole-Hopf transformations," *J. Heat Transf.*, vol. 132, no. 12, pp. 121 302–1–121 302–6, Dec. 2010.

[24] L. M. Jiji, *Heat Conduction*. Berlin, Germany: Springer, 2009.

[25] M. M. Yovanovich, Y. S. Muzychka, and J. R. Culham, "Spreading resistance in isoflux rectangles and strips on compound flux channels," *J. Thermophys. Heat Transf.*, vol. 13, no. 4, pp. 495–500, 1999.

[26] MATLAB Release 2016b, The MathWorks, Inc., Natick, MA, USA, 2016.

[27] ANSYS® Release 16.2, ANSYS, Inc., Canonsburg, PA, USA, 2015.

Chapter 7

Conclusions and Future Work

7.1 Summary and Conclusions

In this thesis, we obtained analytical solutions for the temperature distribution and thermal resistance of 3D flux channels with nonuniform properties and complex structures. These solutions can be very useful for thermal engineers in thermal design analysis and optimization of microelectronics and cooling systems.

In Chapters 2 and 3, we obtained analytical solutions for the temperature field and total thermal resistance of a single-layer isotropic flux channel with nonuniform heat transfer coefficients along the sink plane. The solutions in Chapter 2 account for a concentric heat source, convective cooling along the side edges, and a variable heat transfer coefficient varying in one direction along the sink region. The solutions were obtained using the method of separation of variables combined with the least squares method. In Chapter 3, we generalized the solutions to account for an eccentric heat source and a 2D variable heat transfer coefficient varying in the two horizontal directions along the sink plane. Furthermore, we used these solutions to conduct some parametric studies in order to examine the effects of the different variable heat transfer

coefficient functions with the same average conductance on the temperature distribution and thermal resistance of the flux channel. The results show that although the average total conductance for the different variable heat transfer coefficient functions was fixed at constant value, the temperature distribution and total thermal resistance are strongly dependent on the distribution of the conductance profile along the sink plane.

In Chapter 4, we presented the general solutions of a 3D isotropic flux channel with temperature-dependent thermal conductivity and constant heat transfer coefficient along the sink plane. The solutions were presented by means of the Kirchhoff transform and the inverse Kirchhoff transform. The Kirchhoff transform was used to linearize the nonlinear conduction system, where the solution of the linearized system is obtained using the method of separation of variables. Then we used the solution of the linearized system in obtaining the solution of the original nonlinear system through the inverse Kirchhoff transform. In the general definition of the Kirchhoff transform, the approximate sink plane temperature was used as a reference temperature in order to consider the convective boundary condition through the Kirchhoff transform method. We also presented an explicit approximation for the total thermal resistance based on the solution of the linearized system and the functional relationships between the actual temperature and the apparent temperature. In addition, we used these analytical solutions to study the effects of temperature-dependent thermal conductivity functions on the temperature rise and thermal resistance. The results show noticeable differences in the temperature distribution and thermal resistance for the different temperature-dependent thermal conductivity functions compared with using a constant thermal conductivity.

In Chapters 5 and 6, we studied 3D flux channels of multilayered structures consisting of a finite number of orthotropic layers with constant and temperature-dependent

thermal conductivities, respectively. In Chapter 5 we presented analytical solutions for the temperature distribution and thermal resistance of the multilayered structure with interfacial conductance between the adjacent layers and a uniform conductance along the sink plane. The solutions account for multiple eccentric heat sources in the source plane. The results show how the analytical solutions offer significant computational savings over the numerical FEM solutions.

Finally, in Chapter 6 we presented the general solutions of multilayered orthotropic flux channels with temperature-dependent thermal conductivities by making use of the solutions presented in Chapters 4 and 5. The Kirchhoff transform method presented in Chapter 4 was used to transform the nonlinear governing equations of the multilayered temperature-dependent orthotropic system into a linear system with constant thermal conductivities, representing a special case of the system discussed in Chapter 5. Although the solutions presented in Chapter 6 are obtained for multilayered orthotropic systems with temperature-dependent thermal conductivities, some restrictions on the system exist for obtaining the general analytical solutions in this way. First, all the adjacent layers have to be perfectly attached with no interfacial conductance between the layers. Second, all the thermal conductivity functions in the system must depend on temperature in the same manner.

7.2 Suggestions for Future Research

In the present research, analytical solutions for the temperature distribution and thermal resistance in different types of flux channels have been developed. However, many aspects of thermal issues and thermal analysis in microelectronic devices need further investigations, which would benefit the overall field of thermal management in microelectronics and some other disciplines. Some of these aspects are listed here

as suggestions for future research:

- Analytical solutions for the temperature distribution and thermal resistance in a cylindrical shaped flux tube with a circular heat source in the source plane and a nonuniform heat transfer coefficient along the sink plane.

- Analytical solutions for the temperature distribution and thermal resistance in a multilayered flux tube consisting of a finite number of layers with temperature-dependent thermal conductivities.

- Analytical solutions for the temperature distribution and thermal resistance in multilayered flux tubes of orthotropic materials.

- Analytical solutions for the temperature distribution and thermal resistance in flux channels and flux tubes chosen in different orientations of orthotropic materials.

- Analytical optimization studies for the multiple-heat-source distribution along the source plane.

For cylindrical shaped flux tubes (which represent the other general geometry of microelectronic devices) with a uniform heat transfer coefficient along the sink plane, the heat flow mechanism is similar to that for rectangular shaped flux channels. In addition, the general solutions for the temperature distribution and thermal resistance in flux tubes can be obtained using the method of separation of variables, where the solutions are represented in terms of the orthogonal set of Bessel's functions. However, when the distribution of the heat transfer coefficient along the sink plane is nonuniform, the direct application of the method of separation of variables is not possible. Nevertheless, the analytical solution procedures for rectangular flux channels

with nonuniform heat transfer coefficients, presented in Chapters 2 and 3, can be followed to obtain the analytical solutions for cylindrical flux tubes.

Similarly, the developed analytical solutions in Chapters 5 and 6 for the multilayered flux channels with orthotropic and temperature-dependent thermal conductivities construct mathematical procedures that can be followed to obtain the analytical solutions for similar flux tube models. Moreover, when the flux channel or flux tube is constructed from orthotropic materials in different orientations, the thermal conductivity tensor may have nine nonzero components and this requires the use of other mathematical transformations besides the stretched coordinate transformations in order to obtain the analytical solutions for the temperature distribution and thermal resistance in the channel.

Finally, the developed analytical solutions can be used to conduct analytical optimization studies for the best distribution of the heat sources along the source plane for which the temperature excess is minimized.